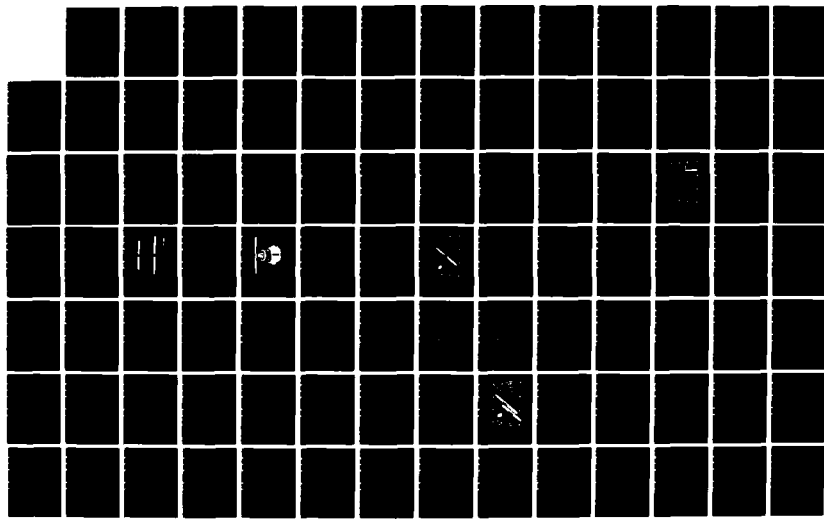
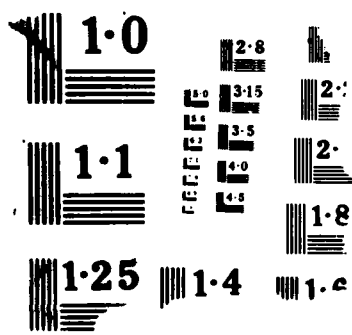


AD-A195 085 ANALYTICAL AND EXPERIMENTAL STUDIES OF BEAM WAVEGUIDE
ABSORBERS FOR STRUCTURAL DAMPING(U) NAVAL POSTGRADUATE
SCHOOL MONTEREY CA G G LEE MAR 88 1/2

UNCLASSIFIED

F/G 13/10.1 NL





DTIC FILE COPY

(2)

NAVAL POSTGRADUATE SCHOOL

Monterey, California

AD-A195 085



DTIC
ELECTED
JUL 14 1988
S H D

THESIS

ANALYTICAL AND EXPERIMENTAL STUDIES OF
BEAM WAVEGUIDE ABSORBERS FOR
STRUCTURAL DAMPING

by

Gi Gon Lee

March 1988

Thesis Advisor
Co-Advisor

Y. S. Shin
K. S. Kim

Approved for public release: distribution is unlimited.

Unclassified

security classification of this page

A195 585

REPORT DOCUMENTATION PAGE

| | | | |
|---|--|--|--|
| 1a Report Security Classification Unclassified | | 1b Restrictive Markings | |
| 2a Security Classification Authority | | 3 Distribution Availability of Report Approved for public release; distribution is unlimited. | |
| 2b Declassification Downgrading Schedule | | | |
| 4 Performing Organization Report Number(s) | | 5 Monitoring Organization Report Number(s) | |
| 6a Name of Performing Organization Naval Postgraduate School | 6b Office Symbol (if applicable) 62 | 7a Name of Monitoring Organization Naval Postgraduate School | |
| 8c Address (city, state, and ZIP code) Monterey, CA 93943-5000 | | 7b Address (city, state, and ZIP code) Monterey, CA 93943-5000 | |
| 8a Name of Funding Sponsoring Organization | 8b Office Symbol (if applicable) | 9 Procurement Instrument Identification Number | |
| 8c Address (city, state, and ZIP code) | | 10 Source of Funding Numbers Program Element No [Project No] Task No Work Unit Accession No | |

11 Title (include security classification) ANALYTICAL AND EXPERIMENTAL STUDIES OF BEAM WAVEGUIDE ABSORBERS FOR STRUCTURAL DAMPING

12 Personal Author(s) Gi Gon Lee

| | | | |
|---------------------------------------|---|--|----------------------|
| 13a Type of Report Master's Thesis | 13b Time Covered From _____ To _____ | 14 Date of Report (year, month, day) March 1988 | 15 Page Count 123 |
|---------------------------------------|---|--|----------------------|

16 Supplementary Notation The views expressed in this thesis are those of the author and do not reflect the official policy or position of the Department of Defense or the U.S. Government.

| | | | |
|----------------|-------|---|--|
| 17 Cosat Codes | | 18 Subject Terms (continue on reverse if necessary and identify by block number) waveguide absorber, viscoelastic, constrained layer, beam ← | |
| Field | Group | Subgroup | |
| | | | |
| | | | |

19 Abstract (continue on reverse if necessary and identify by block number)

The reduction of structural vibrations in ships and submarines is a long standing concern of the Navy. Waveguide absorbers are very effective devices which can be applied to this problem. This study evaluates the increase in vibration damping of a plate structure across a broad frequency range using light weight beam waveguide absorbers. Viscoelastic and constrained layer beam waveguide absorbers were studied both theoretically and experimentally. Impedances of the waveguide absorbers at the attachment point were predicted using both Bernoulli-Euler and Timoshenko beam theory for the viscoelastic beam and using sixth order beam theory for the constrained layer beam. The theoretically predicted impedances were compared with the experimental measurements. Results from random vibration tests of a plate structure showed significant increases in damping over a broad frequency range (100 Hz - 2 KHz) when the waveguide absorbers were attached on the plate.

Regrained:

| | |
|--|---|
| 20 Distribution Availability of Abstract: <input checked="" type="checkbox"/> Inclusive/unlimited <input type="checkbox"/> same as report <input type="checkbox"/> DDCI users | 21 Abstract Security Classification Unclassified |
| 22a Name of Responsible Individual Y. S. Shin | 22b Telephone (include Area code) (408) 373-2341 |
| 22c Office Symbol 608g | |

DD FORM 1473.84 MAR

83 APR edition may be used until exhausted
All other editions are obsolete

security classification of this page

Unclassified

Approved for public release; distribution is unlimited.

ANALYTICAL AND EXPERIMENTAL STUDIES OF BEAM WAVEGUIDE
ABSORBERS FOR STRUCTURAL DAMPING

by

Gi Gon Lee
Lieutenant, Korean Navy
B.S., Naval Academy of Korea, 1982

Submitted in partial fulfillment of the
requirements for the degree of

MASTER OF SCIENCE IN MECHANICAL ENGINEERING

from the

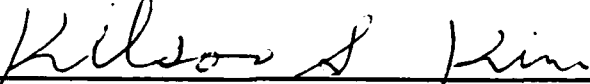
NAVAL POSTGRADUATE SCHOOL
March 1988

Author:


Gi Gon Lee

Approved by:


Y. S. Shin, Thesis Advisor


K. S. Kim, Co-Advisor


A. J. Healey, Chairman,
Department of Mechanical Engineering


Gordon E. Schacher,
Dean of Science and Engineering

ABSTRACT

The reduction of structural vibrations in ships and submarines is a long standing concern of the Navy. Waveguide absorbers are very effective devices which can be applied to this problem. This study evaluates the increase in vibration damping of a plate structure across a broad frequency range using light weight beam waveguide absorbers. Viscoelastic and constrained layer beam waveguide absorbers were studied both theoretically and experimentally. Impedances of the waveguide absorbers at the attachment point were predicted using both Bernoulli-Euler and Timoshenko beam theory for the viscoelastic beam and using sixth order beam theory for the constrained layer beam. The theoretically predicted impedances were compared with the experimental measurements. Results from random vibration tests of a plate structure showed significant increases in damping over a broad frequency range (100 Hz - 2 KHz) when the waveguide absorbers were attached on the plate.



| | |
|---------------|--|
| Accession For | |
| NTIS | RA&I <input checked="" type="checkbox"/> |
| DTIC | CD |
| University | DD |
| Other | EE |
| Date | |
| A-1 | |

TABLE OF CONTENTS

| | |
|--|----|
| I. INTRODUCTION | 1 |
| II. THEORETICAL ANALYSIS | 2 |
| A. LOSS FACTOR CONTRIBUTION OF A WAVEGUIDE ABSORBER | 2 |
| B. IMPEDANCE OF BEAM WAVEGUIDE ABSORBERS FROM WAVE PROPAGATION THEORY | 4 |
| 1. VISCOELASTIC BEAM USING BERNOULLI-EULER BEAM THE- ORY | 4 |
| a. INFINITE VISCOELASTIC BEAM | 6 |
| b. FINITE VISCOELASTIC BEAM | 7 |
| 2. FINITE VISCOELASTIC BEAM USING TIMOSHENKO BEAM THEORY | 8 |
| 3. FINITE CONSTRAINED LAYER BEAM | 11 |
| C. COMPUTER IMPLEMENTATION | 15 |
| III. EXPERIMENT | 25 |
| A. IMPEDANCES OF THE TEST PLATE | 25 |
| B. IMPEDANCES OF THE WAVEGUIDE ABSORBER | 28 |
| C. DAMPING OF THE PLATE | 35 |
| IV. RESULTS AND DISCUSSIONS | 38 |
| A. IMPEDANCES OF THE TEST PLATE | 38 |
| B. IMPEDANCES OF THE WAVEGUIDE ABSORBER | 45 |
| C. DAMPING OF THE PLATE | 53 |
| V. CONCLUSIONS | 74 |
| VI. RECOMMENDATIONS | 75 |
| APPENDIX A. | 76 |

| | |
|--|-----|
| 1. THE IMPEDANCE OF THE INFINITE VISCOELASTIC BEAM USING BERNOULLI-EULER BEAM THEORY | 76 |
| 2. THE IMPEDANCE OF THE FINITE VISCOELASTIC BEAM US- ING BERNOULLI-EULER BEAM THEORY | 78 |
| 3. THE IMPEDANCE OF THE FINITE VISCOELASTIC BEAM US- ING TIMOSHENKO BEAM THEORY | 81 |
| 4. THE IMPEDANCE OF THE FINITE CONSTRAINED LAYER BEAM USING THE SIXTH ORDER BEAM THEORY | 84 |
| APPENDIX B. | 91 |
| LIST OF REFERENCES | 109 |
| INITIAL DISTRIBUTION LIST | 111 |

LIST OF TABLES

| | |
|--|----|
| Table 1. DIMENSIONS AND PROPERTIES OF THE WAVEGUIDE ABSORBER SPECIMENS. | 29 |
|--|----|

LIST OF FIGURES

| | | |
|------------|---|----|
| Figure 1. | Vibrating structure with waveguide absorber. | 3 |
| Figure 2. | Coordinates and sign conventions for a semi-infinite (finite) viscoelastic beam. | 6 |
| Figure 3. | Coordinates and sign conventions for a semi-finite constrained layer beam. | 12 |
| Figure 4. | Real part of the 16" viscoelastic beam waveguide absorber theoretical impedances | 19 |
| Figure 5. | Imaginary part of the 16" viscoelastic beam waveguide absorber theoretical impedances | 20 |
| Figure 6. | Real part of the 16" viscoelastic beam waveguide absorber theoretical impedances | 21 |
| Figure 7. | Imaginary part of the 16" viscoelastic beam waveguide absorber theoretical impedances | 22 |
| Figure 8. | Real part of the 20" constrained layer beam waveguide absorber theoretical impedances. | 23 |
| Figure 9. | Imaginary part of the 20" constrained layer beam waveguide absorber theoretical impedances. | 24 |
| Figure 10. | Arrangement for test plate impedance measurement. | 26 |
| Figure 11. | Test plate impedance measurement configuration. | 27 |
| Figure 12. | Loss factor vs. frequency for a LD-400 and a ISD-112. | 30 |
| Figure 13. | Shear modulus vs. frequency for a LD-400 and a ISD-112. | 31 |
| Figure 14. | Waveguide absorbers. | 32 |
| Figure 15. | Arrangement for waveguide absorber impedance measurement. | 33 |
| Figure 16. | Wilcoxon F4 F7 shaker with waveguide absorber mounted. | 34 |
| Figure 17. | Arrangement for test plate damping measurement. | 36 |
| Figure 18. | Damping measurement configuration. | 37 |
| Figure 19. | Impedance magnitude of test plate at location 1. | 39 |
| Figure 20. | Impedance phase of test plate at location 1. | 40 |
| Figure 21. | Impedance magnitude of test plate at location 2. | 41 |
| Figure 22. | Impedance phase of test plate at location 2. | 42 |
| Figure 23. | Impedance magnitude of test plate at location 3. | 43 |

| | |
|---|----|
| Figure 24. Impedance phase of test plate at location 3 | 44 |
| Figure 25. Real part of the 16" viscoelastic beam waveguide absorber impedances at the center of the beam. | 47 |
| Figure 26. Imaginary part of the 16" viscoelastic beam waveguide absorber impe- dances at the center of beam. | 48 |
| Figure 27. Real part of the 16" constrained layer beam waveguide absorber impe- dances at the center of the beam. | 49 |
| Figure 28. Imaginary part of the 16" constrained layer beam waveguide absorber impedances at the center of beam. | 50 |
| Figure 29. Real part of the 20" constrained layer beam waveguide absorber impe- dances at the center of the beam. | 51 |
| Figure 30. Imaginary part of the 20" constrained layer beam waveguide absorber impedances at the center of beam. | 52 |
| Figure 31. The driving point frequency response of the test plate without a wave- guide absorber. | 56 |
| Figure 32. Modal damping factors vs. frequency of the test plate without a wave- guide absorber. | 57 |
| Figure 33. The driving point frequency response of the test plate with a 20" viscoe- lastic beam waveguide absorber (dashed) at location | 58 |
| Figure 34. Modal damping factors vs. frequency of the test plate with a 20" viscoe- lastic beam waveguide absorber at location 1 and | 59 |
| Figure 35. The driving point frequency response of the test plate with a 20" viscoe- lastic beam waveguide absorber (dashed) at | 60 |
| Figure 36. Modal damping factors vs. frequency of the test plate with a 20" viscoe- lastic beam waveguide absorber at location 2 and | 61 |
| Figure 37. The driving point frequency response of test test plate with a 20" vis- coelastic beam waveguide absorber (dashed) at | 62 |
| Figure 38. Modal damping factors vs. frequency of the test plate with a 20" viscoe- lastic beam waveguide absorber at location 3 and | 63 |
| Figure 39. The driving point frequency response of the test plate with a 16" con- strained layer beam waveguide absorber (dashed) at | 64 |
| Figure 40. Modal damping factors vs. frequency of the test plate with a 16" con- strained layer beam waveguide absorber at location 1 | 65 |
| Figure 41. The test plate with three waveguide absorbers. | 66 |

| | |
|---|-----|
| Figure 42. The driving point frequency response of the test plate with a 20" viscoelastic (at location 1) and 16" constrained layer | 67 |
| Figure 43. Modal damping factors vs. frequency of the test plate with a 20" viscoelastic (location 1) and a 16" constrained layer | 68 |
| Figure 44. The driving point frequency response of the test plate with a 20" viscoelastic (at location 1), a 16" constrained layer (at | 69 |
| Figure 45. Modal damping factors vs. frequency of the test plate with a 20" viscoelastic (location 1), a 16" constrained layer | 70 |
| Figure 46. Magnitude impedances of the test plate at location 1 (solid) and of the 20" viscoelastic beam at the driving point | 71 |
| Figure 47. Magnitude impedances of the test plate at location 2 (solid) and of the 16" constrained layer beam at the driving point | 72 |
| Figure 48. Magnitude impedances of the test plate at location 3 (solid) and of the 16" viscoelastic beam at the driving point | 73 |
| Figure 49. Real part of the 20" viscoelastic beam waveguide absorber impedances at the center of the beam. | 91 |
| Figure 50. Imaginary part of the 20" viscoelastic beam waveguide absorber impedances at the center of the beam. | 92 |
| Figure 51. The driving point frequency response of the test plate with a 16" viscoelastic beam waveguide absorber (dashed) at location | 93 |
| Figure 52. Modal damping factors vs. frequency of the test plate with a 16" viscoelastic beam waveguide absorber at location 1 and | 94 |
| Figure 53. The driving point frequency response of the test plate with a 20" constrained layer beam waveguide absorber (dashed) at | 95 |
| Figure 54. Modal damping factors vs. frequency of the test plate with a 20" constrained layer beam waveguide absorber at location 1 and | 96 |
| Figure 55. The driving point frequency response of the test plate with a 16" viscoelastic beam waveguide absorber (dashed) at location | 97 |
| Figure 56. Modal damping factors vs. frequency of the test plate with a 16" viscoelastic beam waveguide absorber at location 2 and | 98 |
| Figure 57. The driving point frequency response of the test plate with a 16" constrained layer beam waveguide absorber (dashed) at | 99 |
| Figure 58. Modal damping factors vs. frequency of the test plate with a 16" constrained layer beam waveguide absorber at location 2 and | 100 |

- Figure 59. The driving point frequency response of the test plate with a 20° constrained layer beam waveguide absorber (dashed) at 101
- Figure 60. Modal damping factors vs. frequency of the test plate with a 20° constrained layer beam waveguide absorber at location 2 and 102
- Figure 61. The driving point frequency response of the test plate with a 16° viscoelastic beam waveguide absorber (dashed) at location 103
- Figure 62. Modal damping factors vs. frequency of the test plate with a 16° viscoelastic beam waveguide absorber at location 3 and 104
- Figure 63. The driving point frequency response of the test plate with a 16° constrained layer beam waveguide absorber (dashed) at 105
- Figure 64. Modal damping factors vs. frequency of the test plate with a 16° constrained layer beam waveguide absorber at location 3 and 106
- Figure 65. The driving point frequency response of the test plate with a 20° constrained layer beam waveguide absorber (dashed) at 107
- Figure 66. Modal damping factors vs. frequency of the test plate with a 20° constrained layer beam waveguide absorber at location 3 and 108

I. INTRODUCTION

Suppressing noise and vibrations of ships and submarines is very important for the Navy and has been one of the Navy's long-standing concerns. Much work has been done on the development of vibration control means such as isolation, detuning, viscoelastic damping and dynamic absorption. All of these approaches have been studied rather thoroughly including their range of applicability and definite limits on their vibration and noise reduction capability within acceptable weight and volume increases.

Recently, a waveguide absorber concept has been developed [Ref. 1], which can provide simple and highly effective vibration control over a wide frequency range. A "Waveguide" is a structure along which vibrational waves can travel. If one end of a waveguide is attached to a vibrating structure, some vibration energy will travel along the waveguide in wave forms. If the waveguide is treated with a high energy dissipation scheme, the damping of the waveguide causes the amplitude of the waves to decrease as they travel and the waveguide may be expected to remove vibrational energy from the structure.

In previous studies by Ungar and Kurzweil [Ref. 2] and by Ungar and Williams [Ref. 3], semi-infinite beams and exponentially tapered semi-infinite beam waveguide absorbers were studied. However, theoretical prediction of the driving point impedances showed wide discrepancy from the experimental results since the experiments were performed with finite length beams and the effects of viscoelastic materials on beams were not considered in theoretical calculations.

In this investigation, two kinds of high damping beam waveguide absorber are subjected to study: viscoelastic beam and constrained layer beam waveguide absorbers. The driving point impedances are theoretically predicted for the finite length beams of highly viscoelastic behavior. Experimental studies are also performed on the impedances of these waveguide specimens and on their contribution to damping increase of a test plate structure.

II. THEORETICAL ANALYSIS

A. LOSS FACTOR CONTRIBUTION OF A WAVEGUIDE ABSORBER

Consider a linear structure, S , under a harmonic load

$$F = f_0 \sin \omega t \quad (2.1)$$

at location c (Figure 1 on page 3). The structure S will vibrate with the energy of vibration

$$W_0 = \frac{1}{2} M V_m^2 \quad (2.2)$$

where M represents the total mass of the structure and V_m is the magnitude of average velocity. The energy dissipated in S per cycle, D_0 , depends on the original loss factor, η_0 , of the structure and the following relation holds:

$$\eta_0 = \frac{D_0}{2\pi W_0} \quad (2.3)$$

For a lightly damped structure, η_0 is much smaller than 1 and D_0 is much smaller than $2\pi W_0$. If a point a of a second body B , a waveguide absorber, is attached to body S at location b of body S , internal force, F_b , will interact between body S and body B and some vibration energy, D will be dissipated in body B (Figure 1 on page 3). Moreover, this internal force influences the vibrational motion of body S and may reduce the energy of vibration, W , of body S under the same harmonic load at the same location c .

The interaction between bodies S and B depends on the impedances of bodies S and B at the attachment point, Z , and Z_b . Impedance is the ratio of the harmonic force, F , acting on a point a of the structure to the velocity, V , of the point.

$$Z = \frac{F}{V} \quad (2.4)$$

and can be described by a complex number,

$$Z = R + iV \quad (2.5)$$

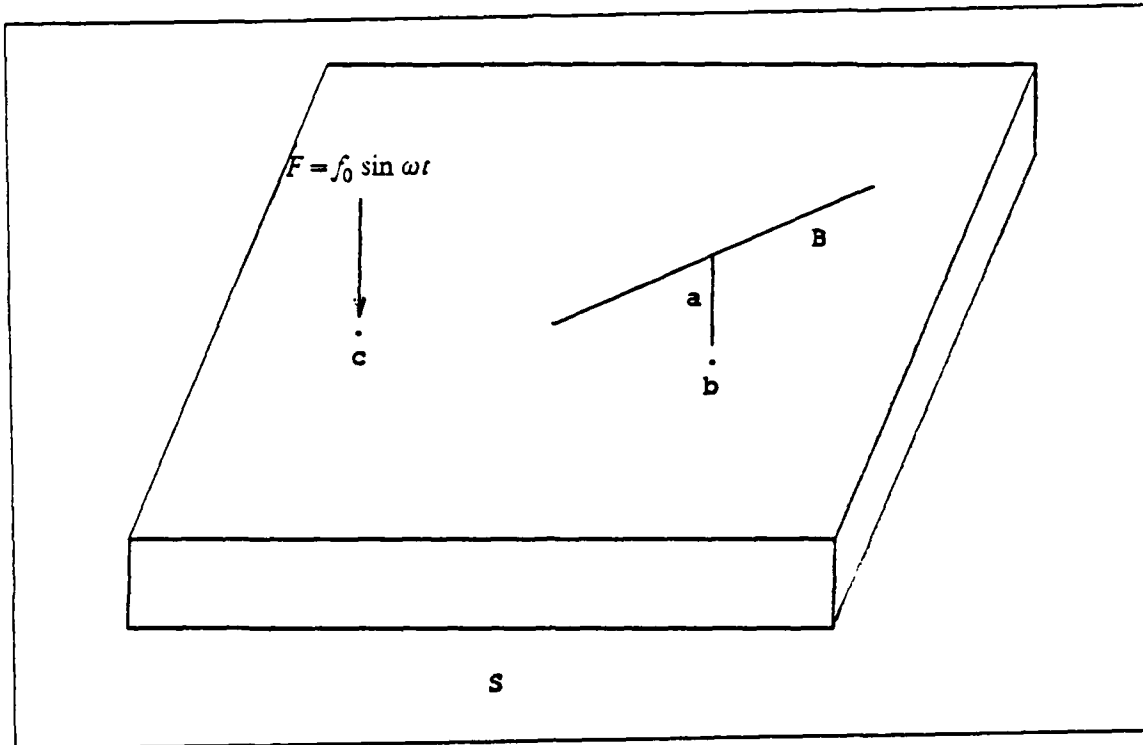


Figure 1. Vibrating structure with waveguide absorber.

where R is the real part of Z and resistance component, or simply resistance, and X is the imaginary part of Z and reactive component, or reactance.

The energy loss per cycle, D , of a structure by an attached waveguide absorber is, as shown by the previous study [Ref. 2 . and Ref. 3],

$$D = \frac{\pi R_h}{\omega} \frac{|V_s|^2}{|1 + \frac{Z_h}{Z_s}|^2} \quad (2.6)$$

where ω denotes the vibration frequency in radian sec, V_s represents the velocity of the structure at the attachment point of the structure before the attachment of the waveguide absorbers, Z_h and Z_s denote the impedance of the waveguide absorber and the structure at the attachment point, and R_h represents the real part of the impedance Z_h .

From the equations 2.2, 2.3 and 2.6, the energy loss factor, η , due to the contribution of an attached waveguide absorber can be expressed as follows:

$$\eta = \frac{R_p}{\omega M} \frac{\left| \frac{V_s}{V_\infty} \right|^2}{\left| 1 + \frac{Z_b}{Z_s} \right|^2} \quad (2.7)$$

Equation (2.6) shows that the vibration energy loss of a structure through the waveguide absorber depends on the magnitude of the velocity, V_s , at the attachment point on the structure. If this attachment point is a node for which $V_s = 0$, then the energy loss factor, η , equals zero. If the attachment point is an antinode, then $\left| \frac{V_s}{V_\infty} \right|^2$ can be relatively large. Equation (2.7) indicates that the loss factor contribution is small if the impedance of the beam, Z_b , is considerably greater than the impedance of the structure, Z_s . If Z_b is much smaller than Z_s , then the structure will not be affected by the absorber and the vibration energy of the structure, W_0 in equation (2.2), will not be reduced much. Therefore, impedance matching between the structure and the waveguide absorber is important to get the highest energy loss factor, η . So, analytic methods which can predict the impedance of beams using the theory of elastic wave propagation in beams are developed in the next section.

B. IMPEDANCE OF BEAM WAVEGUIDE ABSORBERS FROM WAVE PROPAGATION THEORY

I. VISCOELASTIC BEAM USING BERNOULLI-EULER BEAM THEORY

Previous research [Ref. 3] considers the impedances of the infinite viscoelastic beam using Bernoulli-Euler beam theory. In this section, this previous work is expanded to include the finite viscoelastic beam. The viscoelastic beam will be excited harmonically at its center by a transverse force, F as shown in Figure 2 on page 6. For a beam which is free of lateral loading and under an assumption that cross-sectional areas remain plane and normal to the neutral axis, the equation of motion becomes [Ref. 2].

$$E^* I \frac{\partial^4 y}{\partial x^4} + \rho A \frac{\partial^2 y}{\partial t^2} = 0 \quad (2.8)$$

where $y(x,t)$ is the transverse displacement, and E^* is the complex moduli of the beam:

$$E^* = E(1 + i\eta_{ve}), \quad (2.9)$$

and,

E : modulus of elasticity of the beam

η_{ve} : loss factor of the viscoelastic material

m : mass per unit length of the beam

ρ : density of the beam material

A : cross sectional area of the beam

I : moment of inertia of the cross sectional area

The general form of $y(x,t)$ for a propagating harmonic wave in this Bernoulli-Euler beam is

$$y(x,t) = Y_0 e^{i(k^x x - \omega t)} \quad (2.10)$$

where k^x is the complex wave number, and ω is the frequency of the propagating wave.

Inserting the wave equation (2.10) into the equation of motion (equation 2.8), the dispersion relation is obtained as follow:

$$E^x I(k^x)^4 = \rho A \omega^2 \quad (2.11)$$

This equation gives the four different complex wave numbers as function of frequencies,

$$k_1^x = ik(\sqrt{1 + \eta_{ve}^2})^{-1/4} [\cos(\frac{\tan^{-1}\eta_{ve}}{4}) - i \sin(\frac{\tan^{-1}\eta_{ve}}{4})] \quad (2.12.a)$$

$$k_2^x = -ik(\sqrt{1 + \eta_{ve}^2})^{-1/4} [\cos(\frac{\tan^{-1}\eta_{ve}}{4}) - i \sin(\frac{\tan^{-1}\eta_{ve}}{4})] \quad (2.12.b)$$

$$k_3^x = -k(\sqrt{1 + \eta_{ve}^2})^{-1/4} [\cos(\frac{\tan^{-1}\eta_{ve}}{4}) - i \sin(\frac{\tan^{-1}\eta_{ve}}{4})] \quad (2.12.c)$$

$$k_4^x = k(\sqrt{1 + \eta_{ve}^2})^{-1/4} [\cos(\frac{\tan^{-1}\eta_{ve}}{4}) - i \sin(\frac{\tan^{-1}\eta_{ve}}{4})] \quad (2.12.d)$$

where subscript ve is an abbreviation of Viscoelastic beam using Bernoulli-Euler beam theory and k is the wave number, given by

$$k^4 = \frac{\omega^2 m}{EI} = \frac{\omega^2 \rho A}{EI} = \left(\frac{\omega}{rc_l} \right)^2 \quad (2.13)$$

r denotes the radius of gyration of the cross sectional area, ($\sqrt{\frac{I}{A}}$) and c_l denotes the longitudinal wavespeed in the beam material ($\sqrt{\frac{E}{\rho}}$). Therefore, the equation (2.10) is expanded using wave number k_1^x , k_2^x , k_3^x and k_4^x .

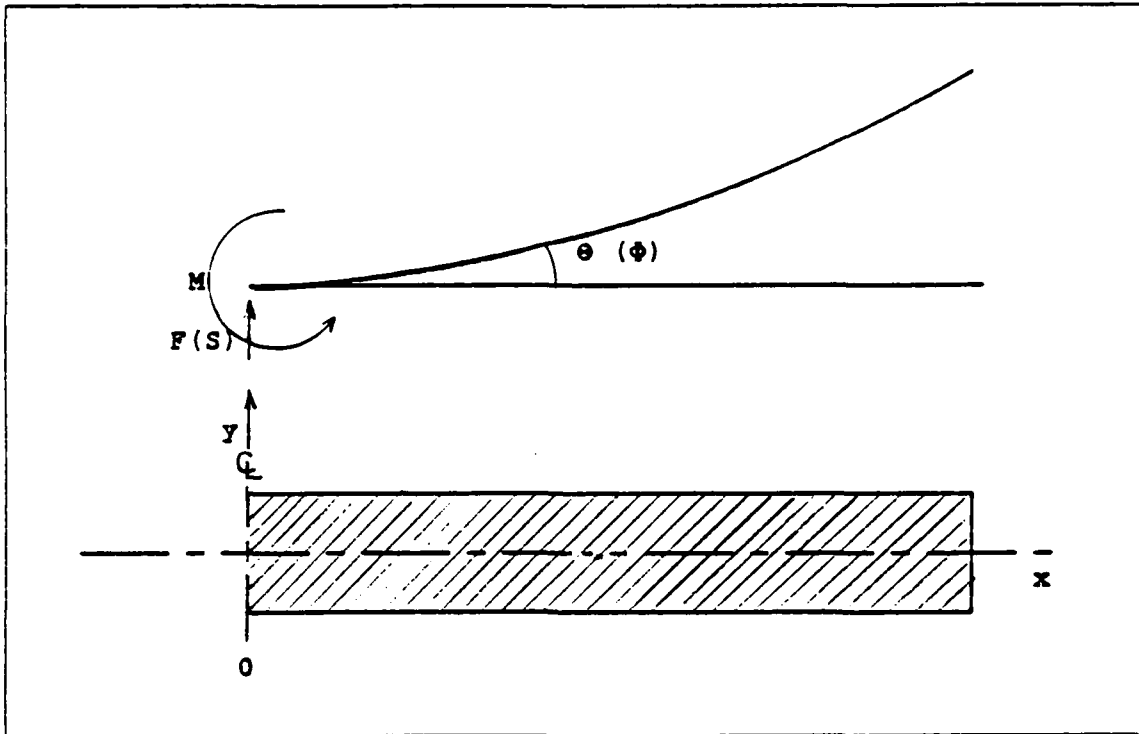


Figure 2. Coordinates and sign conventions for a semi-infinite (finite) viscoelastic beam.

$$y(x,t) = (Y_1 e^{ik_1^x x} + Y_2 e^{ik_2^x x} + Y_3 e^{ik_3^x x} + Y_4 e^{ik_4^x x}) e^{-i\omega t} \quad (2.14)$$

where Y_1 , Y_2 , Y_3 and Y_4 are constants whose values depend on the boundary conditions and x is the axial coordinate. The complex transverse force, F , is denoted by

$$F(x) = E^x I \frac{d^3 y(x)}{dx^3} \quad (2.15)$$

a. INFINITE VISCOELASTIC BEAM

Let's consider the infinite viscoelastic beam. If $y(x)$ is to remain finite for a large x , then Y_4 must vanish. If there is no wave coming toward the origin from the positive x direction, then Y_2 must vanish. Y_1 and Y_3 in equation (2.14) are determined from two boundary conditions at $x = 0$, as functions of y and θ , as follows:

$$y(0) = y \quad (2.16)$$

$$\frac{dy(0)}{dx} = \theta \quad (2.17)$$

At the driving point, the input transverse force, $F(0)$, can be calculated using the equation (2.15), which can be expressed using impedance and velocity at $x = 0$ as follows:

$$F(0) = Z_1 V(0) + Z_2 \Omega(0) \quad (2.18)$$

The complex transverse velocity, V , and the complex angular velocity, Ω , are related to the corresponding displacement, y and θ of equations (2.16 and 2.17), as follows:

$$\frac{V}{y} = \frac{\Omega}{\theta} = -i\omega \quad (2.19)$$

Z_1 represents the impedances of the transverse force at the driving point of the center of the infinite viscoelastic beam. If there is no rotation at the center of the beam, that is $\Omega(0) = 0$, the equation (2.18) becomes

$$F(0) = Z_1 V(0) \quad (2.20)$$

Therefore, the impedance of an infinite Bernoulli-Euler beam at the driving point, Z_{∞} , can be calculated from

$$Z_{ive}(0) = \frac{F_{ive}(0)}{i\omega} \frac{1}{y} \quad (2.21)$$

where subscript *ive* is an abbreviation of the Infinite Viscoelastic beam using Bernoulli-Euler beam theory.

b. FINITE VISCOELASTIC BEAM

For a finite beam, four constants Y_1 , Y_2 , Y_3 and Y_4 , are determined from four boundary conditions at $x = 0$ and $x = l$, as follows:

$$y(0) = y \quad (2.22)$$

$$\frac{dy(0)}{dx} = \theta \quad (2.23)$$

$$-E^* I \frac{d^2 y(l)}{dx^2} = 0 \quad (2.24)$$

$$E^* I \frac{d^3 y(l)}{dx^3} = 0 \quad (2.25)$$

From the same considerations as those in the previous section, the impedance $Z_{\text{v.e.}}$,

$$Z_{\text{fve}}(0) = \frac{F_{\text{fve}}(0)}{i\omega} \frac{1}{y} \quad (2.26)$$

is determined as function of frequencies, where the subscript *fve* is the abbreviation of the Finite Viscoelastic beam using Bernoulli-Euler beam theory.

2. FINITE VISCOELASTIC BEAM USING TIMOSHENKO BEAM THEORY

The Bernoulli-Euler beam theory was obtained using two assumptions which neglect shear deformation and rotational inertia. The Bernoulli-Euler beam theory may be useful for low frequencies and long wavelengths. However, the Timoshenko beam theory gives more accurate simulation at wider frequency ranges and wave lengths. Therefore we will analyze the impedances of the finite viscoelastic beam using Timoshenko beam theory in this section. Two independent variables, the transverse displacement, $y(x,t)$, and angular displacement, $\phi(x,t)$, are defined in Timoshenko beam theory. Beam motions are governed by the following equations [Ref. 4].

$$a_1^2 \left(\frac{\partial^2 y}{\partial x^2} - \frac{\partial \phi}{\partial x} \right) = \frac{\partial^2 y}{\partial t^2} \quad (2.27)$$

$$a_2^2 \frac{\partial^2 \phi}{\partial x^2} + a_1^2 k_0^2 \left(\frac{\partial y}{\partial x} - \phi \right) = \frac{\partial^2 \phi}{\partial t^2} \quad (2.28)$$

where $a_1^2 = \frac{\kappa G^*}{\rho}$, $a_2^2 = \frac{E^*}{\rho}$ and $k_0^2 = \frac{A}{I}$. The complex moduli G^* and E^* are defined as:

$$G^* = G(1 + i\eta_{vt}) \quad (2.29)$$

$$E^* = E(1 + i\eta_{vt}) \quad (2.30)$$

where subscript *vt* is an abbreviation of Viscoelastic beam using Timoshenko beam theory, and

G : shear modulus of the beam

E : elastic modulus of the beam

η_{vt} : loss factor of the viscoelastic material

A : cross sectional area of the beam

I : moment of the inertia of the cross sectional area

ρ : density of the beam material

κ : shear deformation factor

The general forms $y(x,t)$ and $\phi(x,t)$ for the propagating harmonic wave in a Timoshenko beam are

$$y(x,t) = Y_0 e^{ik^x x - \omega t} \quad (2.31)$$

$$\phi(x,t) = \Phi_0 e^{ik^x x - \omega t} \quad (2.32)$$

where k^x is the complex wave number, and ω is the frequency of the propagating wave. Inserting the wave equations (2.31 and 2.32) into the governing beam equations (2.27 and 2.28) becomes

$$(\omega^2 - a_1^2(k^x)^2)Y_0 + (-ia_1^2 k^x)\Phi_0 = 0 \quad (2.33)$$

$$(ia_1^2 k_0^2 k^x)Y_0 + (\omega^2 - a_1^2 k_0^2 - a_2^2(k^x)^2)\Phi_0 = 0 \quad (2.34)$$

The dispersion relation of waves is obtained from equations (2.33 and 2.34)

$$a_1^2 a_2^2 (k^x)^4 - (a_1^2 + a_2^2) \omega^2 (k^x)^2 + (\omega^4 - a_1^2 k_0^2 \omega^2) = 0 \quad (2.35)$$

with the relationship between Y_0 and Φ_0 ,

$$\Phi_0 = \frac{\rho \omega^2 - \kappa G^x (k^x)^2}{i \kappa G^x k^x} Y_0 = R_0 Y_0 \quad (2.36)$$

where

$$R_0 = \frac{\rho \omega^2 - \kappa G^x (k^x)^2}{i \kappa G^x k^x} \quad (2.37)$$

The equation (2.35) gives the four different wave numbers as function of wave frequencies,

$$k_1^x = \sqrt{\frac{(a_1^2 + a_2^2)\omega^2 + \sqrt{(a_1^2 + a_2^2)^2 \omega^4 - a_1^2 a_2^2 (\omega^4 - a_1^2 k_0^2 \omega^2)}}{2a_1^2 a_2^2}} \quad (2.38.a)$$

$$k_2^* = - \sqrt{\frac{(a_1^2 + a_2^2)\omega^2 + \sqrt{(a_1^2 + a_2^2)^2\omega^4 - a_1^2 a_2^2(\omega^4 - a_1^2 k_0^2 \omega^2)}}{2a_1^2 a_2^2}} \quad (2.38.b)$$

$$k_3^* = \sqrt{\frac{(a_1^2 + a_2^2)\omega^2 - \sqrt{(a_1^2 + a_2^2)^2\omega^4 - a_1^2 a_2^2(\omega^4 - a_1^2 k_0^2 \omega^2)}}{2a_1^2 a_2^2}} \quad (2.38.c)$$

$$k_4^* = - \sqrt{\frac{(a_1^2 + a_2^2)\omega^2 - \sqrt{(a_1^2 + a_2^2)^2\omega^4 - a_1^2 a_2^2(\omega^4 - a_1^2 k_0^2 \omega^2)}}{2a_1^2 a_2^2}} \quad (2.38.d)$$

Therefore, the equations (2.31 and 2.32) are expanded using k_1^* , k_2^* , k_3^* and k_4^*

$$y(x,t) = (Y_1 e^{ik_1^* x} + Y_2 e^{ik_2^* x} + Y_3 e^{ik_3^* x} + Y_4 e^{ik_4^* x}) e^{-i\omega t} \quad (2.39)$$

$$\phi(x,t) = (\Phi_1 e^{ik_1^* x} + \Phi_2 e^{ik_2^* x} + \Phi_3 e^{ik_3^* x} + \Phi_4 e^{ik_4^* x}) e^{-i\omega t} \quad (2.40)$$

The equation (2.40) becomes the following equation

$$\Phi(x) = R_1 Y_1 e^{ik_1^* x} + R_2 Y_2 e^{ik_2^* x} + R_3 Y_3 e^{ik_3^* x} + R_4 Y_4 e^{ik_4^* x} \quad (2.41)$$

where

$$R_n = \frac{\rho \omega^2 - \kappa G^* (k_n^*)^2}{i\kappa G^* k_n^*} \quad (2.42)$$

for $n = 1, 2, 3, 4$.

For a finite viscoelastic beam with a length l , which is free at $x = l$ and excited at $x = 0$, four boundary conditions are defined as:

$$y(0) = y \quad (2.43)$$

$$\phi(0) = \phi \quad (2.44)$$

$$M(l) = E^* I \frac{\partial \phi(l)}{\partial x} = 0 \quad (2.45)$$

$$S(l) = \kappa G^* I \left(\frac{\partial y}{\partial x} - \phi \right) = 0 \quad (2.46)$$

From those boundary conditions, the constants Y_1 , Y_2 , Y_3 and Y_4 are determined as functions of y and ϕ . At the driving point, $x = 0$, input transverse force,

$F(0) = -S(0)$, can be calculated using equation (2.46), which can be expressed using impedances and velocity at the driving point as follows:

$$F(0) = Z_1 V(0) + Z_2 \Phi(0) \quad (2.47)$$

where the complex transverse velocity, V , and the complex angular velocity, Φ , are related to the corresponding displacement as follows:

$$\frac{V}{y} = \frac{\Phi}{\phi} = -i\omega \quad (2.48)$$

If there is no angular displacement, ϕ , at the center of the beam, that is, $\Phi(0) = 0$, the equation (2.47) becomes

$$F(0) = Z_1 V(0) \quad (2.49)$$

Therefore, the impedance of the Timoshenko beam at the driving point, Z_{fv} , can be calculated using the following equation.

$$Z_{fvt}(0) = \frac{F_{fvt}(0)}{-i\omega} \frac{1}{y} \quad (2.50)$$

where subscript *fvt* is an abbreviation of the Finite Viscoelastic beam using Timoshenko beam theory.

3. FINITE CONSTRAINED LAYER BEAM

In this section, impedances of the constrained layer beam, which has viscoelastic material between the two elastic layers, are studied. The theory of a damped sandwich beam was developed by R.A. Ditaranto [Ref. 5], who extended Kerwin's [Ref. 6] basically similar analysis. D.J. Mead and S. Markus [Ref. 7] expanded the concept by considering these earlier works. The result of their efforts is a sixth order differential equation of motion which is expressed in terms of the transverse displacement, y , and longitudinal displacement, u , for the constrained layer beam. The constrained layer beam will be excited harmonically at its center by a shear force, S , as shown in Figure 3 on page 12. This equation of motion leads to the impedances of the sandwich beams with six boundary conditions, which are used for evaluating impedances depending on frequency, viscoelastic material property, and two elastic material properties.

From the [Ref. 7], the governing sixth order differential equation is

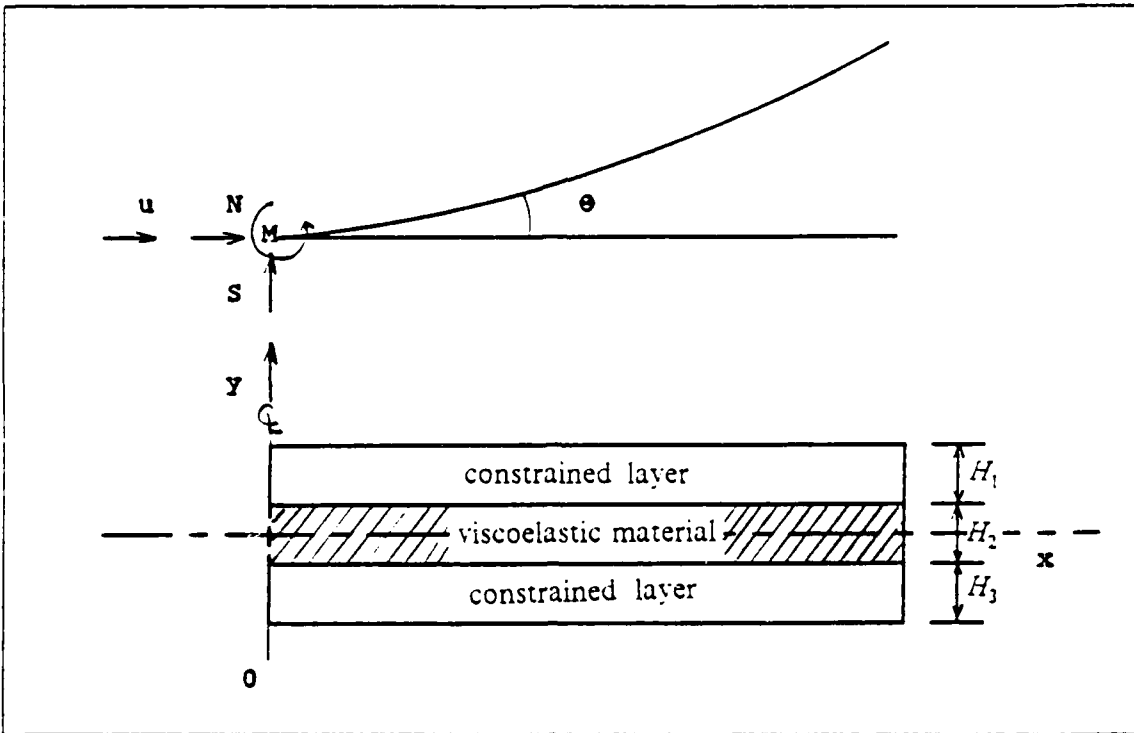


Figure 3. Coordinates and sign conventions for a semi-finite constrained layer beam.

$$\frac{\partial^6 v}{\partial x^6} - B_b(1+Z) \frac{\partial^4 v}{\partial x^4} = \frac{1}{D_d} \left(\frac{\partial^2 p}{\partial x^2} - D_d p \right) \quad (2.51)$$

where

$$p = -m \frac{\partial^2 v}{\partial t^2} \quad (2.52)$$

with the relationship between $v(x,t)$ and $u(x,t)$ expressed as:

$$\frac{\partial^2 u}{\partial x^2} - B_b u = \frac{B_b Z D_d}{E_3 I_3 C_c} \frac{\partial v}{\partial x} \quad (2.53)$$

The parameters in this equation are defined as follows:

$$B_b = \frac{G^x}{H_2} \left(\frac{1}{E_1 H_1} + \frac{1}{E_3 H_3} \right) \quad (2.54.a)$$

$$Z = \frac{C^2}{D_d} + \frac{E_1 H_1 E_3 H_3}{E_1 H_1 + E_3 H_3} \quad (2.54.b)$$

$$D_d = E_1 I_1 + E_3 I_3 \quad (2.54.c)$$

$$C_s = H_2 + \frac{1}{2} (H_1 + H_3) \quad (2.54.d)$$

$$I_1 = \frac{H_1^3}{12} \quad (2.54.e)$$

$$I_3 = \frac{H_3^3}{12} \quad (2.54.f)$$

$$G^* = G(1 + i\eta_c) \quad (2.55)$$

where subscript *c* is an abbreviation of constrained layer beam, and

G : shear modulus of the viscoelastic layer

E : elastic modulus of the elastic layer

η_c : loss factor of the viscoelastic layer

I : moment of the inertia of the cross sectional area

H : thickness of the constrained layer beam

m : mass per unit length of the whole three layer section.

The general form of transverse displacement, $y(x,t)$, and longitudinal displacement, $u(x,t)$, for the propagating harmonic waves in a constrained layer beam are

$$y(x,t) = Y_0 e^{i(k' x - \omega t)} \quad (2.56)$$

$$u(x,t) = U_0 e^{i(k' x - \omega t)} \quad (2.57)$$

where k' is a complex wave number and ω is the frequency of the propagating wave.

After inserting the wave equations (2.56 and 2.57) into the sixth order beam equation (2.51), the dispersion relation is obtained as follows:

$$(k'^*)^6 + B_t(1+Z)(k'^*)^4 - \frac{m\omega^2}{D_d}(k'^*)^2 - \frac{B_3 m \omega^2}{D_d} = 0 \quad (2.58)$$

There are six different roots with six different complex wave numbers in the above equation, which means a wave of six different modes propagate through the constrained layer beam. From the equations (2.56 and 2.57), we may rearrange equation (2.53)

$$U_0 = R_0 Y_0 \quad (2.59)$$

where

$$R_0 = \frac{iB_b Z D_d k_x^*}{E_3 H_3 C_c ((k_x^*)^2 + B_b)} \quad (2.60)$$

The general form of the transverse displacement equation (2.56), y , and longitudinal displacement equation (2.57), u , are obtained using the six complex wave numbers and a ratio R_0 . The equations (2.56, 2.57 and 2.59) as follow:

$$y(x,t) = (Y_1 e^{ik_1^* x} + Y_2 e^{ik_2^* x} + Y_3 e^{ik_3^* x} + Y_4 e^{ik_4^* x} + Y_5 e^{ik_5^* x} + Y_6 e^{ik_6^* x}) e^{-i\omega t} \quad (2.61)$$

$$\begin{aligned} u(x,t) = & (R_1 Y_1 e^{ik_1^* x} + R_2 Y_2 e^{ik_2^* x} + R_3 Y_3 e^{ik_3^* x} + R_4 Y_4 e^{ik_4^* x} \\ & + R_5 Y_5 e^{ik_5^* x} + R_6 Y_6 e^{ik_6^* x}) e^{-i\omega t} \end{aligned} \quad (2.62)$$

where

$$R_n = \frac{iB_b Z D_d k_n^*}{((k_n^*)^2 + B_b) E_3 H_3 C_c} \quad (2.63)$$

$n = 1, 2, 3, 4, 5, 6$ For a constrained layer beam with a finite length l which is free at $x = l$ and excited at one end at $x = 0$, the six boundary conditions are defined as follows [Ref. 7]:

$$y(0) = y \quad (2.64)$$

$$\frac{dy(0)}{dx} = \theta \quad (2.65)$$

$$u(l) = u \quad (2.66)$$

$$S(l) = D_d \frac{\partial^3 y}{\partial x^3} - D_d B_b Z \frac{\partial y}{\partial x} + \frac{D_d B_b Z}{C_c} \left(\frac{E_1 H_1 + E_3 H_3}{E_1 H_1} \right) u = 0 \quad (2.67)$$

$$M(l) = D_3 \frac{\partial^2 y}{\partial x^2} - C E_3 I_3 \frac{\partial u}{\partial x} = 0 \quad (2.68)$$

$$N(l) = E_3 I_3 \frac{\partial u}{\partial x} = 0 \quad (2.69)$$

The six constants Y_i ($i=1, 2, 3, 4, 5$ and 6) are determined from these six boundary conditions and are a function of y , θ and u . At the driving point, $x=0$, the input transverse force, $F(0) = -S(0)$, moment, $M(0)$, and normal force, $N(0)$, can be calculated using equations (2.67, 2.68 and 2.69). These input force and moment can be expressed using impedances and velocities and angular velocity at the driving point as follows:

$$F(0) = Z_1 V(0) + Z_2 \Omega(0) + Z_3 U(0) \quad (2.70)$$

Where the complex transverse velocity, V , and the complex angular velocity, Ω , and the complex longitudinal velocity, U , are related to the corresponding displacement as follows:

$$\frac{V}{y} = \frac{\Omega}{\theta} = \frac{U}{u} = -i\omega \quad (2.71)$$

If there is no rotational displacement, θ , and no longitudinal displacement, u , at the center of the beam, Z_1 represents the impedances of the transverse force at the driving point of the constrained layer beam. That is, $\Omega(0) = 0$ and $U(0) = 0$. Therefore, the equation (2.70) becomes

$$F(0) = Z_1 V(0) \quad (2.72)$$

Therefore, the impedances of the constrained layer beam at the driving point, Z_c , can be calculated using the following equation.

$$Z_c(0) = \frac{F_c(0)}{-i\omega} \frac{1}{y} \quad (2.73)$$

Where subscript c is an abbreviation of the constrained layer beam.

C. COMPUTER IMPLEMENTATION

The computer programs using Reduce and FORTRAN languages are used for calculation of the theoretical impedances from the beam theories in this paper. Reduce was developed by Anthony C. Hearn [Ref. 8], and is a programming language which solves

algebraic operations non-numerically. It can manipulate polynomials in a variety of forms (substitution, differentiation and integration) and solves one or more simultaneous algebraic equations. After the impedances were evaluated by a Reduce program with constant variables, a FORTRAN program calculated the impedance with real dimensions and properties of the viscoelastic and constrained layer beam waveguide absorber for the 0-2000Hz frequency range. All constant variables of the Reduce program were defined in each FORTRAN program. We tried to use the same notations for the Reduce program, the FORTRAN program and the text (Appendix A).

Three Reduce programs and a FORTRAN program were used to study each theory. The first Reduce program defined the moment, force and displacements which included the constants Y_n , where n equals 1 and 3 for an infinite viscoelastic beam; n equals 1, 2, 3 and 4 for a finite viscoelastic beam and n equals 1, 2, 3, 4, 5, and 6 for a constrained layer beam. Y_n can be solved with boundary conditions. After running the first Reduce program, new constant terms are defined for Y_n . The second Reduce program includes those new constant variables which were the results of the first Reduce program. The second Reduce program gives the constant variables Y_n . Finally, the third Reduce program can evaluate the impedance of the beam with longitudinal and angular displacement (and normal displacement for the constrained layer beam). The process of the constrained layer beam is similar up to the second Reduce program. However, the computer finds it hard to handle 6 simultaneous equations with 6 non-numerical variables, Y_n . Therefore, we solved Y_1 , Y_5 and Y_6 in the second Reduce program and then substitute these values to Y_1 , Y_2 and Y_3 in the third Reduce program.

Wave numbers as functions of frequencies, *i.e.* dispersion relation, of waves in waveguide absorbers were described in previous sections. It was easy to find the wave number of a viscoelastic beam through Bernoulli-Euler beam theory and Timoshenko beam theory in equations (2.12 and 2.38). However, wave numbers of the constrained layer beam were expressed with a complex six order polynomial. Therefore, they were calculated using Newton's method. The equation (2.58) is rearranged using *real* constants b_r , c_r and d_r and *imaginary* constants b_i and d_i .

$$(K^x)^3 + (b_r + i b_i)(K^x)^2 + c_r(K^x) + (d_r + i d_i) = 0 \quad (2.74)$$

where

$$K^x = (k^x)^2 \quad (2.75.a)$$

$$b_r = Re(B_b + B_b Z) \quad (2.75.b)$$

$$b_i = Im(B_b + B_b Z) \quad (2.75.c)$$

$$c_r = \frac{-m\omega^2}{D_d} \quad (2.75.d)$$

$$d_r = Re\left(\frac{-B_b m\omega^2}{D_d}\right) \quad (2.75.e)$$

$$d_i = Im\left(\frac{-B_b m\omega^2}{D_d}\right) \quad (2.75.f)$$

Let the complex variable $K^* = t + iq$ (t and q are *real* numbers). The equation (2.74) becomes two equations coupled with two variables (t and q).

$$f(t,q) = t^3 + b_r t^2 + (-3q^2 - 2b_i q + c_r)t + (-b_r q^2 + d_r) \quad (2.76)$$

$$g(t,q) = q^3 + b_i q^2 + (-3t^2 - 2b_r t - c_i)q + (-b_i t^2 - d_i) \quad (2.77)$$

Starting from initial guesses (t_0, q_0) which are near the roots iteration was continued until either the successive t and q values converged to the certain values or the value of the function is sufficiently near zero. After a few iterations of equations (2.76 and 2.77) using a FORTRAN program (Appendix A), we can get three different square of wave number values, K^* , were obtained. So, finally, this method calculates six different wave numbers, k_n , from $\pm \sqrt{K^*}$, where n equals 1, 2, 3, 4, 5, and 6.

Impedances of a 20" viscoelastic beam were calculated using these computer programs for viscoelastic beam properties of 200,000 psi constant shear modulus and 0.2 energy loss factor. The results of these simulations are shown in Figure 4 on page 19 and Figure 5 on page 20 which reflect sharp resonance frequencies. These sharp resonance phenomena reduced for the same beam with higher energy loss factor of 0.5. For cases using the Bernoulli-Euler beam theory, the impedances of the finite viscoelastic beam approached to the infinite viscoelastic beam waveguide absorber with increasing energy loss factor and with increasing frequency. The impedance using Timoshenko beam theory differs from the impedance from the Bernoulli-Euler beam theory (Figure 6 on page 21 and Figure 7 on page 22), because Timoshenko beam theory considers shear deformation and rotary inertia effect of the viscoelastic beam.

Impedances of a 20" constrained layer beam with viscoelastic layer properties of 200 psi constant shear modulus and 0.5 and 1.0 energy loss factors were calculated. Figure 8 on page 23 and Figure 9 on page 24 compare the impedances vs. frequency depending on the energy loss factor of the constrained layer beam. The impedance of the high damping constrained layer beam shows the smooth and shifted resonance frequencies compared with the low damping constrained layer beam.

IMPEDANCES VS. FREQUENCY

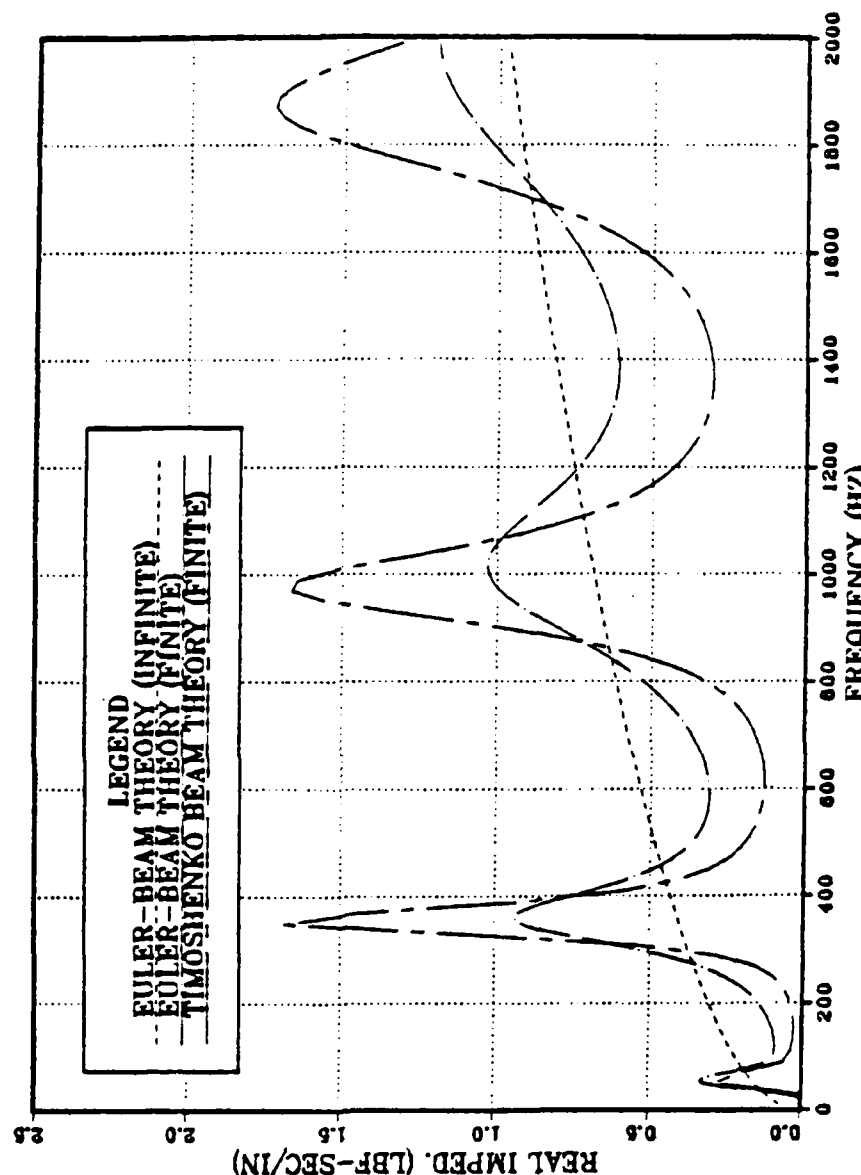


Figure 4. Real part of the 16" viscoelastic beam waveguide absorber theoretical impedances ($\eta = 0.2$).

IMPEDANCES VS. FREQUENCY

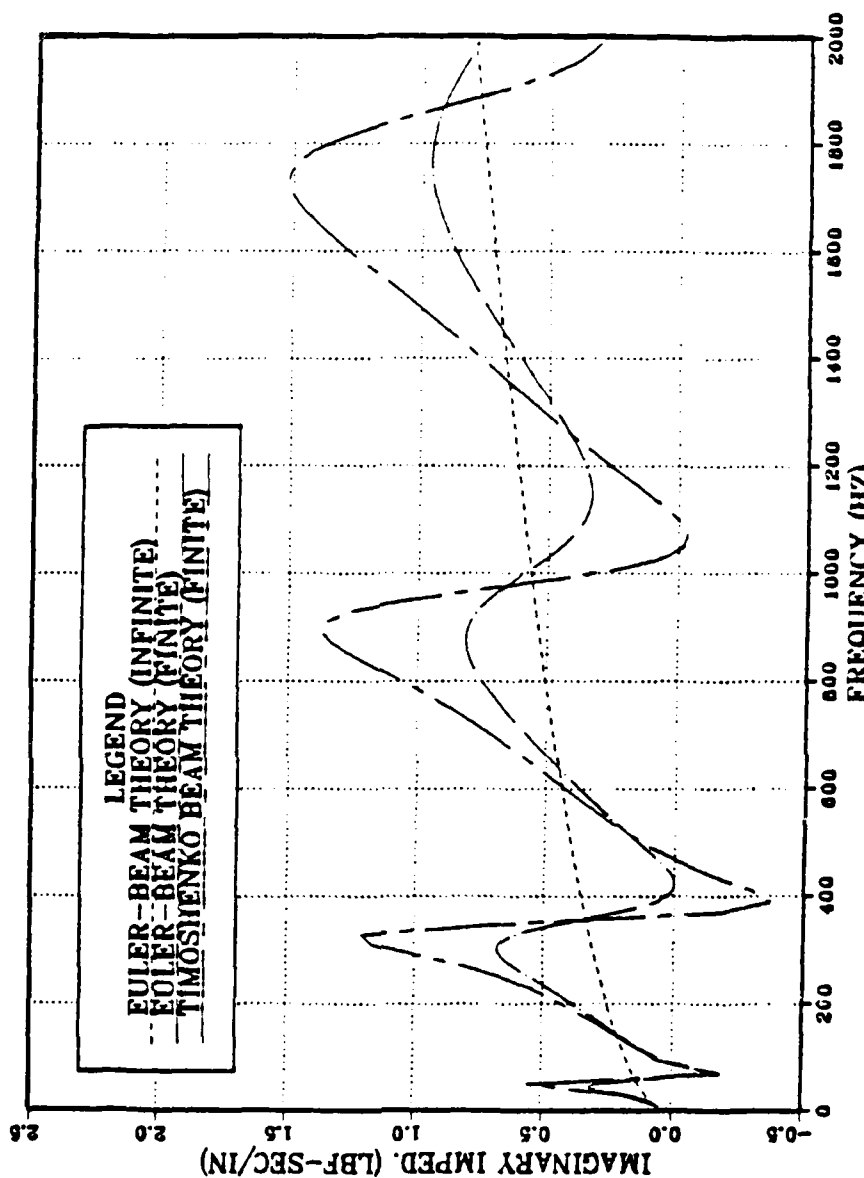


Figure 5. Imaginary part of the 16" viscoelastic beam waveguide absorber theoretical impedances ($\eta = 0.2$).

IMPEDANCES VS. FREQUENCY

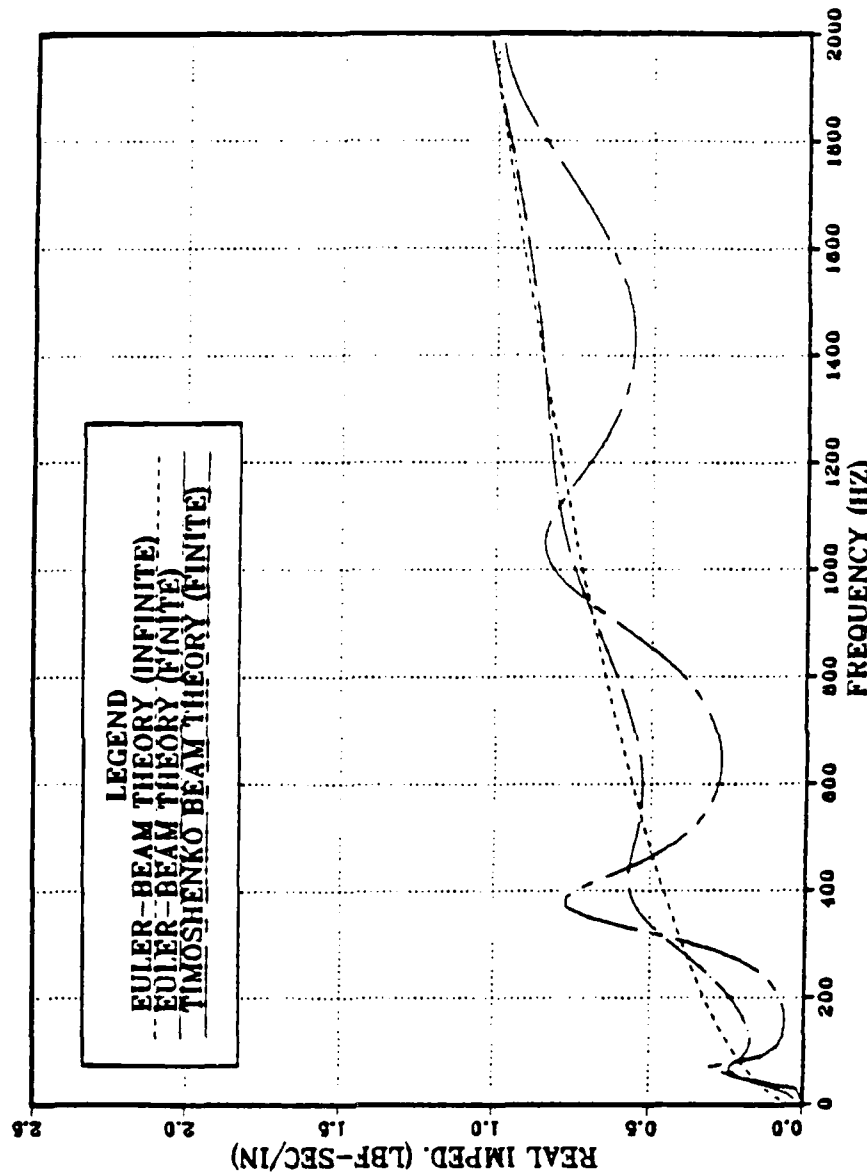


Figure 6. Real part of the 16" viscoelastic beam waveguide absorber theoretical impedances ($\eta = 0.5$) .

IMPEDANCES VS. FREQUENCY

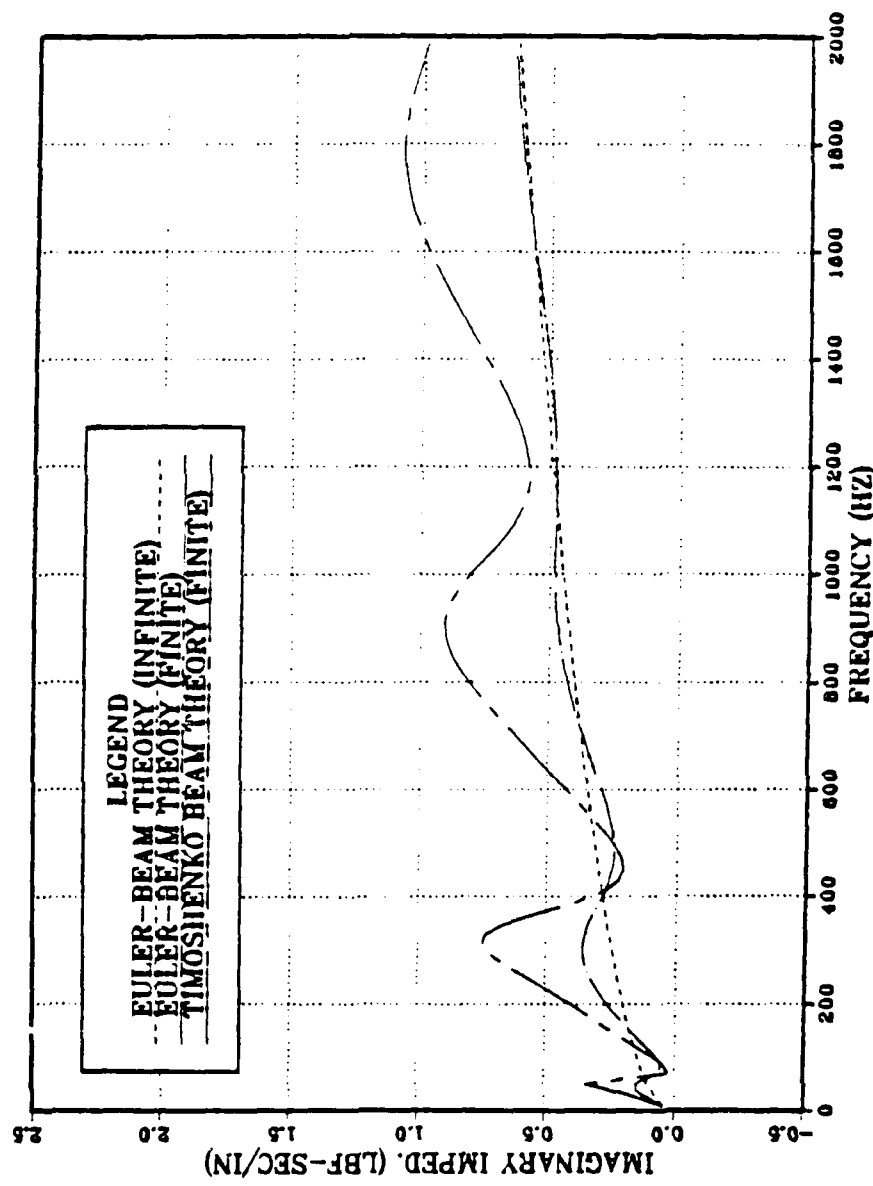


Figure 7. Imaginary part of the 16" viscoelastic beam waveguide absorber theoretical impedances ($\eta = 0.5$).

IMPEDANCES VS. FREQUENCY

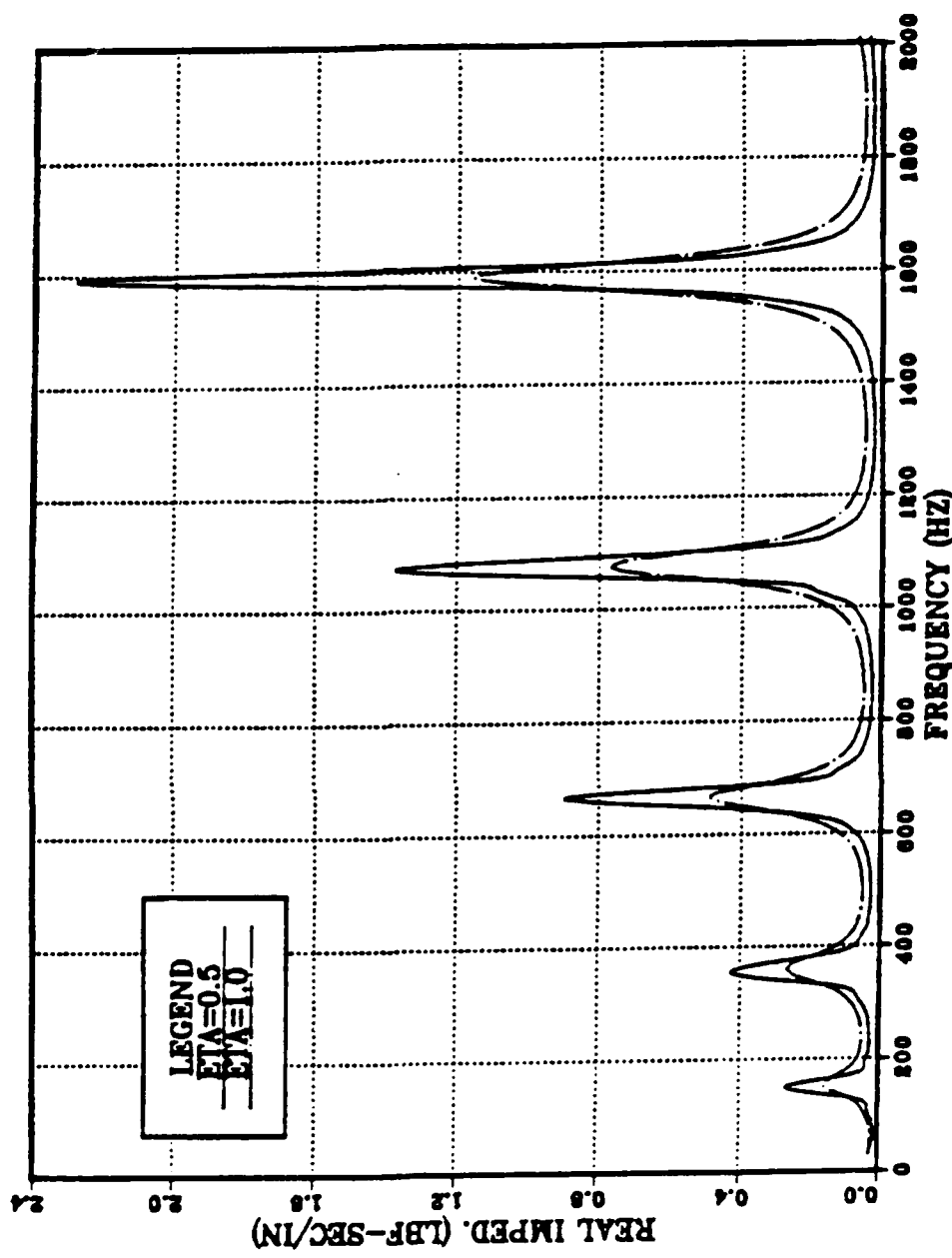


Figure 8. Real part of the 20" constrained layer beam waveguide theoretical impedances.

IMPEDANCES VS. FREQUENCY

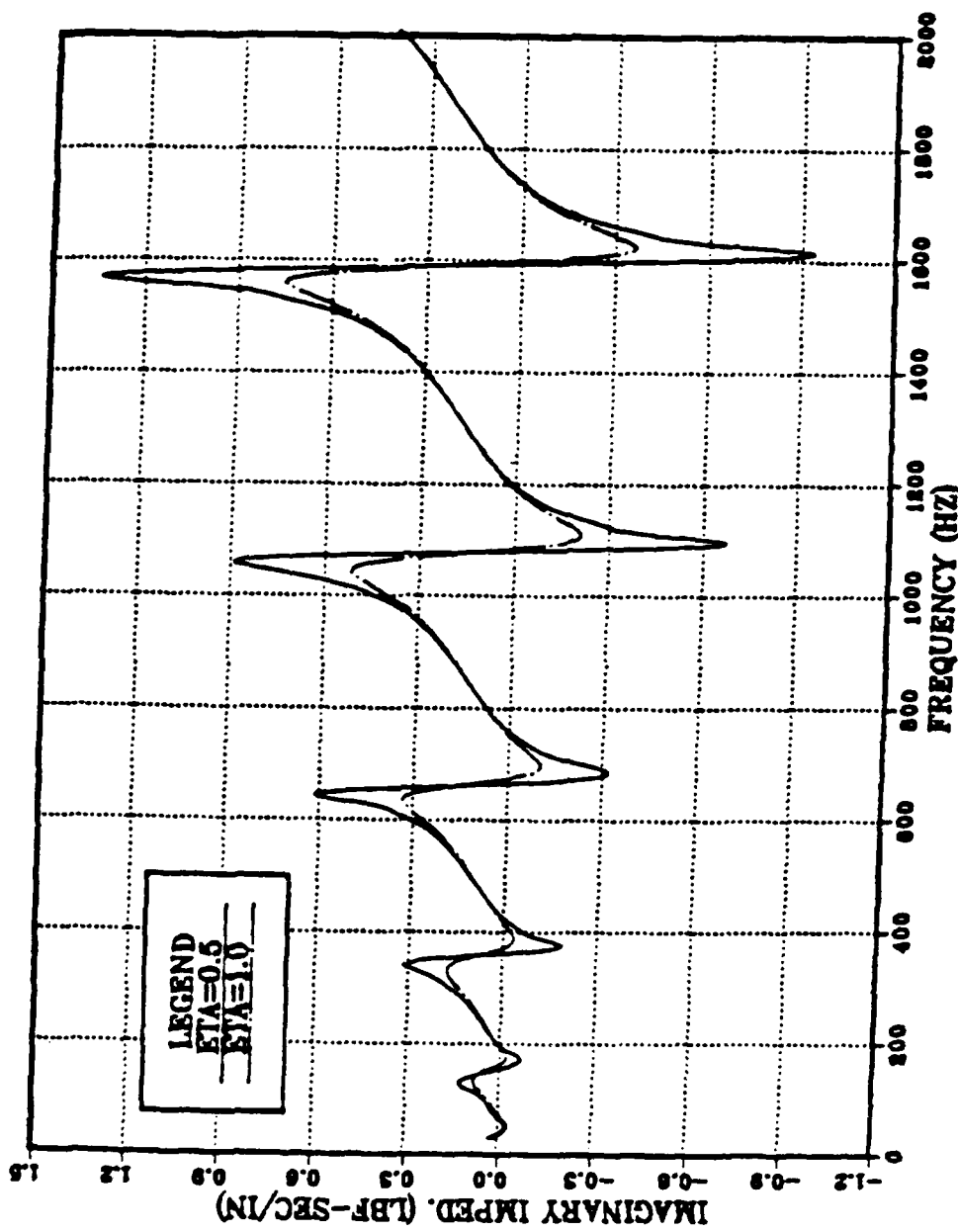


Figure 9. Imaginary part of the 20" constrained layer beam waveguide absorber theoretical impedances.

III. EXPERIMENT

A. IMPEDANCES OF THE TEST PLATE

A rectangular aluminum plate with clamped boundary condition was selected as the test structure, because it has enough closely space modes in the frequency range (100Hz-2Kz). An aluminum block (30" x 22" x 2") was carved inside to make a 24" x 16" x 0.3125" plate with clamp boundary condition.

The impedances of the test plate were measured from impact hammer tests. The aluminum plate was excited by a PCB 086B03 impact hammer. Input impact force was measured by a force transducer at the tip of the impact hammer. Responses were measured by an Endevco 2250A-10 piezoelectric accelerometer which was attached under the impact point for locations 1, 2 and 3 (Figure 10 on page 26 and Figure 11 on page 27). Location 1 is the center of the plate. Location 2 is the symmetric point of location 4, where a shaker will be attached during the damping measurement tests. Location 3 is a general point which is not on any line of symmetry. A baseband measurement for each location was taken from 0 to 2000Hz. An average of 15 data samples was taken for each measurement and analyzed using a HP-3562A dynamic signal analyzer. Impedance of the aluminum plate at each location was determined after a predetermined data processing procedure using the HP-3562A dynamic signal analyzer.

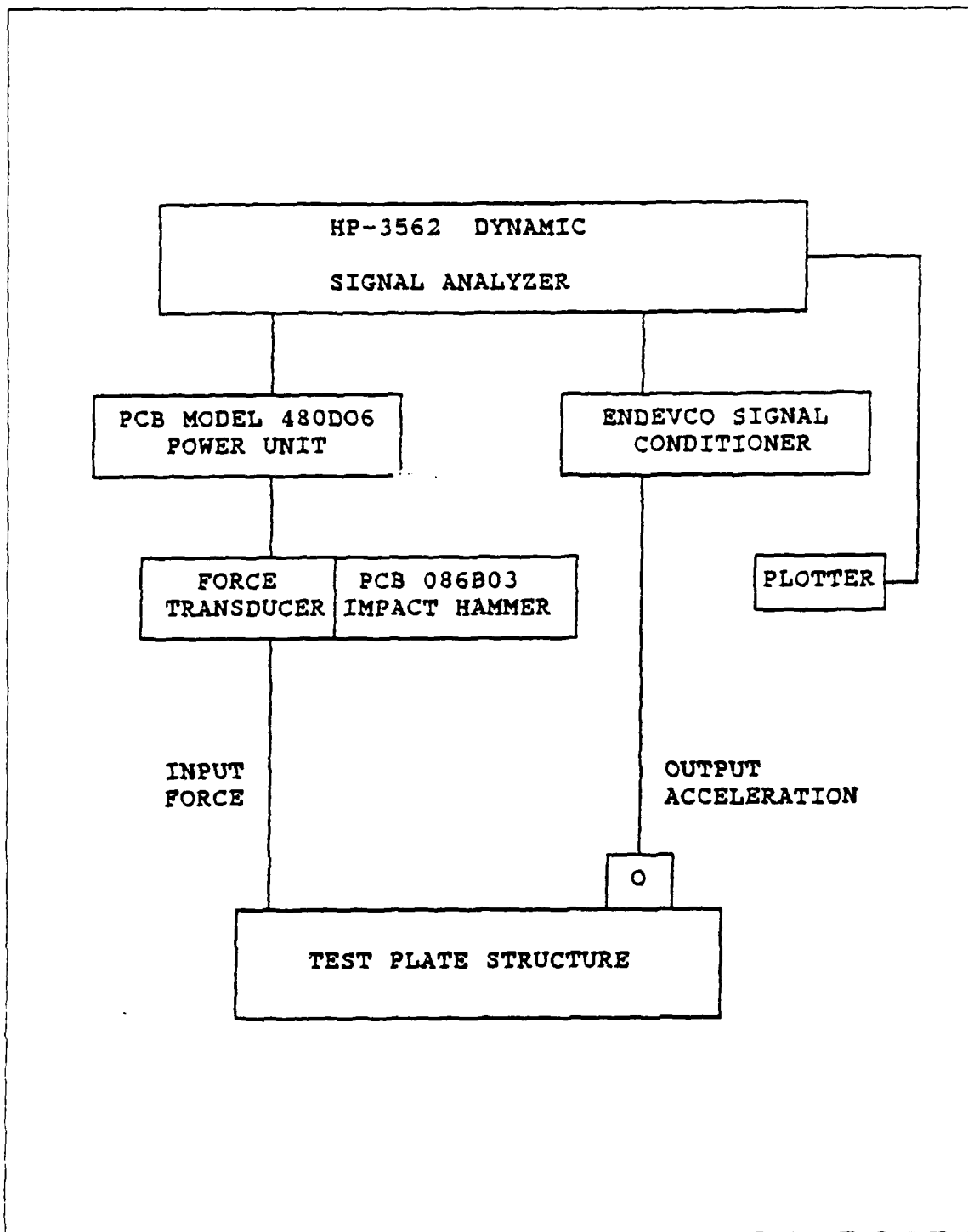


Figure 10. Arrangement for test plate impedance measurement.

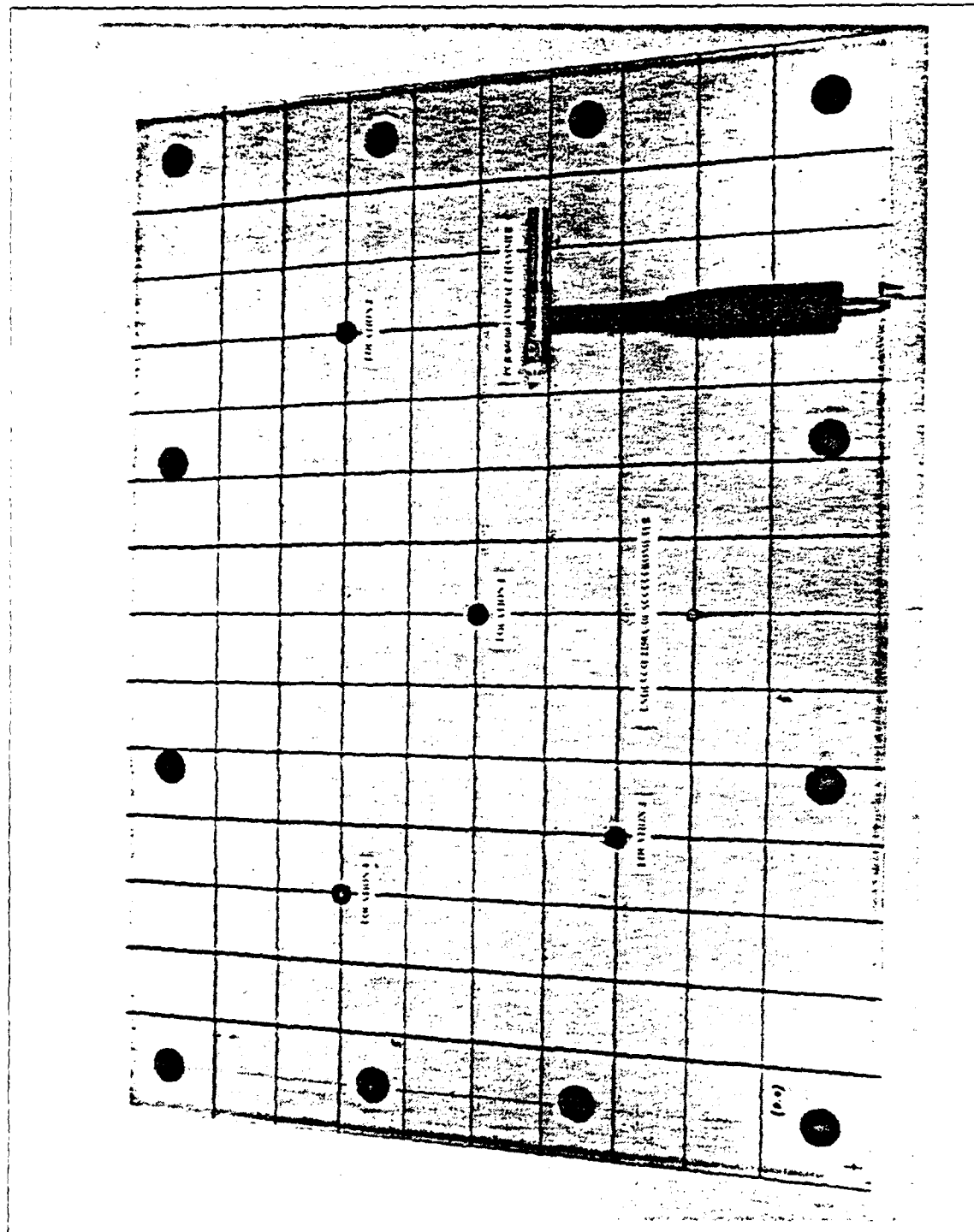


Figure 11. Test plate impedance measurement configuration.

B. IMPEDANCES OF THE WAVEGUIDE ABSORBER

Two viscoelastic beams and two constrained layer beams were selected as the waveguide absorber specimens. Dimensions and physical properties are shown in Table 1. Mechanical properties of a viscoelastic material depend on temperature and vibration frequencies. The loss factors and shear moduli of the viscoelastic material used in the specimens at room temperature (75°F) are shown in Figure 12 on page 30 and Figure 13 on page 31. These data were obtained from Design Data Sheets in a book by Nashif, et. al. [Ref. 9]. Analytic expressions of the loss factors and shear moduli were determined from curve fits to these data. The following four equations represent the loss factors and shear moduli of the LD-400 and ISD-112 viscoelastic material.

$$\eta_v = 0.65e^{[-0.52732(\log(\frac{f}{52}))^{1.95}]} \quad (3.1)$$

$$\eta_c = 1.1e^{[-0.3996(\log(\frac{f}{300}))^{1.93}]} \quad (3.2)$$

$$G_v = 0.00002503f^3 - 0.1752f^2 + 457.5883f + 29280 \quad (3.3)$$

$$G_c = -0.00001258f^2 + 0.2472f + 74.988 \quad (3.4)$$

f represents the frequency. η_v and η_c represent the loss factor of LD-400 and ISD-112 viscoelastic material. G_v and G_c represent the shear modulus of LD-400 and ISD-112 viscoelastic material. Figure 14 on page 32 shows waveguide absorbers which were used in this study.

Impedances of waveguide absorbers at the attachment points were determined from steady state random vibration tests. The waveguide absorber was excited by a Wilcoxon F4 F7 vibration generator using a band limited white noise signal (0-2000Hz) from a HP-3562A dynamic signal analyzer (Figure 15 on page 33). The waveguide absorber was mounted on the Wilcoxon F4 F7 vibration generator (Figure 16 on page 34). Force and acceleration were measured using a force transducer and a piezoelectric accelerometer in the impedance head of the Wilcoxon F4 F7 shaker. These signals were analyzed by a HP-3562A dynamic signal analyzer. 100 data samples were averaged for each measurement.

The measurement of impedances included the impedances of bolts and nuts and connecting aluminum pieces. Therefore, the impedances of bolts, nuts, and connecting aluminum pieces, the so-called mass effect, were measured separately. Total impedances

minus mass effect represented the impedances of the waveguide absorbers. These experimental results are compared with the theoretical predictions in Chapter IV.

Table 1. DIMENSIONS AND PROPERTIES OF THE WAVEGUIDE ABSORBER SPECIMENS.

| | | SPECI-MEN 1 | SPECI-MEN 2 | SPECI-MEN 3 | SPECI-MEN 4 |
|---|--------------------|---------------|---------------|--------------------|--------------------|
| WAVEGUIDE ABSOR-BER TYPE | | VISCO-ELASTIC | VISCO-ELASTIC | CON-STRAINED LAYER | CON-STRAINED LAYER |
| MATE-RIAL | VISCO-ELASTIC | LD-400 | LD-400 | ISD-112 | ISD-112 |
| | CON-STRAINED LAYER | | | Al | Al |
| LENGTH (in) | | 16.0 | 20.0 | 16.0 | 20.0 |
| WIDTH (in) | | 1.0 | 1.0 | 1.0 | 1.0 |
| THICK-NESS (in) | VISCO-ELASTIC | 0.35 | 0.35 | 0.065 | 0.065 |
| | CON-STRAINED LAYER | | | 0.0625 | 0.0625 |
| DEN-SITY ($\frac{\text{lb}}{\text{in}^3}$) | VISCO-ELASTIC | 0.05505 | 0.05505 | 0.03663 | 0.03663 |
| | CON-STRAINED LAYER | | | 0.09832 | 0.09832 |

LOSS FACTOR VS. FREQUENCY

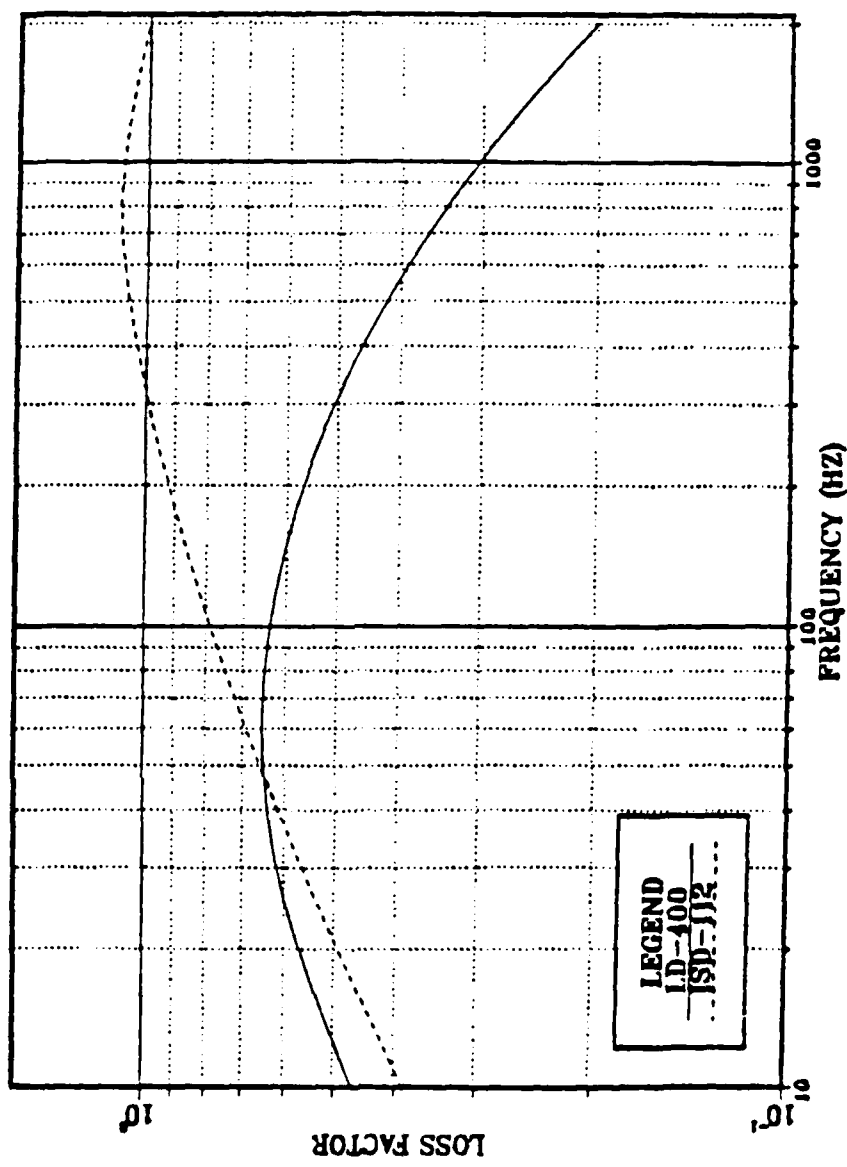


Figure 12. Loss factor vs. frequency for a LD-400 and a ISD-112.

SHEAR MODULUS VS. FREQUENCY

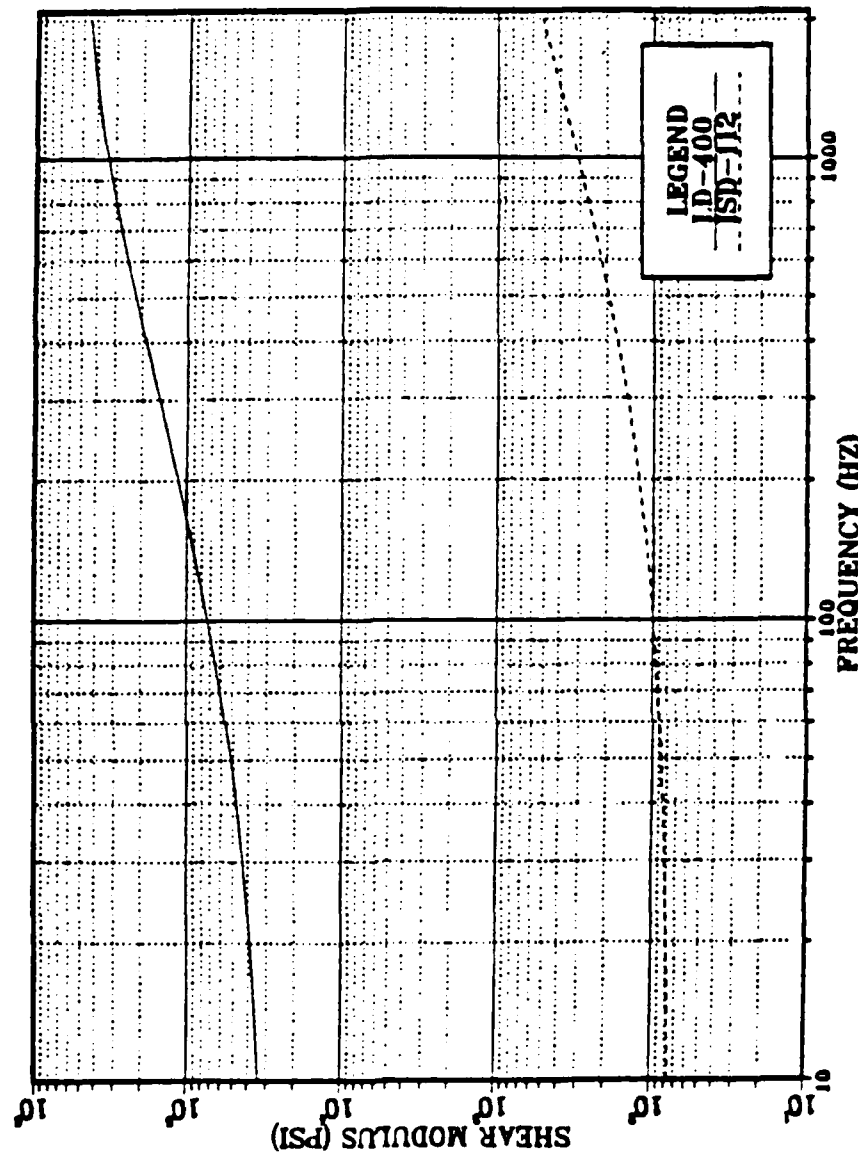


Figure 13. Shear modulus vs. frequency for a LD-400 and a ISD-112.

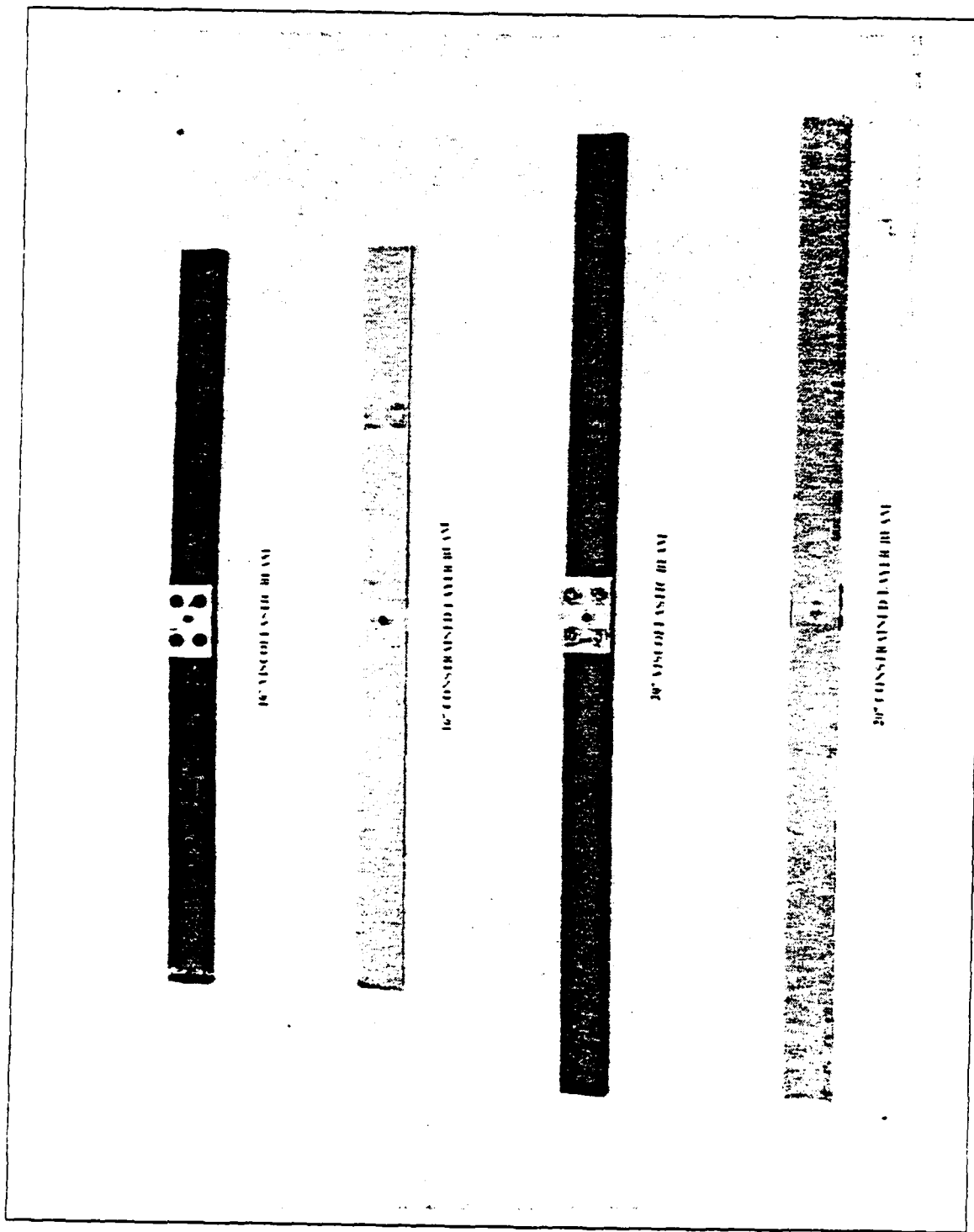


Figure 14. Waveguide absorbers.

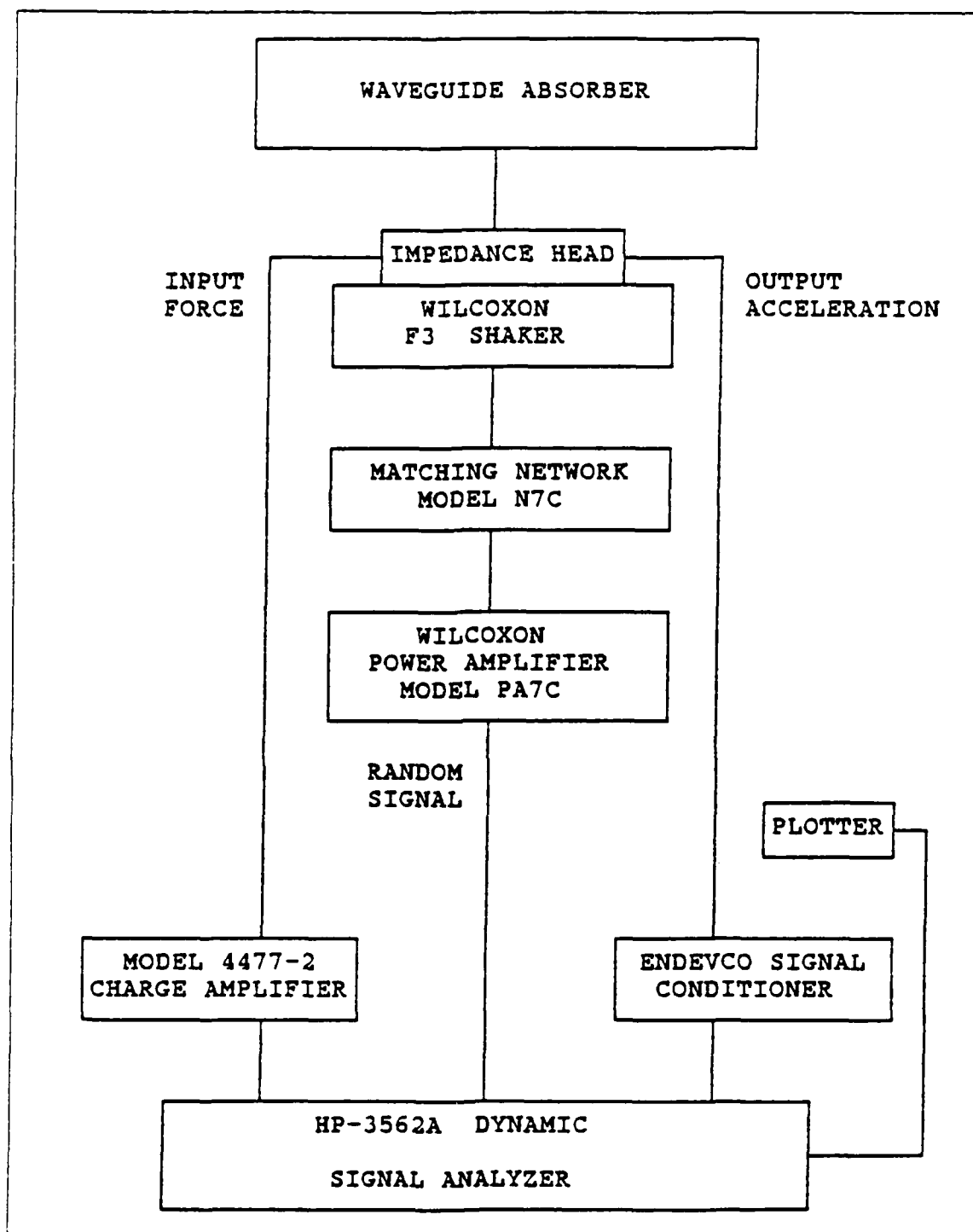


Figure 15. Arrangement for waveguide absorber impedance measurement.

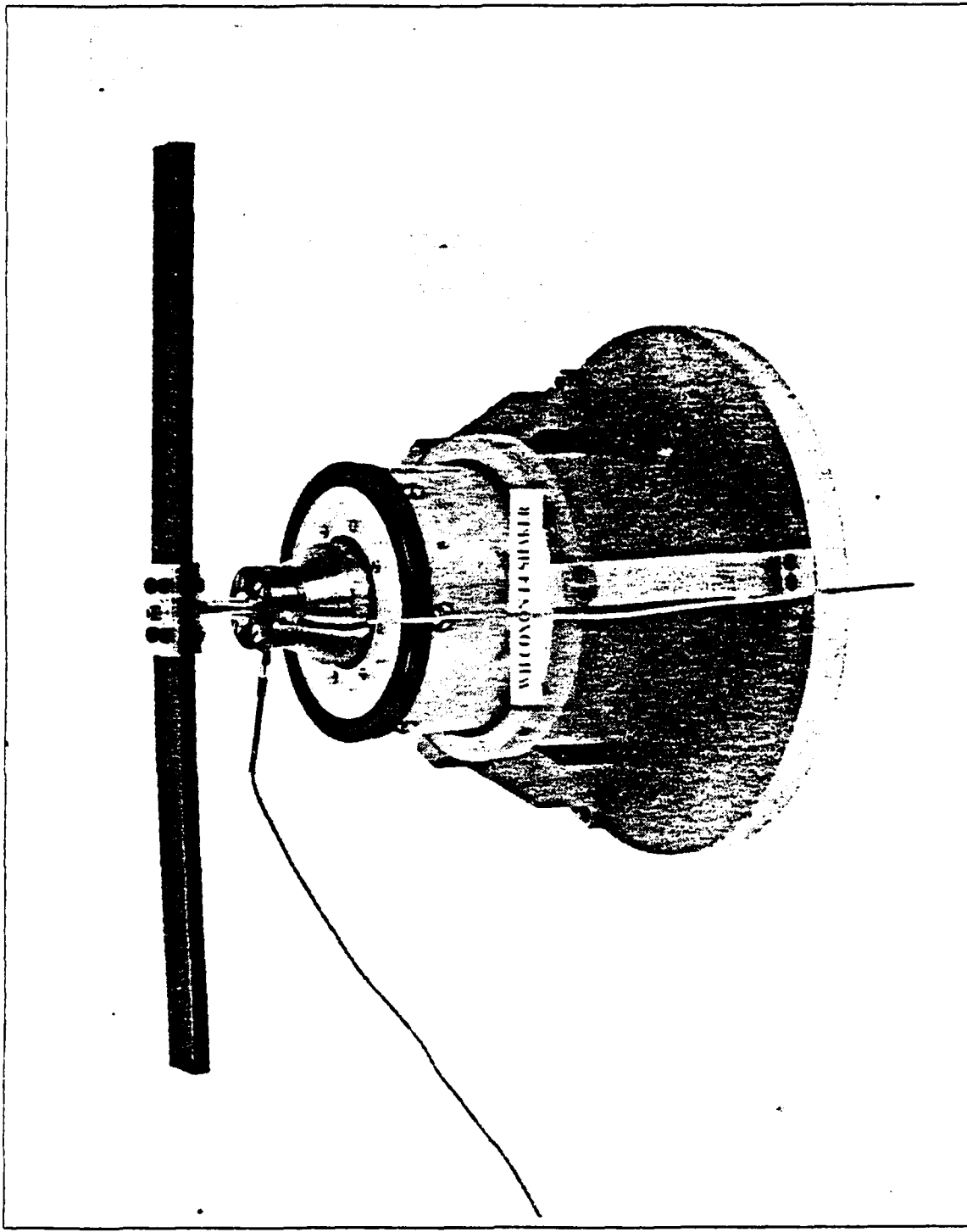


Figure 16. Wilcoxon F4/F7 shaker with waveguide absorber mounted.

C. DAMPING OF THE PLATE

Modal damping values of the plate were determined from structural transfer functions at a driving point and between input and output points on the test plate which were measured using random excitations. The HP-3562A dynamic signal analyzer was used in the measurement of the transfer functions. The Wilcoxon F3 vibration generator excited the plate at location 4 using random oscillation signals from a HP-3562A dynamic signal analyzer. Input forces and output responses at the driving point were measured using a force transducer and a piezoelectric accelerometer in the impedances head of Wilcoxon F3 shaker (Figure 17 on page 36). The damping measurement configuration is shown in Figure 18 on page 37. It was necessary to measure responses at several points other than the driving point to accurately measure damping values of closely spaced modes. These were measured using the Endevco 2250A-10 piezoelectric accelerometer. Modal damping values of all the modes in the frequency range of 100-2000Hz were determined from the response functions using the Half power Band Width method [Ref. 10] and a curvefit method [Ref. 11].

Modal damping values of the plate without a waveguide absorber were measured as the baseline. A waveguide absorber was attached to the plate at location 1. The waveguide absorber was changed after each measurement of the damping for four different waveguide absorbers which were described in section 4-B. After the damping was measured at location 1, measurements were taken at location 2 and location 3.

The most effective waveguide absorber at each location was selected. The 20" viscoelastic beam waveguide absorber, the 16" constrained layer beam waveguide absorber and the 16" viscoelastic beam waveguide absorber were most effective at location 1, 2 and 3, respectively. Therefore, the damping with two waveguide absorbers attached at locations 1 and 2, and the damping with three waveguide absorbers at locations 1, 2 and 3 were also measured, to see the effect of multiple waveguide absorbers.

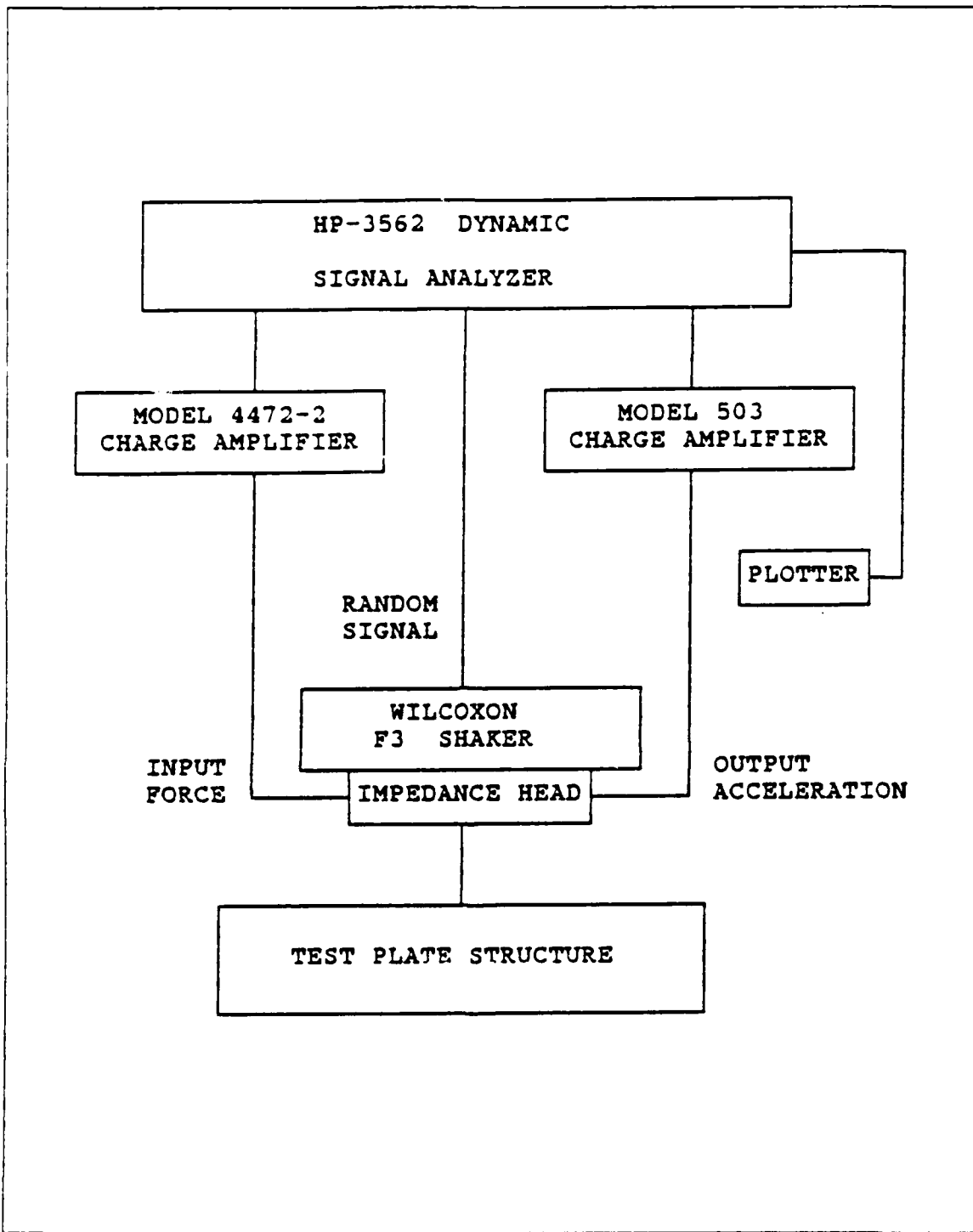


Figure 17. Arrangement for test plate damping measurement.

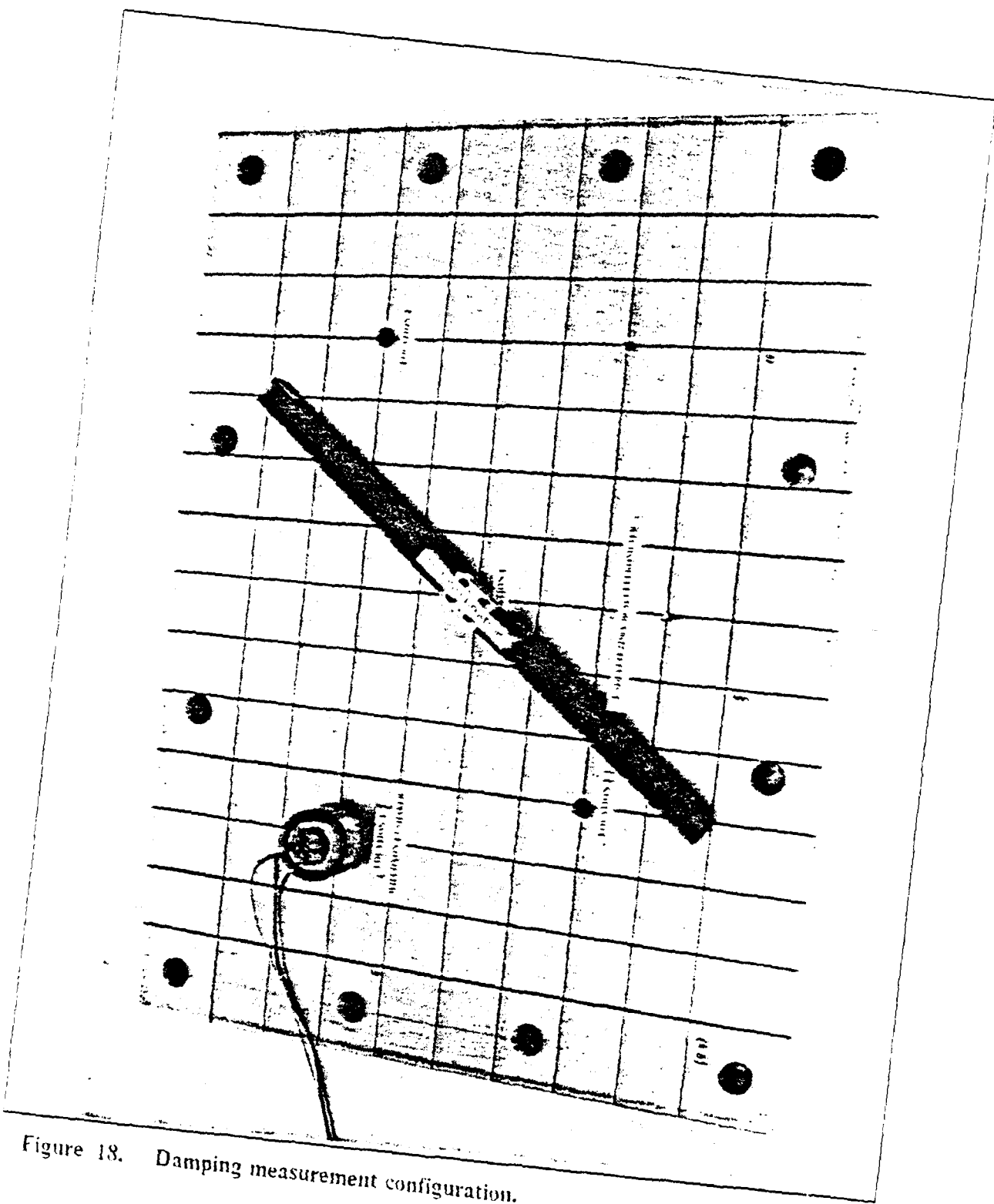


Figure 18. Damping measurement configuration.

IV. RESULTS AND DISCUSSIONS

A. IMPEDANCES OF THE TEST PLATE

Impedances of the test plate were measured from input hammer tests as described in Section 3.A. Since the aluminum test plate is a lightly damped structure, the impedances at resonance frequencies are very low and at anti-resonance frequencies are very high. Phases with 180° phase shift are near $\pm 90^\circ$ both at the resonance and at the anti-resonance frequencies.

Since location 1 is the center point of the plate, only small numbers of resonance and anti-resonance frequencies appear (Figure 19 on page 39 and Figure 20 on page 40). Neither location 2 nor location 3 are on any line of symmetry of the test plate; all the resonance and anti-resonance points appear in the impedance vs. frequency diagrams. (Figure 21 on page 41, Figure 22 on page 42, Figure 23 on page 43 and Figure 24 on page 44). However, the anti-resonance frequencies at location 2 and those at location 3 are different.

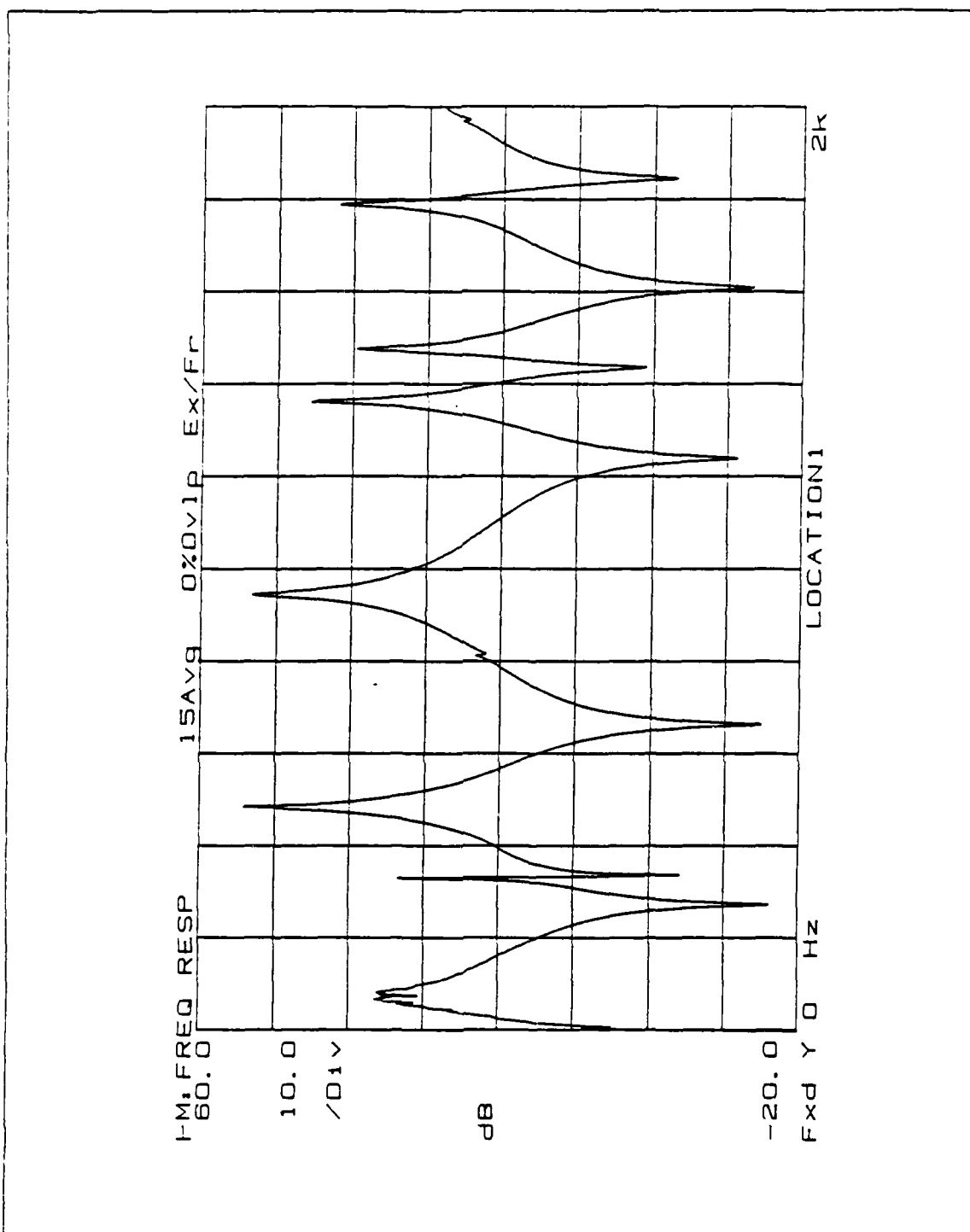


Figure 19. Impedance magnitude of test plate at location 1.

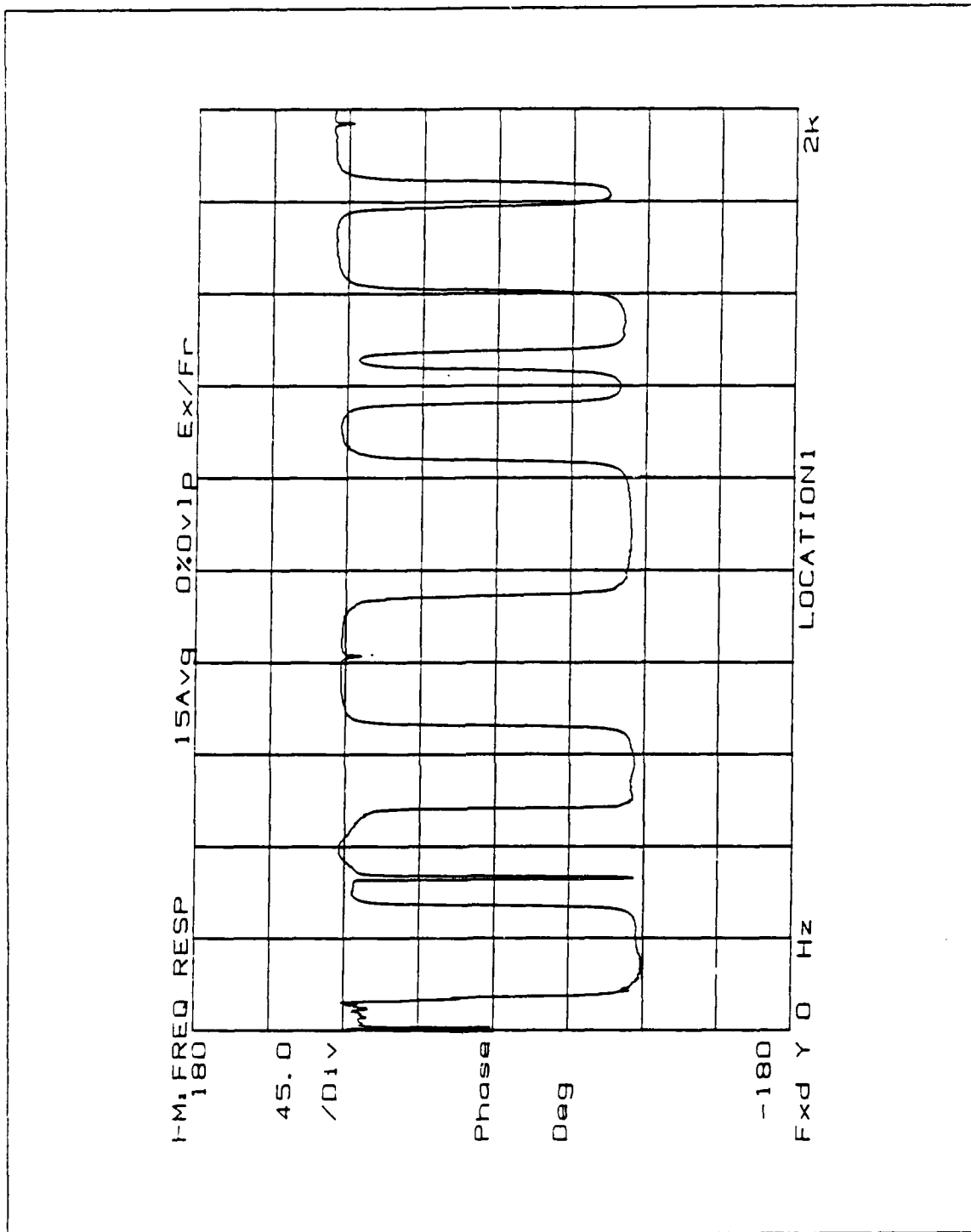


Figure 20. Impedance phase of test plate at location 1.

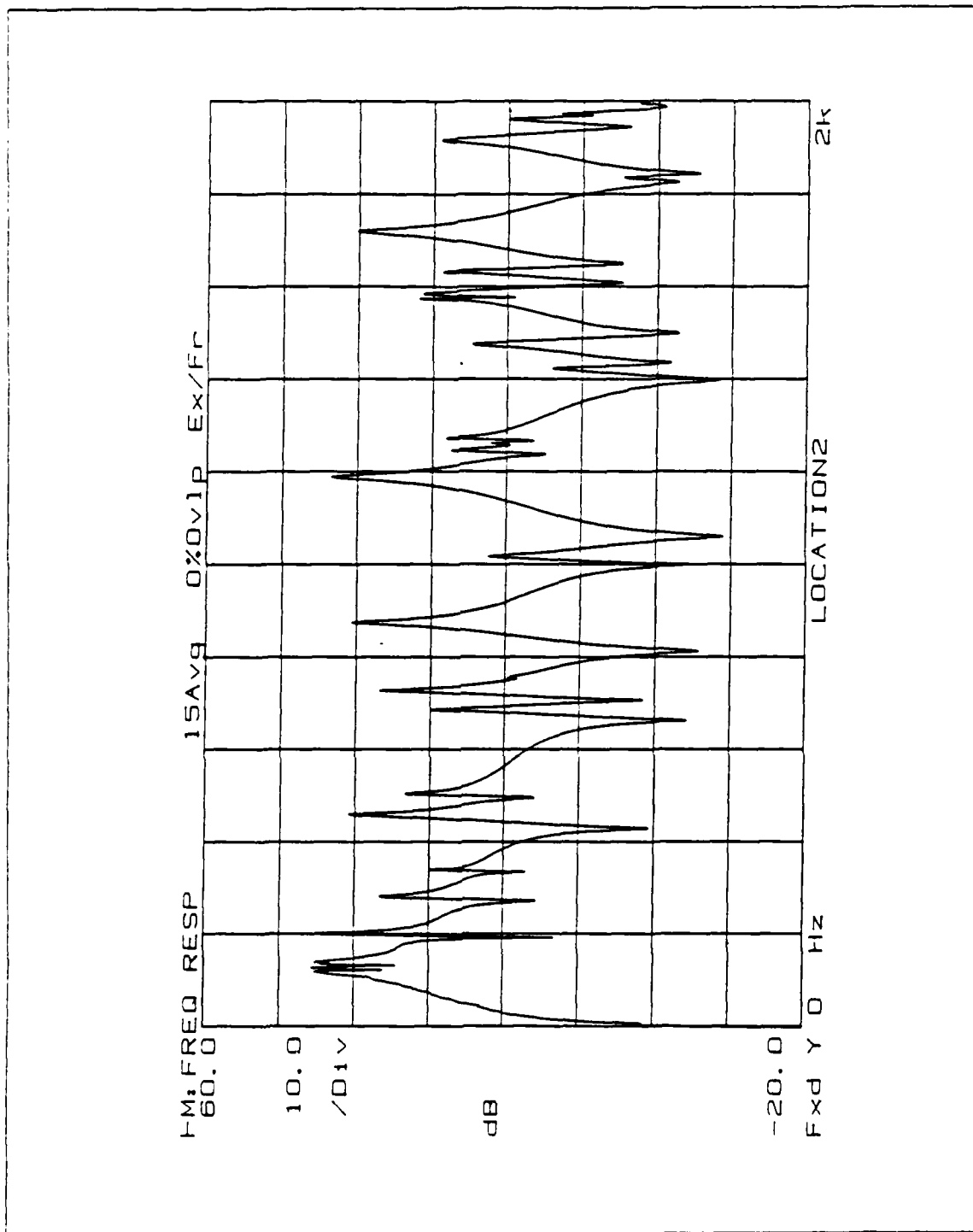


Figure 21. Impedance magnitude of test plate at location 2.

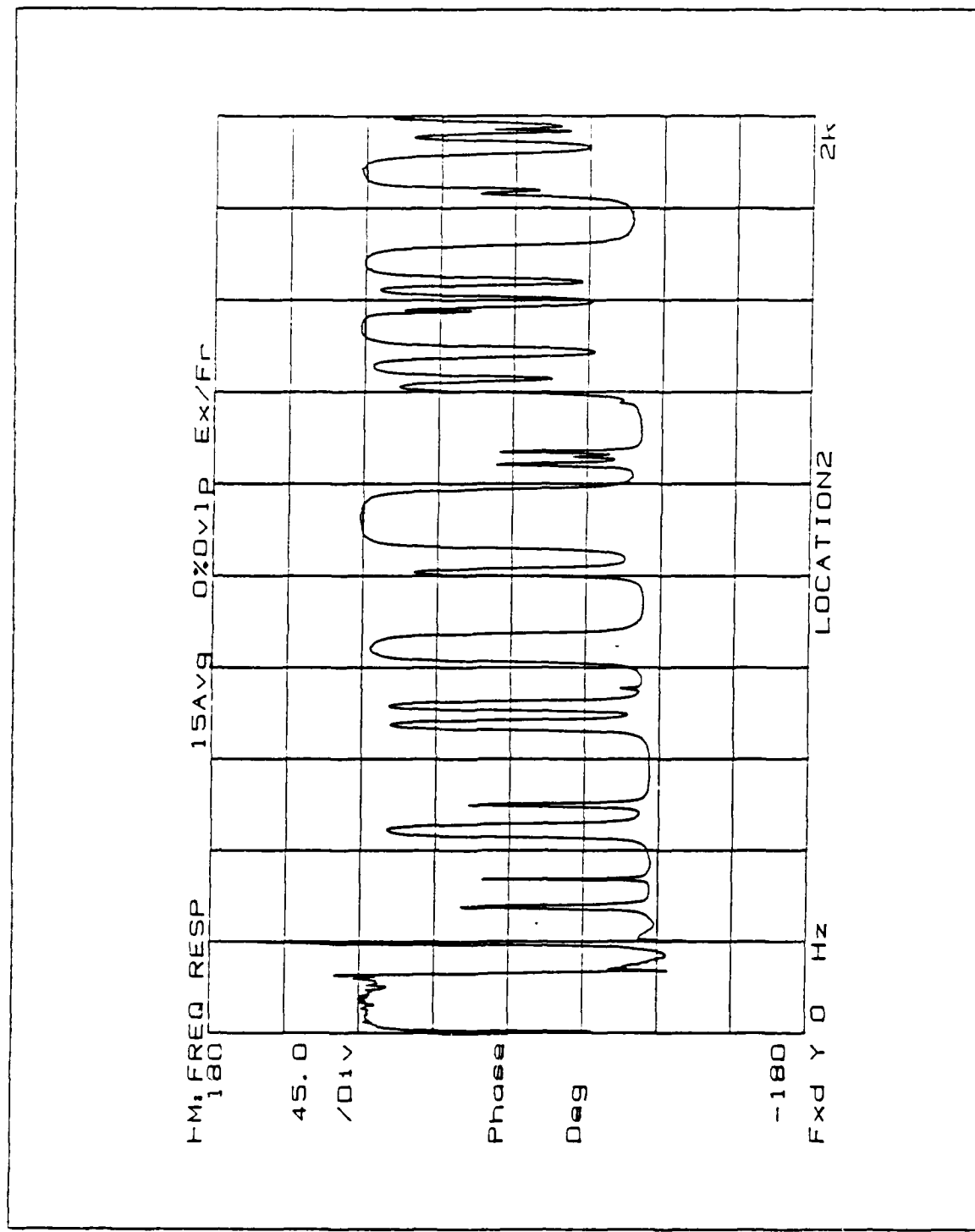


Figure 22. Impedance phase of test plate at location 2.

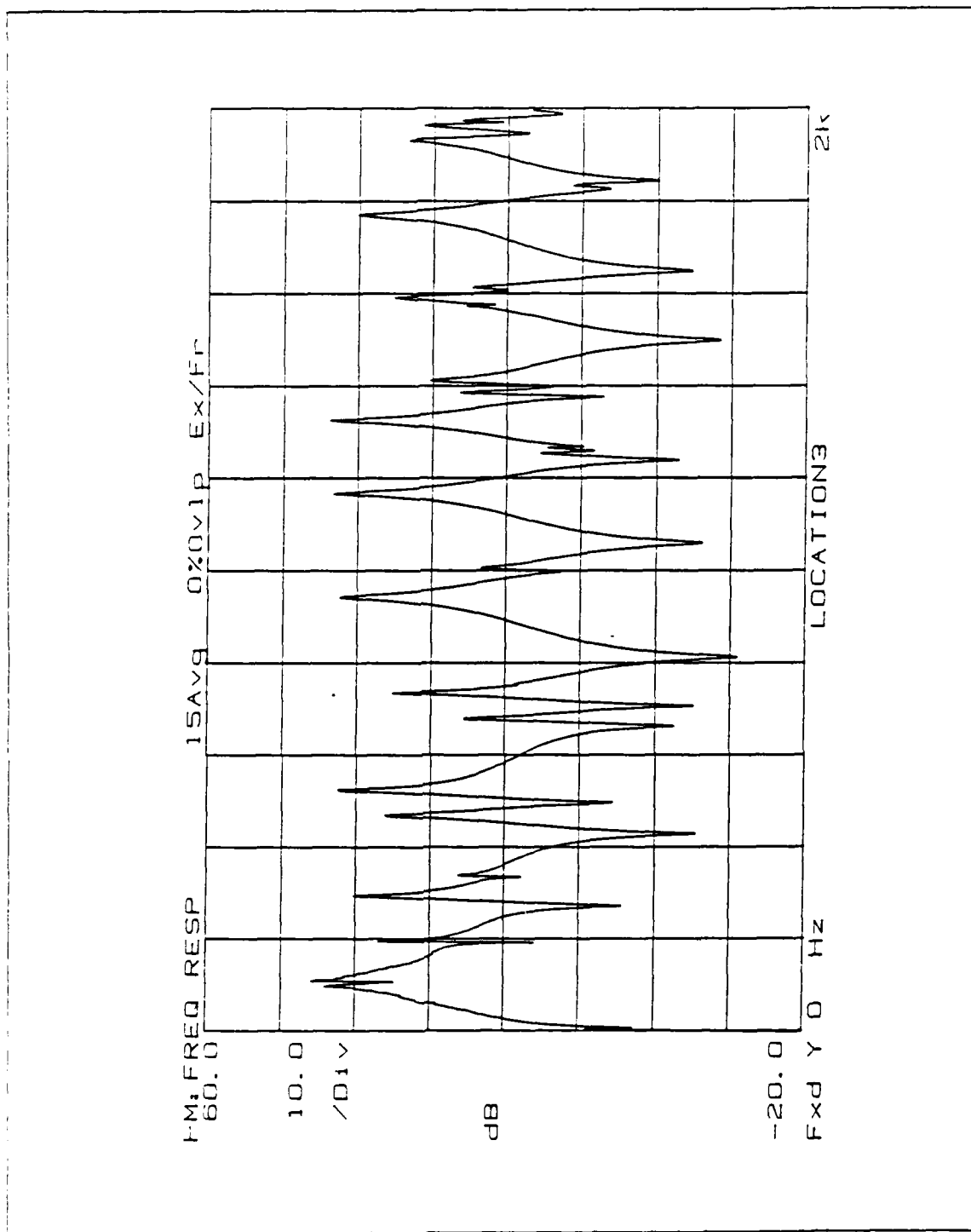


Figure 23. Impedance magnitude of test plate at location 3.

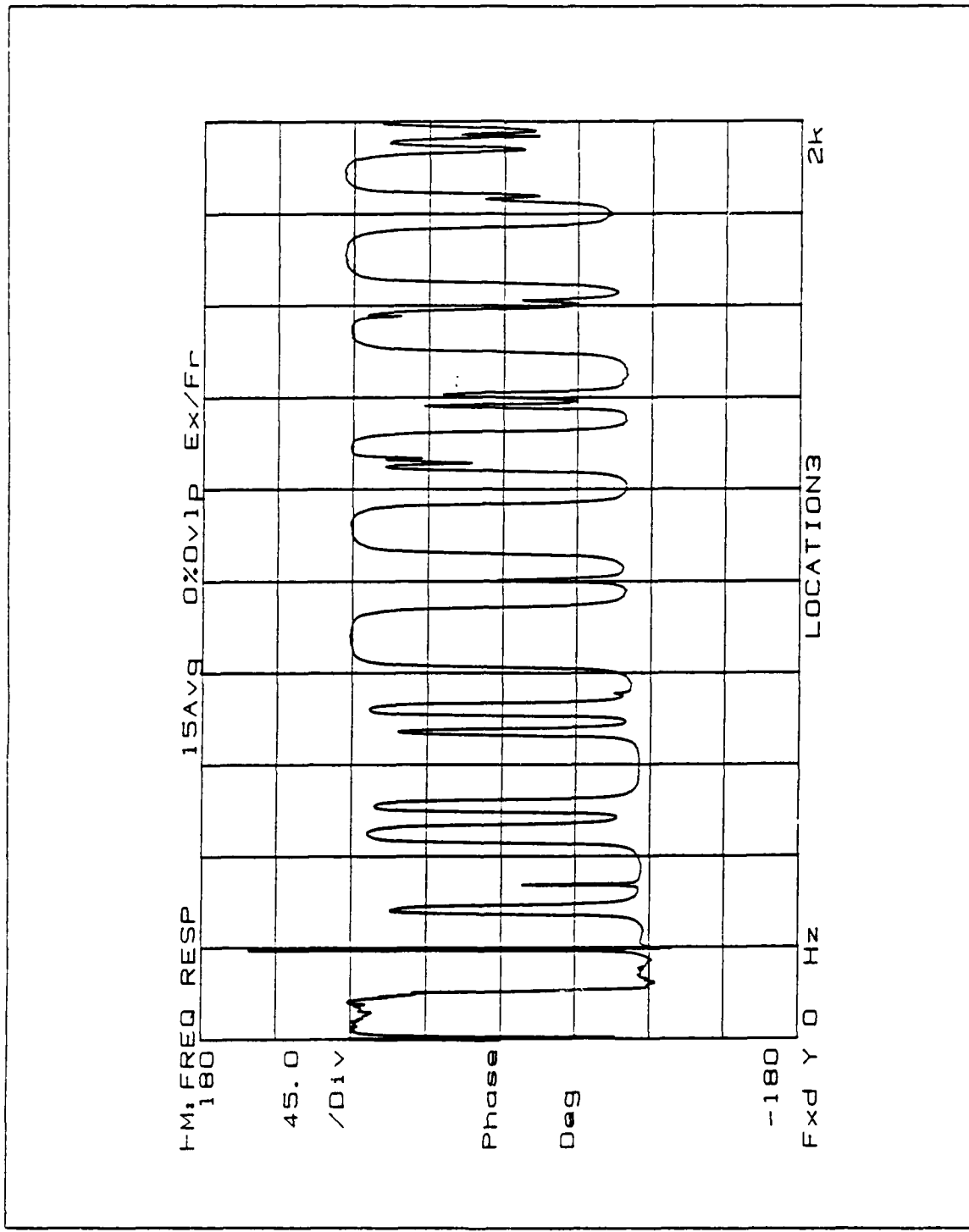


Figure 24. Impedance phase of test plate at location 3.

B. IMPEDANCES OF THE WAVEGUIDE ABSORBER

Two different kinds of waveguide absorbers, a viscoelastic beam and a constrained layer beam, are investigated in this study. In a previous study by Ungur and Williams [Ref. 3], impedances were predicted only for the infinite viscoelastic beam using Bernoulli-Euler beam theory and the theoretical prediction showed wide difference from the experimental results. In this study, this previous work is extended to include the impedances for the finite viscoelastic beam. Since Bernoulli-Euler beam theory does not include the shear deformation and rotary inertia effect of the viscoelastic beam, the predictions from the Timoshenko beam theory are studied to investigate these effects on wave propagation and impedances, and are compared with the results from the Bernoulli-Euler beam theory. The impedances of the constrained layer beam waveguide absorber were predicted using the sixth order beam theory.

The impedances from these theoretical predictions are compared with the impedances from the experimental measurements for the 16" and 20" length waveguide absorbers of two different kinds. In the calculation of theoretical predictions, the loss factors and shear moduli of viscoelastic material were varied as function of frequency as described in Section 3.B. During the experiment, the Wilcoxon F4 F7 vibration generator produced characteristic errors which occurred at different frequencies depending on the mass of the waveguide absorbers. Therefore the viscoelastic beam has unreliable data around 700Hz and the constrained layer beam has unreliable data around 350Hz.

Figure 25 on page 47 and Figure 26 on page 48 show the three theoretical impedances compared with experimental data. The Bernoulli-Euler beam theory for finite beams shows some standing wave effect at low frequency range due to reflection at the free end of the beam, but approaches the results of the infinite beam as frequency increases. The results of the Bernoulli-Euler beam theory do not quite correspond to experimental results for the viscoelastic beam. Impedances from the Timoshenko beam theory closely follow the experimental results for viscoelastic beams as shown in Figure 25 on page 47 and Figure 26 on page 48. These show that the shear deformation and rotary inertia effects are significant for the impedance prediction of beam type waveguide absorbers.

Figure 27 on page 49 and Figure 28 on page 50 represent the real and imaginary parts of the 16" constrained layer beam waveguide absorber and Figure 29 on page 51 and Figure 30 on page 52 represent the real and imaginary parts of the 20" constrained layer beam waveguide absorber. In both beams, the theoretical results of the impedances

using the sixth order beam theory and the resonance frequency patterns are almost the same as the experimental result.

Both Timoshenko beam theory and the sixth order beam theory predict resonance frequencies shifted amount from the experimental results as frequency increases, and the impedance magnitudes of experimental results are bigger than the theoretical results. These difference between theoretical and experimental impedances may derive from the inaccuracy of shear modulus and loss factors which values were selected from 75° F room temperature and changed depending on frequency. However, the theoretical prediction using Timoshenko beam theory for the viscoelastic beam and the sixth order beam theory for the constrained layer beam follow the same trend (Figure 12 on page 30 and Figure 13 on page 31).

Impedances of waveguide absorbers are very low and do not show any sharp variation for all frequencies in the range tested, which are quite different from the impedance of the test plate of very lightly damped structures.

IMPEDANCES VS. FREQUENCY

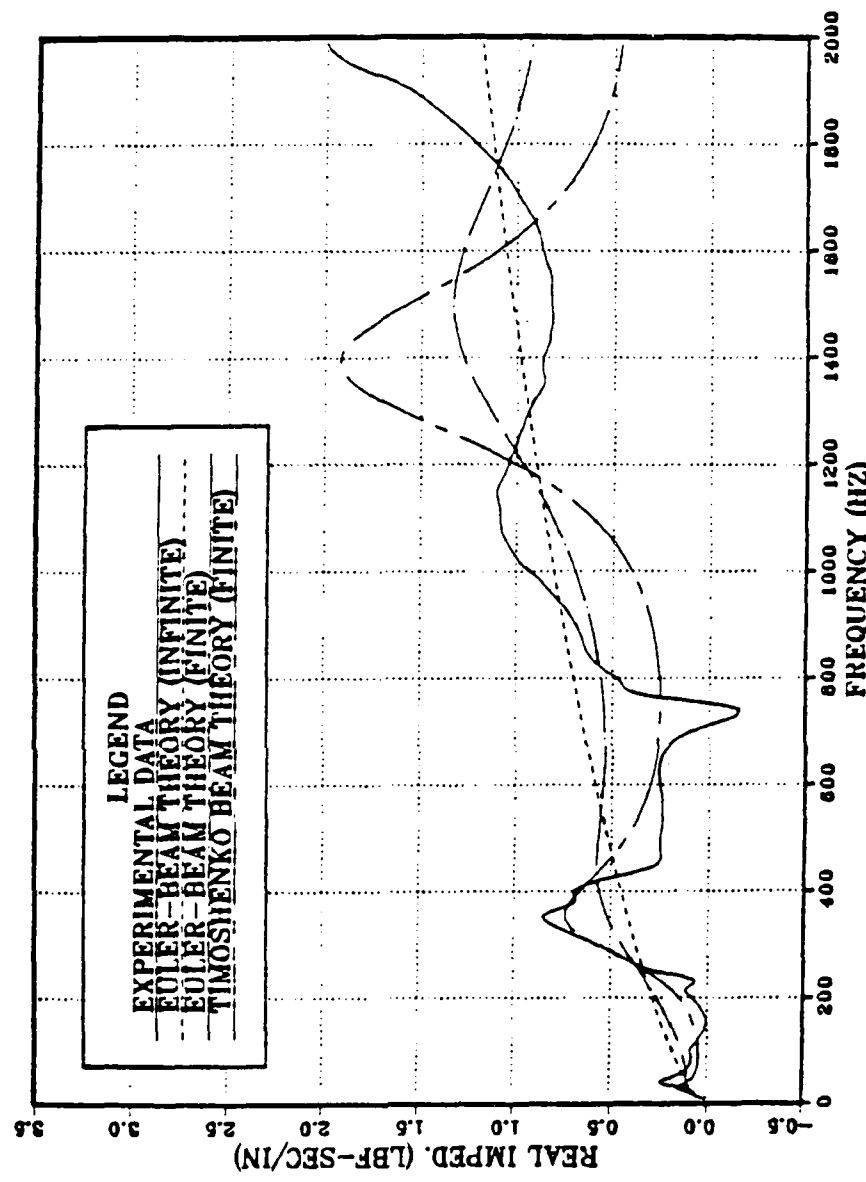


Figure 25. Real part of the 16" viscoelastic beam waveguide absorber impedances at the center of the beam.

IMPEDANCES VS. FREQUENCY

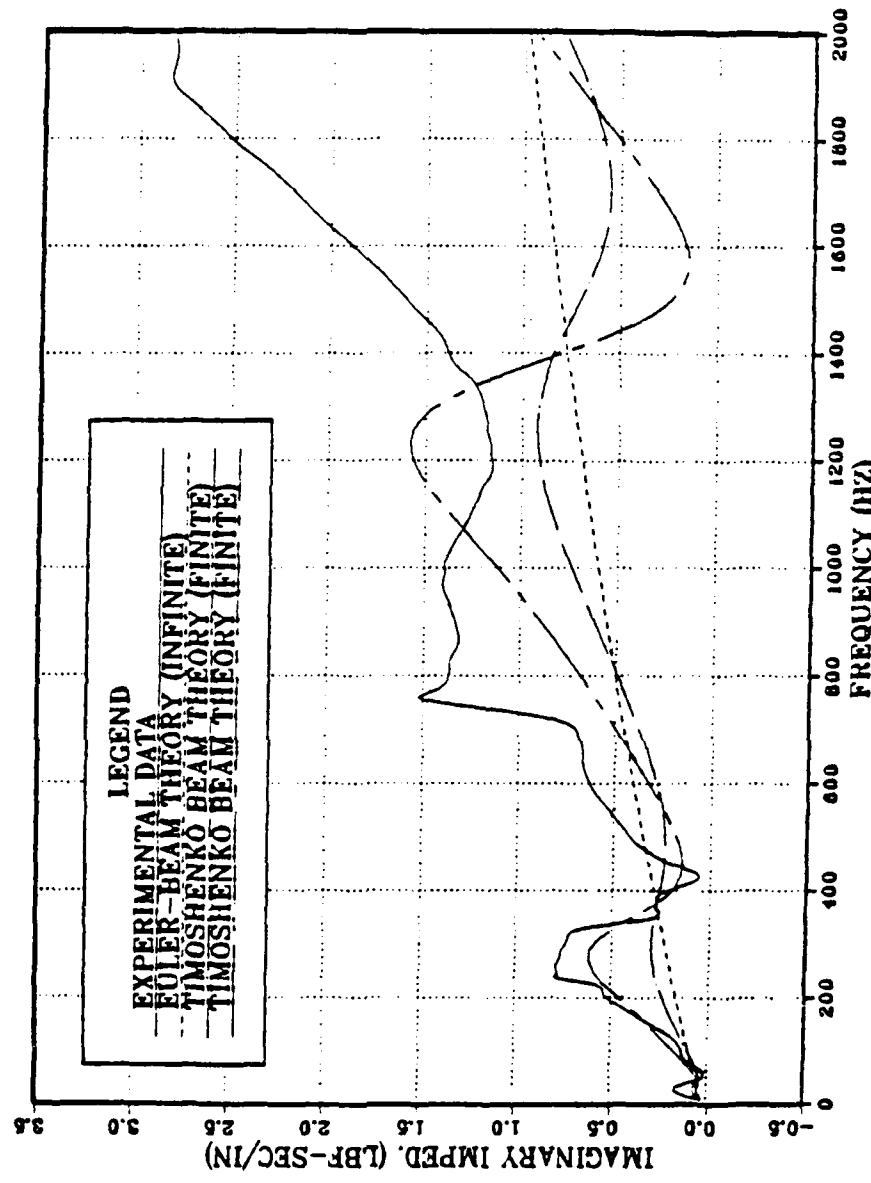


Figure 26. Imaginary part of the 16" viscoelastic beam waveguide impedances at the center of beam.

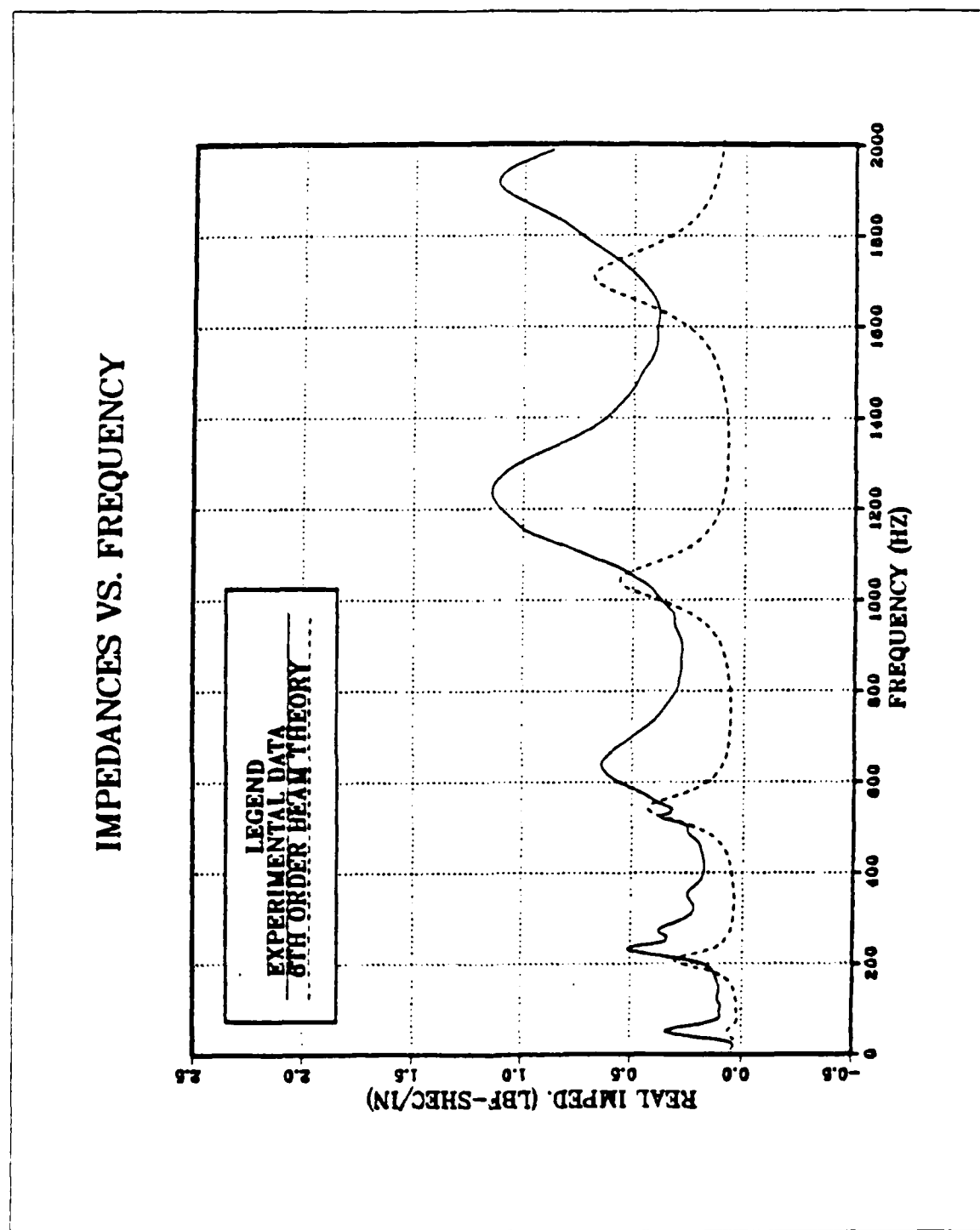


Figure 27. Real part of the 16" constrained layer beam waveguide absorber impedances at the center of the beam.

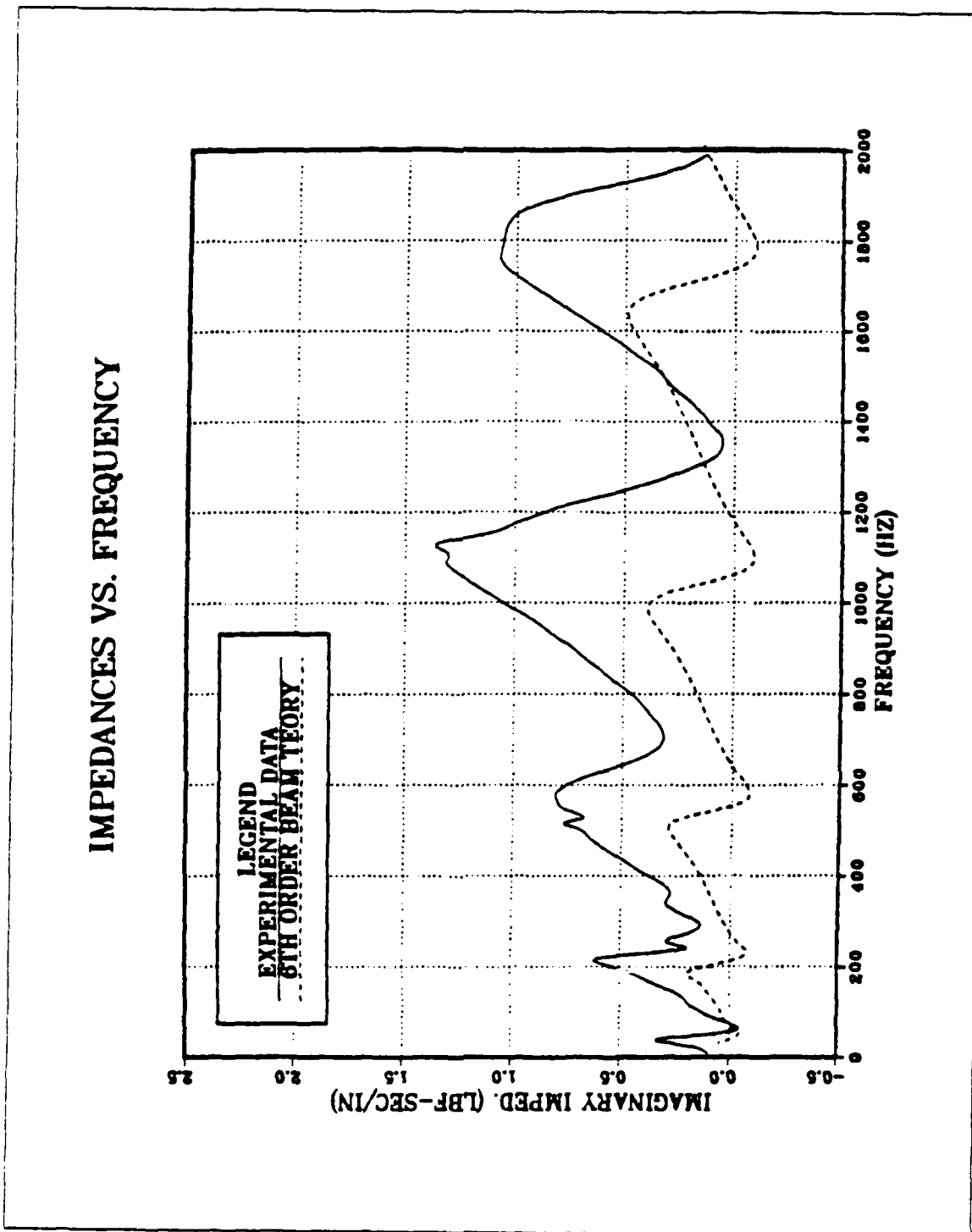


Figure 28. Imaginary part of the 16" constrained layer beam waveguide absorber impedances at the center of beam.

IMPEDANCES VS. FREQUENCY

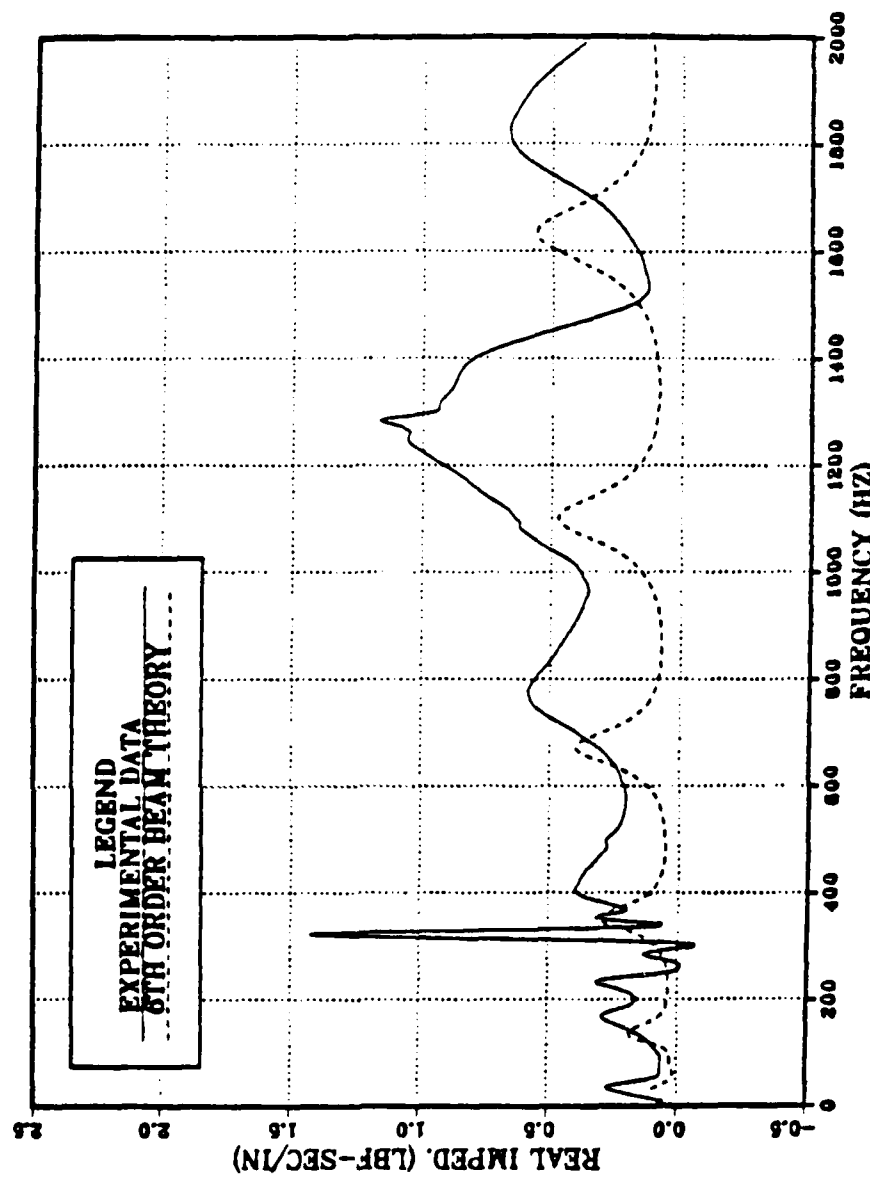


Figure 29. Real part of the 20" constrained layer beam waveguide absorber impedances at the center of the beam.

IMPEDANCES VS. FREQUENCY

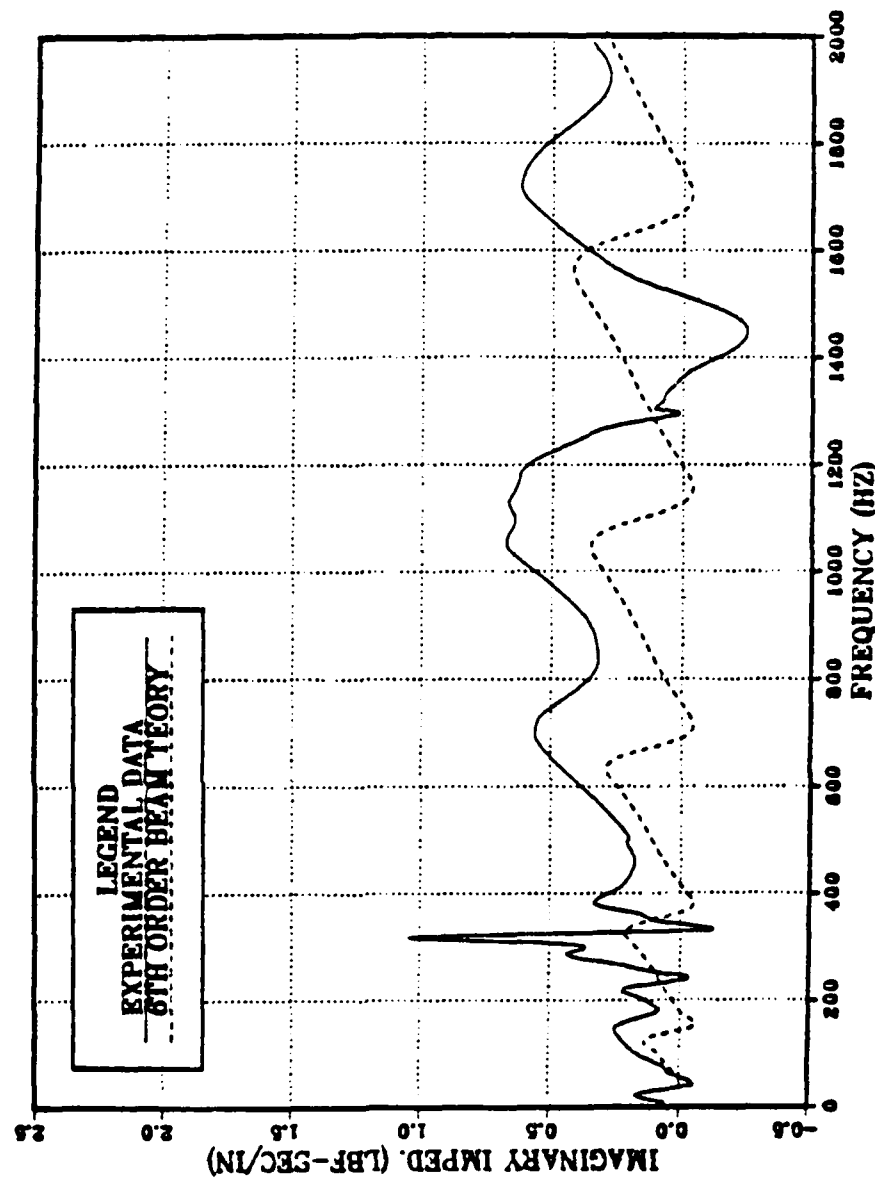


Figure 30. Imaginary part of the 20" constrained layer beam waveguide absorber impedances at the center of beam.

C. DAMPING OF THE PLATE

The purpose of this experiment is to investigate the effect of light weight waveguide absorbers on damping increase in plate type structures over a wide frequency range. Damping of the test plate structure was measured with an attachment of each one of four different waveguide absorbers (16" or 20" viscoelastic or constrained layer beam) at three different locations. The frequency response and the modal damping values of the aluminum test plate with a waveguide absorber were compared with those of the same plate without any waveguide absorber over a wide frequency range (0-2000Hz).

The modal damping values of the test plate without a waveguide absorber are shown in Figure 31 on page 56 and Figure 32 on page 57. They show that more than 20 lightly damped modes are in the frequency range between 100Hz to 2000Hz with the lowest frequency 195Hz.

The damping contribution of the same waveguide absorber to a same plate was different depending on the location of the waveguide absorber attachment point. For the 20" viscoelastic beam waveguide absorber, there was marked damping increase for modes lower than 1100Hz when it was attached at location 1 (Figure 33 on page 58 and Figure 34 on page 59). However, it was more effective for modes higher than 1200Hz when it was attached at location 2 (Figure 35 on page 60 and Figure 36 on page 61). When it was attached at location 3 its contribution to plate damping increase was effective for wider frequency range of 250Hz-1500Hz (Figure 37 on page 62 and Figure 38 on page 63). This trend applies to other waveguide absorbers, though the magnitude of damping contribution and the frequency ranges were different for each case (Figures in Appendix B).

Different modal damping effects with a different waveguide absorber at the same location were also observed. At location 1, the 20" viscoelastic beam waveguide absorber was most effective for the frequency range lower than 1100Hz (Figure 33 on page 58 and Figure 34 on page 59) and the 16" constrained layer beam waveguide absorber was most effective for the frequency range higher than 1200Hz (Figure 39 on page 64 and Figure 40 on page 65). At location 2, the 20" and 16" viscoelastic beam waveguide absorbers showed moderate contribution to plate damping and the 20" constrained layer beam waveguide absorber contributed the least amount to plate damping. For frequency ranges over 1200Hz, the 16" constrained layer beam waveguide absorber produced the largest damping increase. At location 3, the 20" and 16" viscoelastic beam waveguide absorbers and the 20" constrained layer beam waveguide absorber produced moderate

damping increase over a wide frequency range of 250Hz-1500Hz. However, the 16" constrained layer beam waveguide absorber showed the least damping increase.

After the selection of optimum damping at each location, two wave guide absorbers (20" viscoelastic and 16" constrained layer beam) were attached at locations 1 and 2 and three waveguide absorbers (20" viscoelastic, 16" constrained layer and 16" viscoelastic beam) were attached at locations 1, 2 and 3 to see the effect of multiple waveguide absorbers on the test plate damping (Figure 41 on page 66). Figure 42 on page 67 and Figure 43 on page 68 represent frequency response and modal damping of the plate with two waveguide absorbers. Figure 44 on page 69 and Figure 45 on page 70 represent frequency response and modal damping of the plate with three waveguide absorbers. Damping of the plate increased with increasing number of the waveguide absorbers (Figure 42 on page 67 and Figure 44 on page 69). The damping increase resulting from attachment of two or more absorbers resemble the sum of the separate result of each.

Impedance of the test plate at location 1 is compared with the driving point impedance of the 20" viscoelastic beam in Figure 46 on page 71. This figure shows that at resonance frequencies the impedance of the test plate is much smaller than that of the waveguide absorber. Figure 47 on page 72 and Figure 48 on page 73 show the comparison between the impedances of the test plate at location 2 and location 3 with the driving point of the 16" constrained layer beam and 16" viscoelastic beam, respectively. These figures show that at low frequency range (<400Hz) the impedances of the test plate were higher than those of waveguide absorbers and at high frequency range (>400Hz) impedances of waveguide absorbers were higher at some resonance frequencies.

From equation (2.7), the loss factor contribution, η , of a waveguide absorber is proportional to the following 3 terms:

$$R_b \quad (4.1)$$

$$\frac{1}{|1 + \frac{Z_s}{Z_p}|^2} \quad (4.2)$$

$$|\frac{V_s}{V_m}|^2 \quad (4.3)$$

The first term is determined from waveguide characteristics only and the second term is determined from the impedance ratio between the test structure and a waveguide absorber at the attachment point. However, the third term depends on the interaction between the test structure and a waveguide absorber and the whole response of the test plate. If Z_s is much smaller than Z_a , then V_L will remain constant before and after the attachment of a waveguide absorber. Previous studies [Ref. 2 and Ref. 3] were based on this assumption and gave misleading indications that experimental loss factors would be much higher than theoretical predictions. In the present study, as shown in Figure 46 on page 71, Figure 47 on page 72 and Figure 48 on page 73, the impedances of the test plate were similar in magnitude to impedances of waveguide absorbers at resonance frequencies and the loss factor contribution due to waveguide absorbers could not be predicted using equation (2.7).

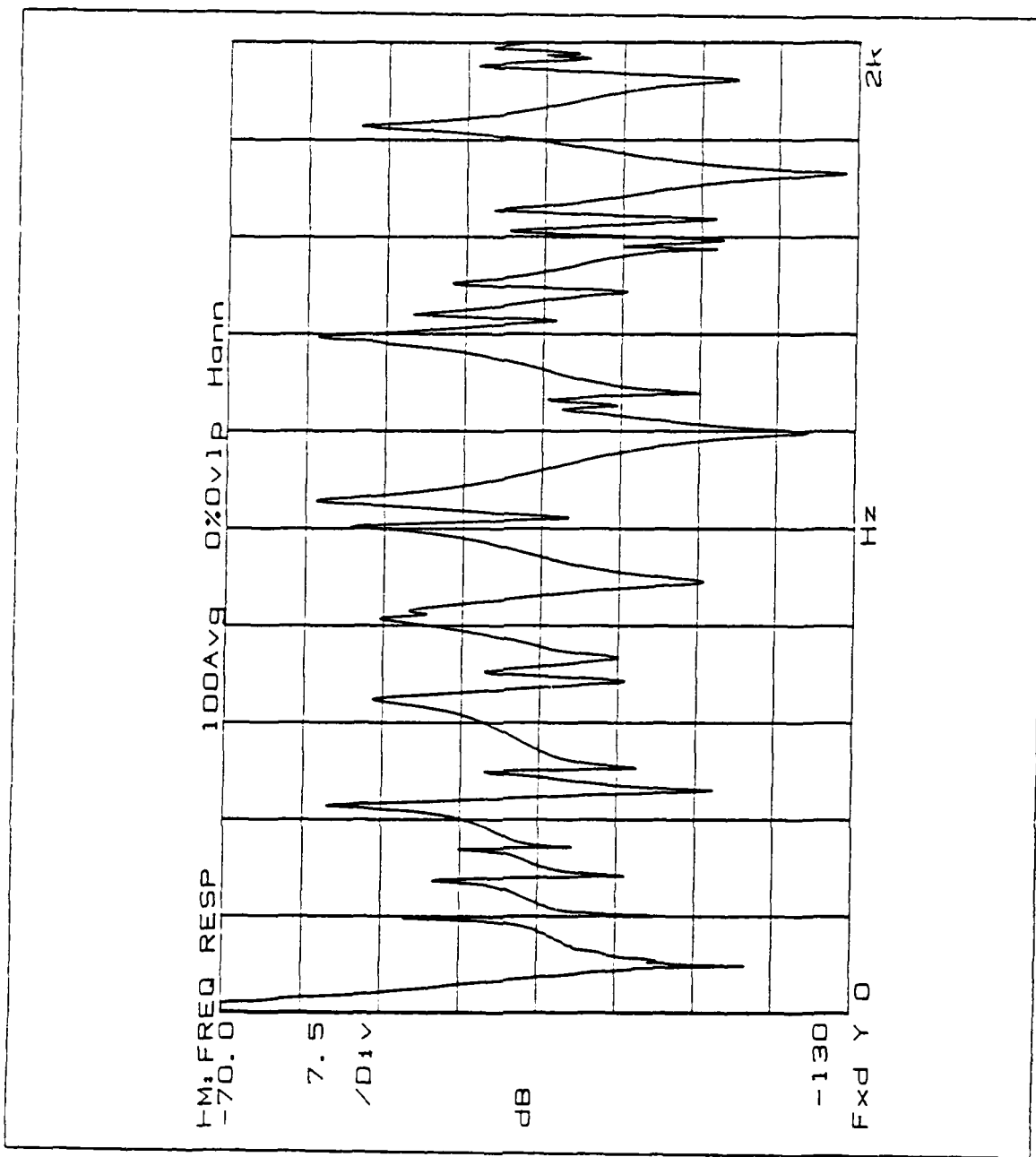


Figure 31. The driving point frequency response of the test plate without a wave-guide absorber.

MODAL DAMPING VS. FREQUENCY

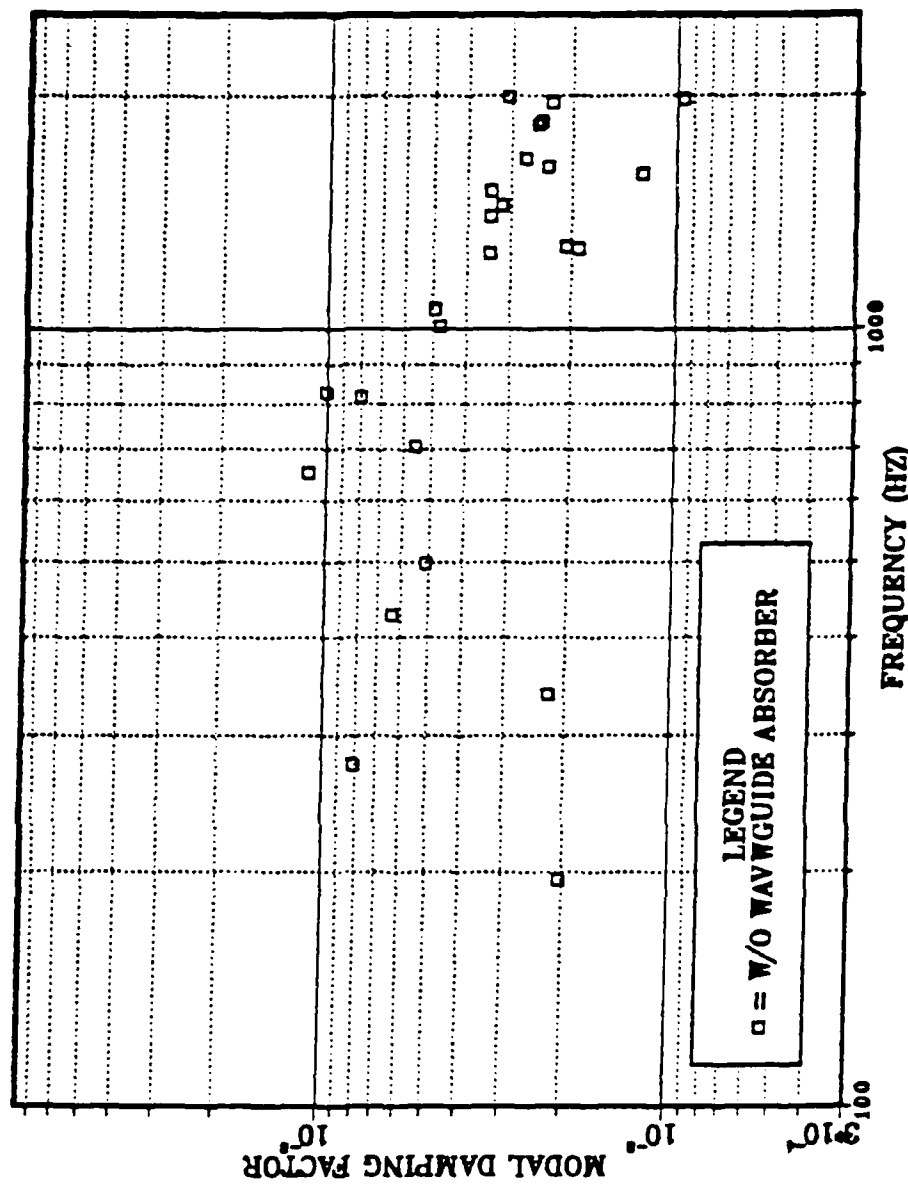


Figure 32. Modal damping factors vs. frequency of the test plate without a wave-guide absorber.

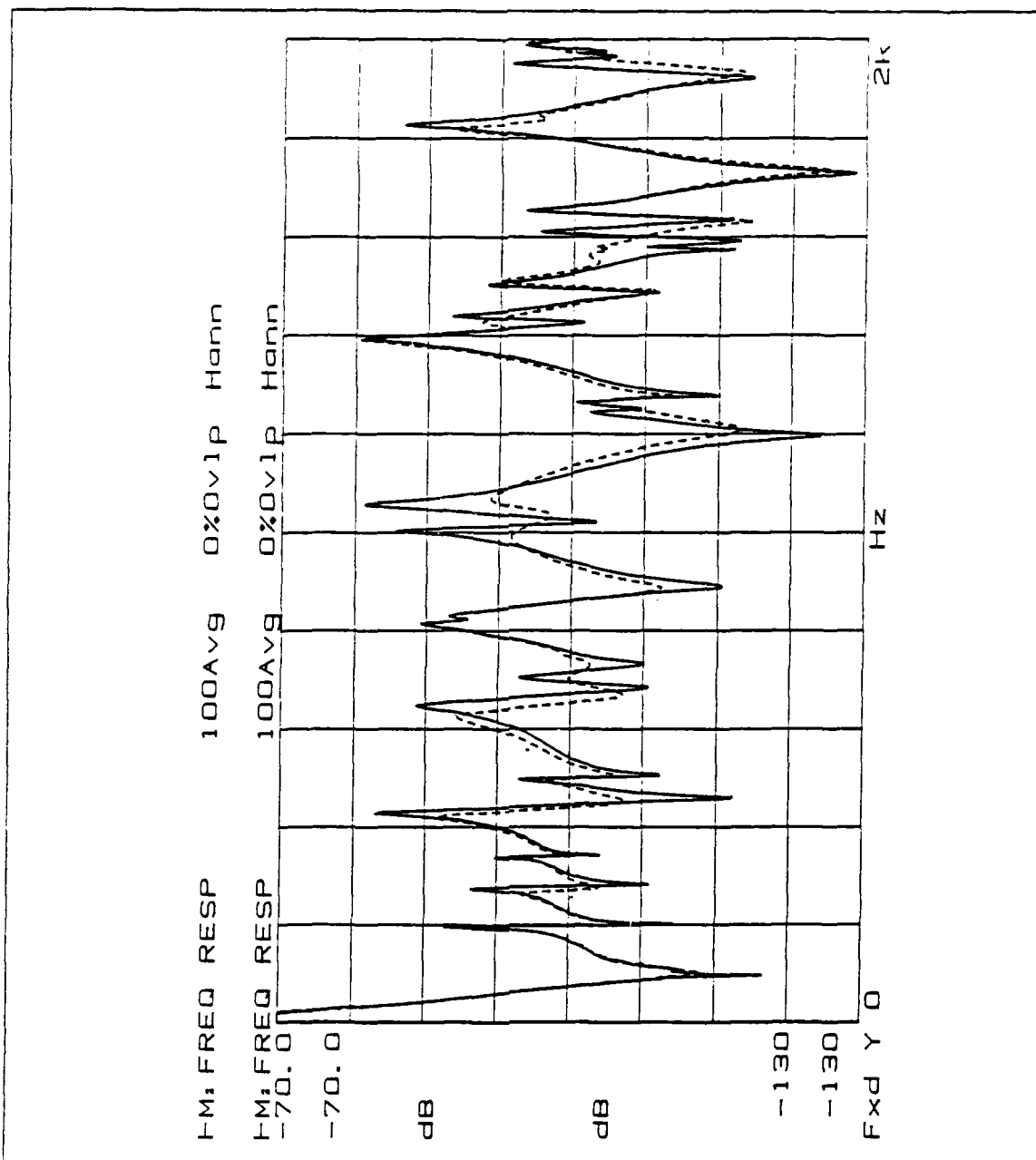


Figure 33. The driving point frequency response of the test plate with a 20" viscoelastic beam waveguide absorber (dashed) at location 1 and without (solid).

MODAL DAMPING VS. FREQUENCY

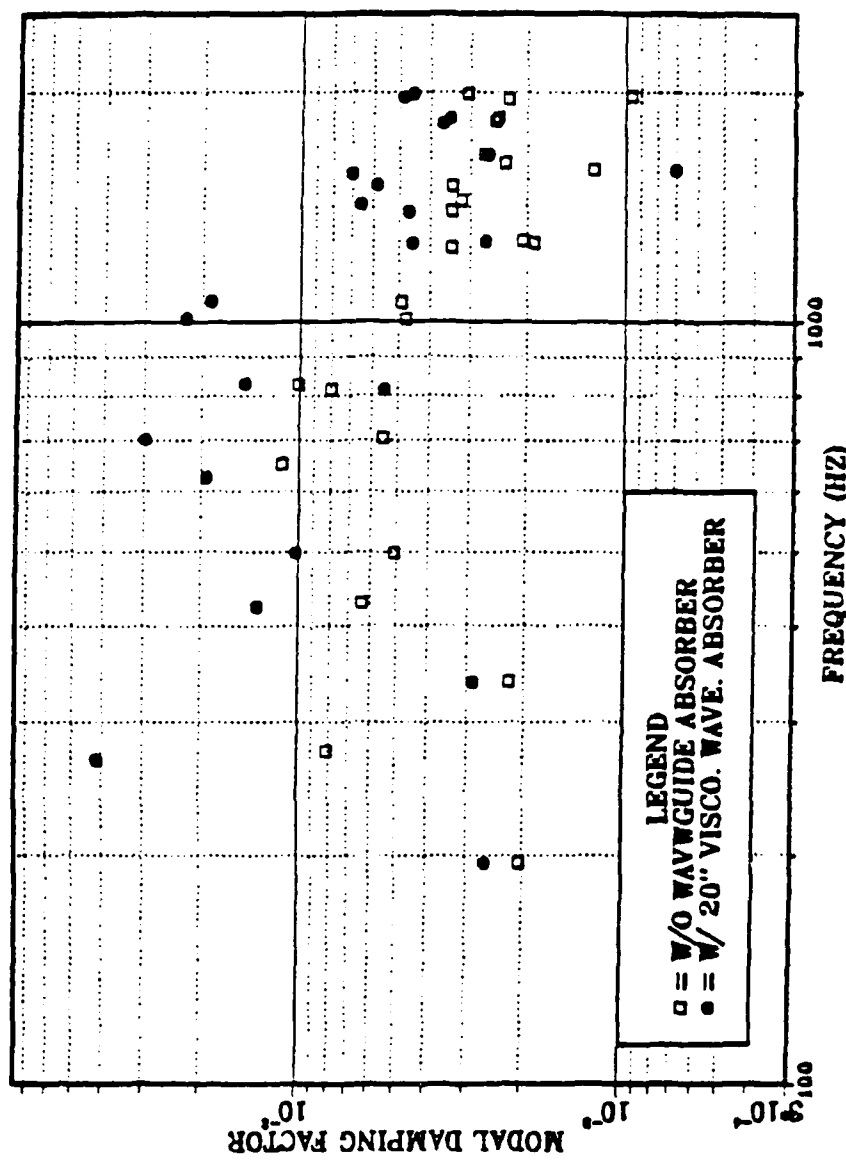


Figure 34. Modal damping factors vs. frequency of the test plate with a 20" viscoelastic beam waveguide absorber at location 1 and without.

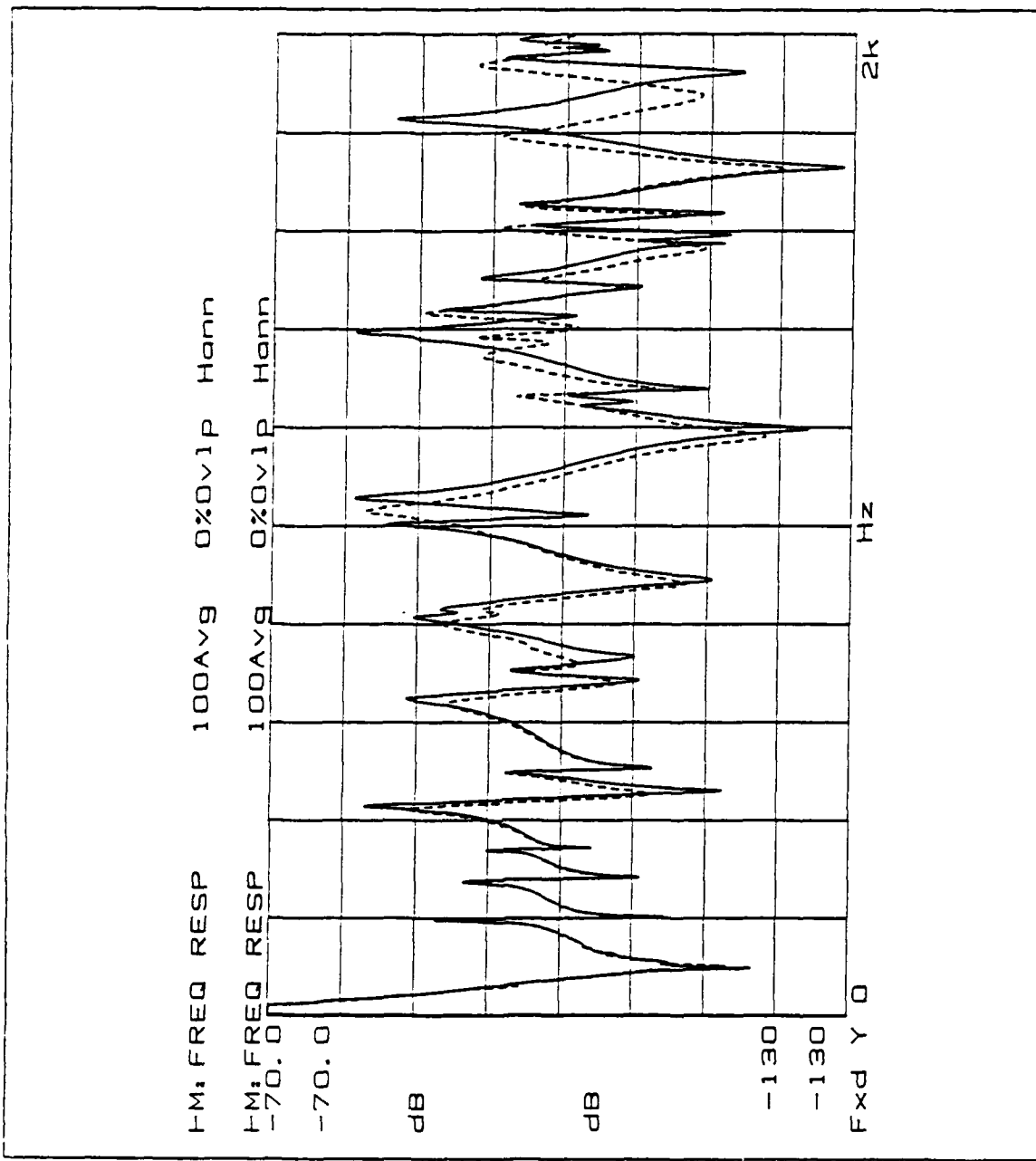


Figure 35. The driving point frequency response of the test plate with a 20" viscoelastic beam waveguide absorber (dashed) at location 2 and without (solid).

MODAL DAMPING VS. FREQUENCY

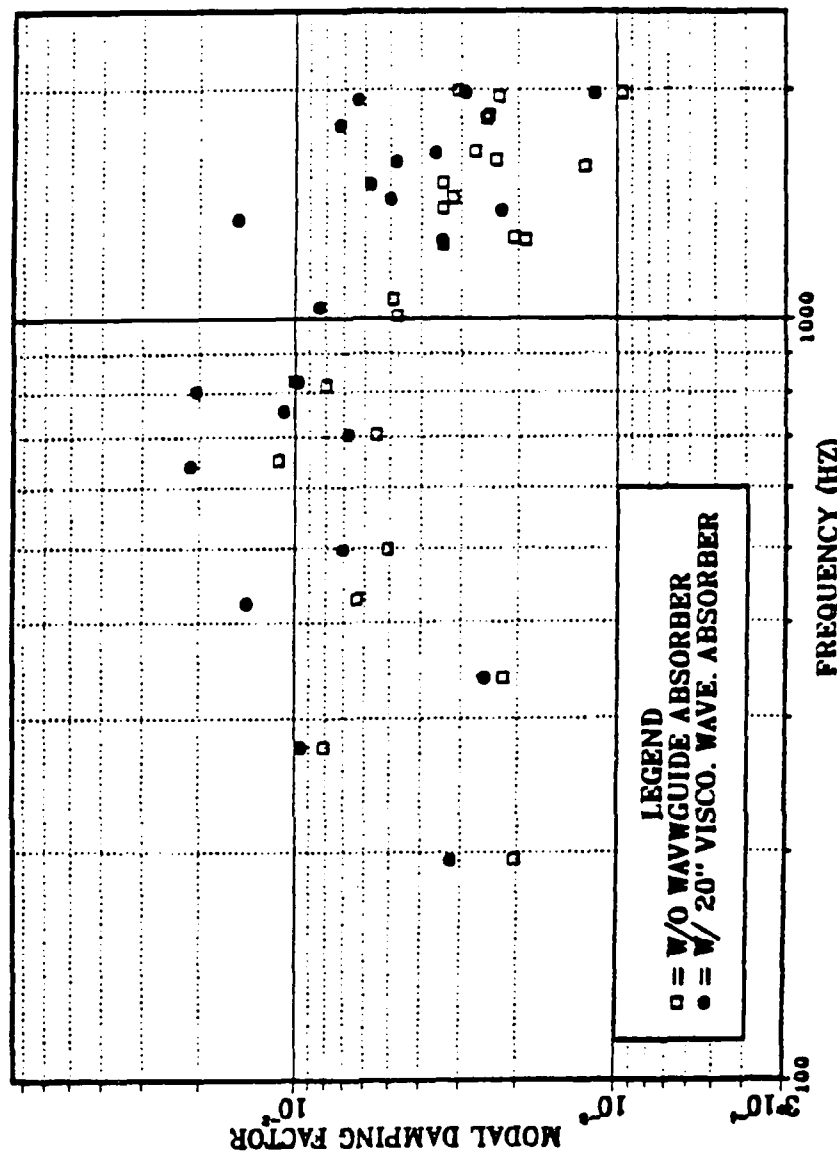


Figure 36. Modal damping factors vs. frequency of the test plate with a 20" viscoelastic beam waveguide absorber at location 2 and without.

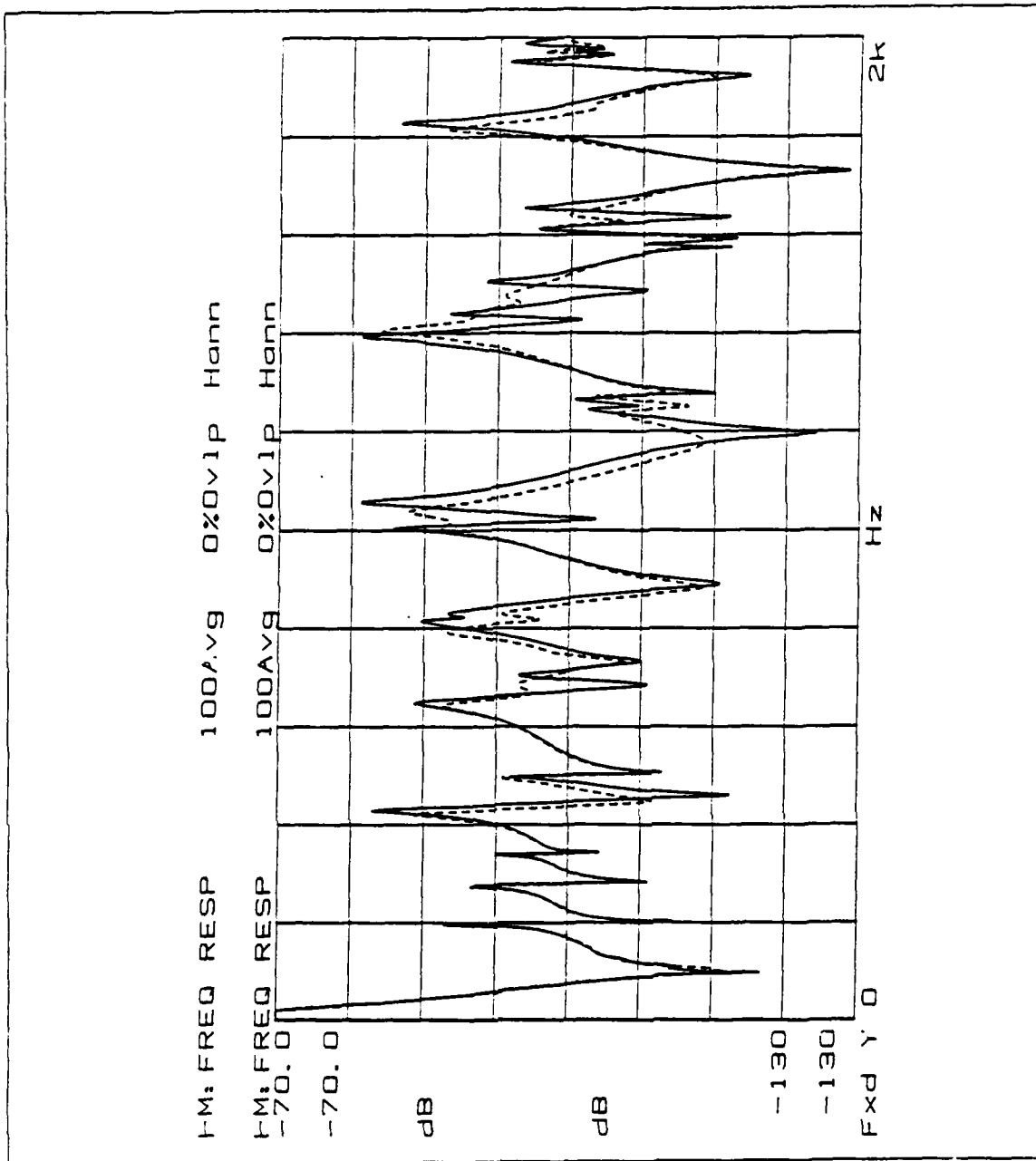


Figure 37. The driving point frequency response of test test plate with a 2.0" viscoelastic beam waveguide absorber (dashed) at location 3 and without (solid).

MODAL DAMPING VS. FREQUENCY

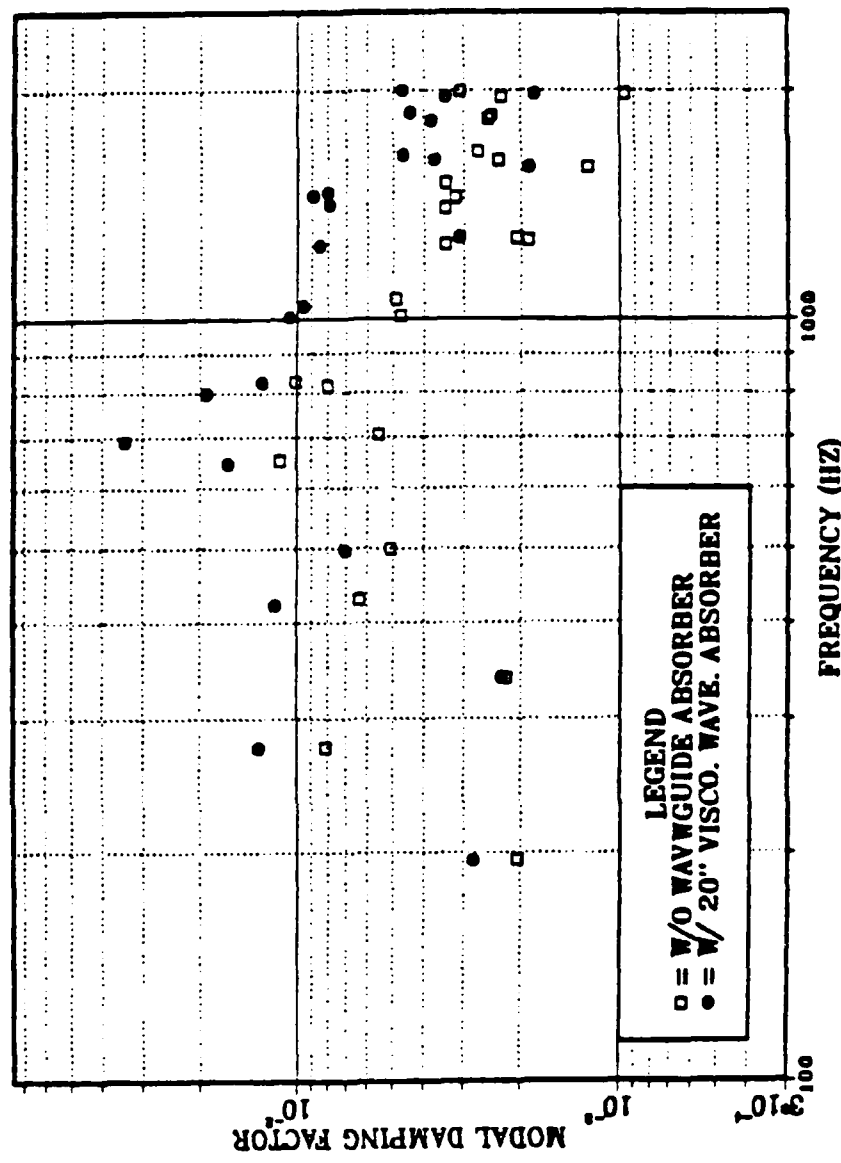


Figure 38. Modal damping factors vs. frequency of the test plate with a 20" viscoelastic beam waveguide absorber at location 3 and without.

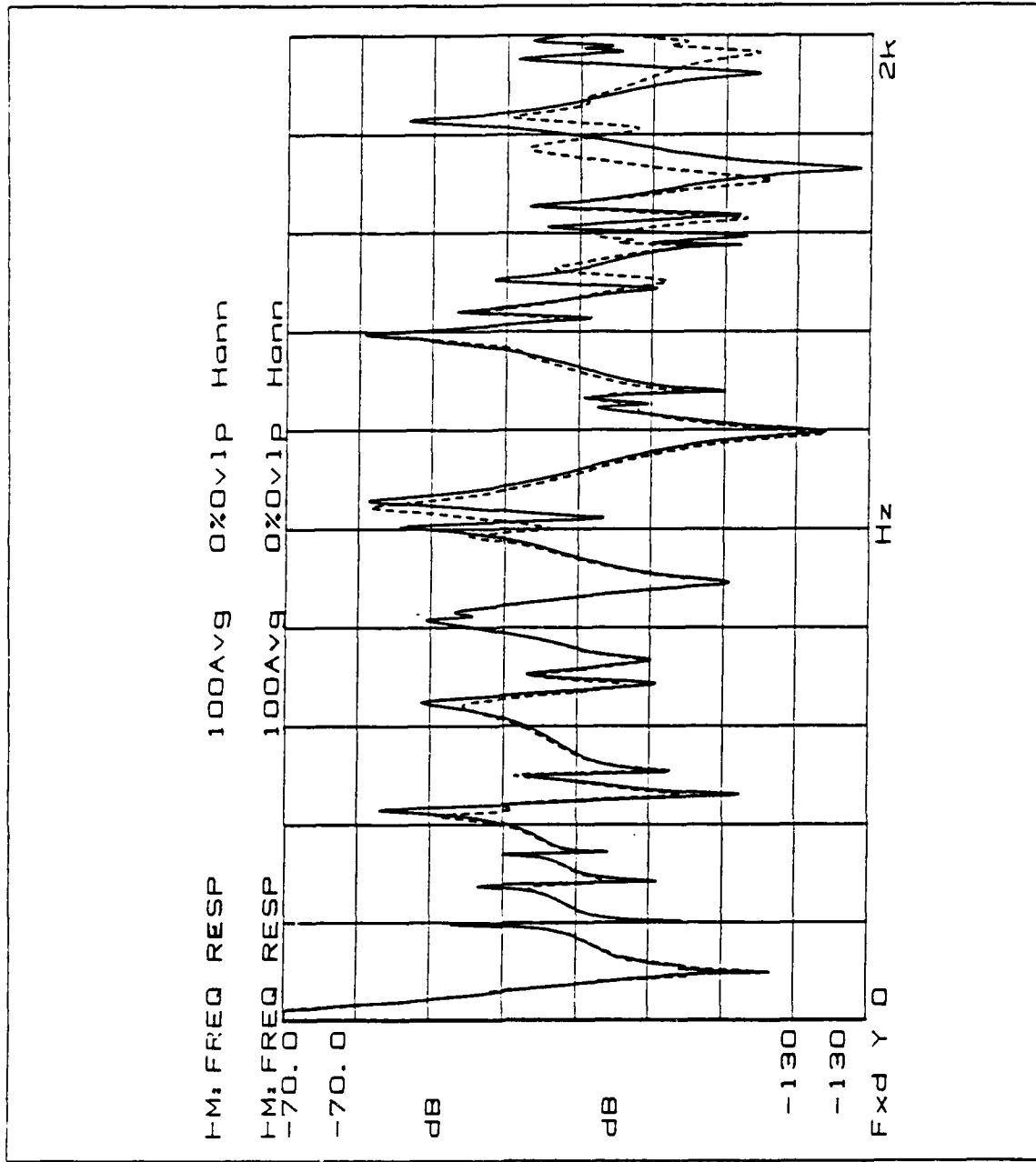


Figure 39. The driving point frequency response of the test plate with a 16" constrained layer beam waveguide absorber (dashed) at location 1 and without (solid).

MODAL DAMPING VS. FREQUENCY

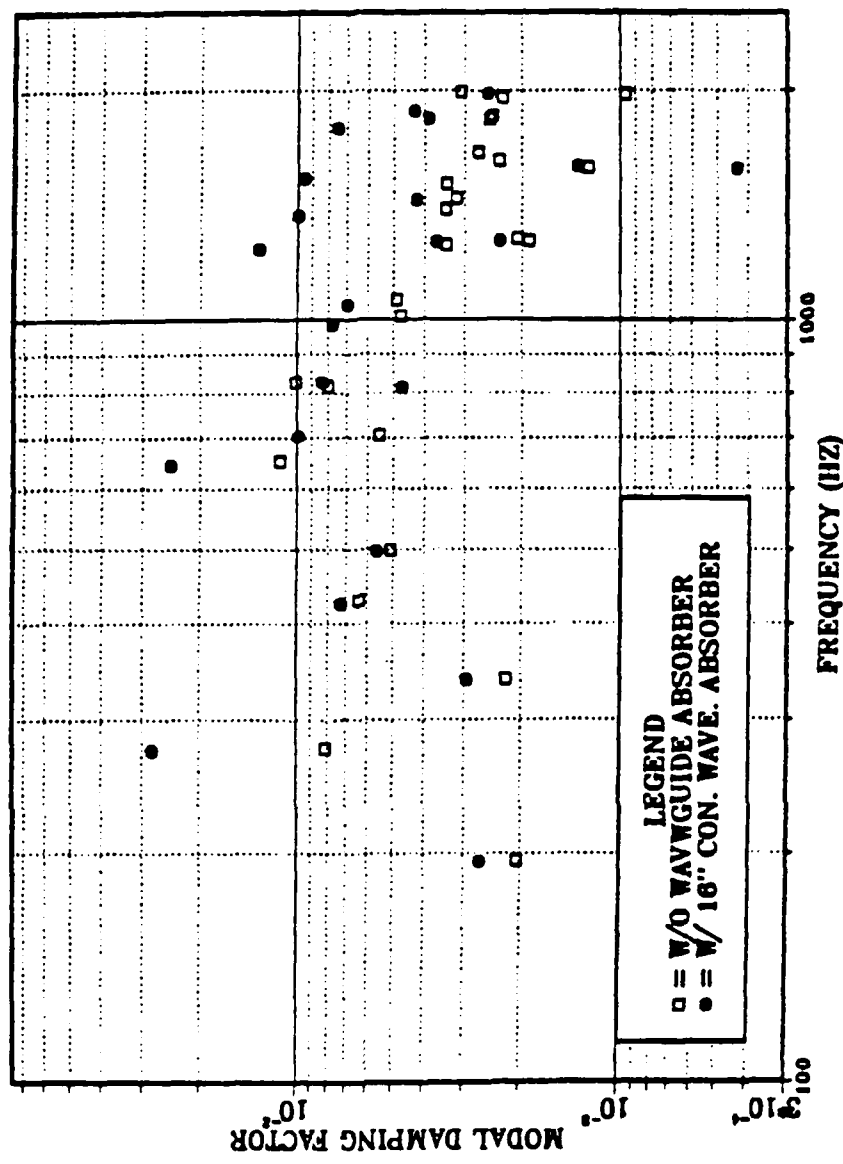


Figure 40. Modal damping factors vs. frequency of the test plate with a 16" constrained layer beam waveguide absorber at location 1 and without.

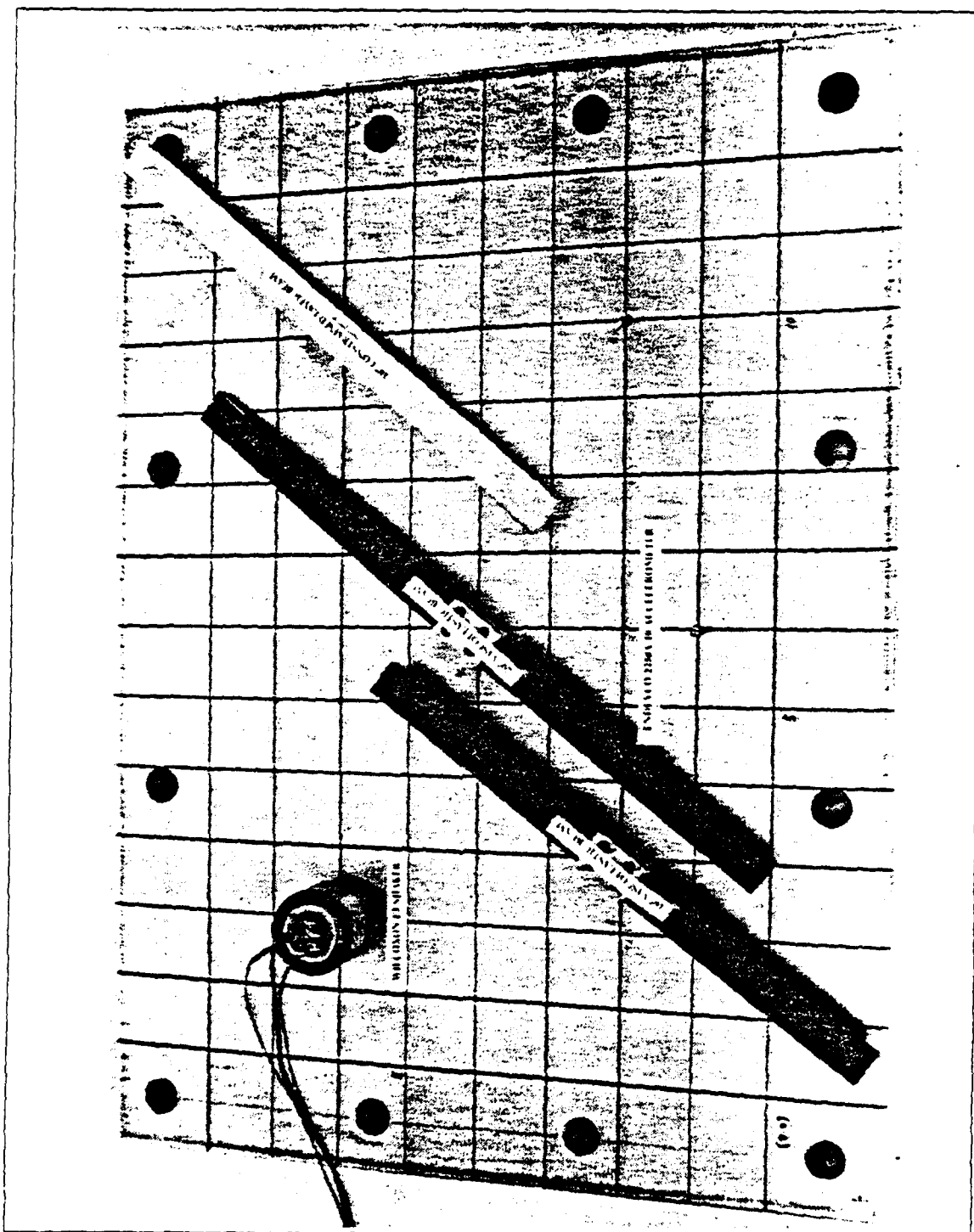


Figure 41. The test plate with three waveguide absorbers.

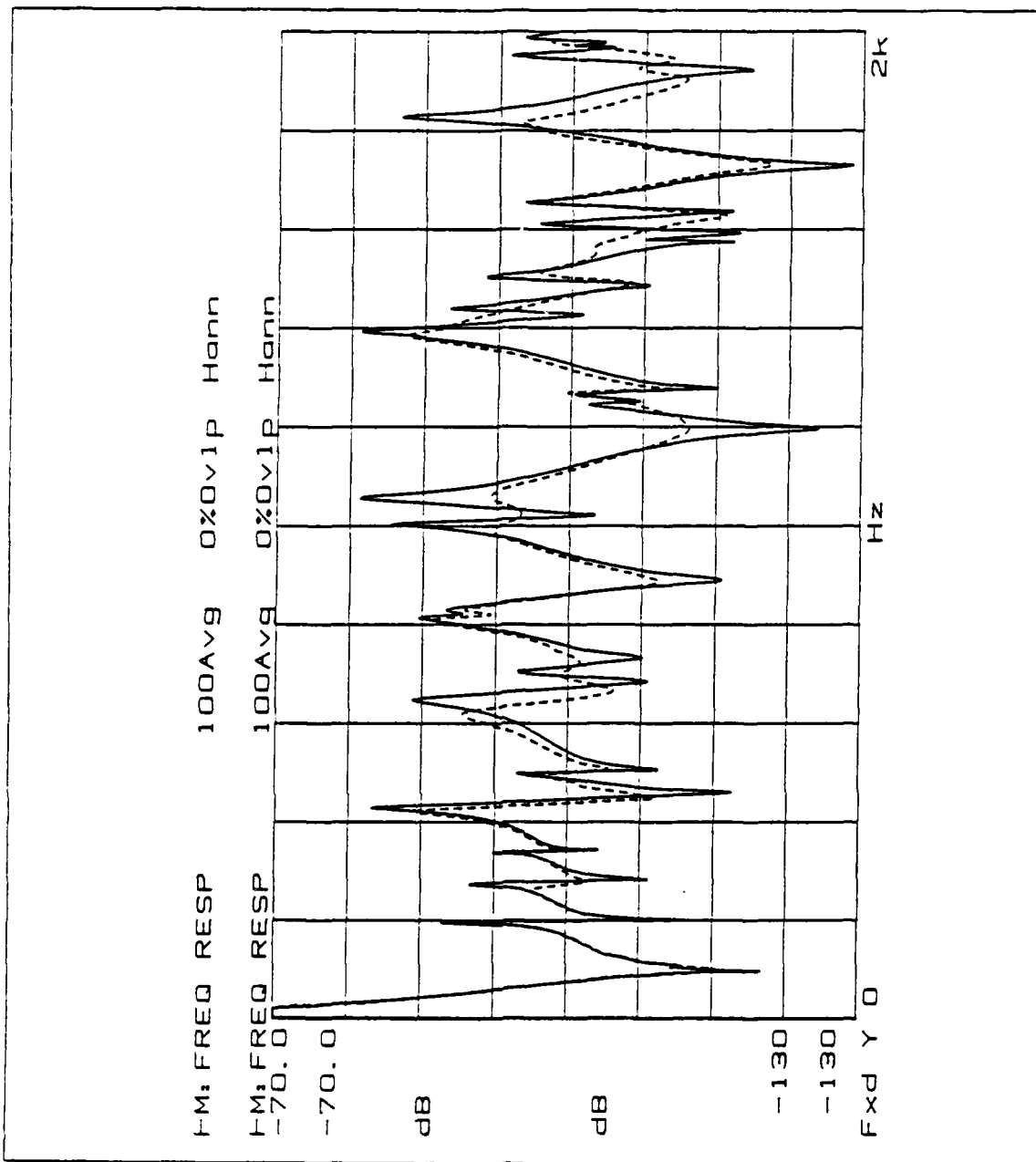


Figure 42. The driving point frequency response of the test plate with a 20" viscoelastic (at location 1) and 16" constrained layer (at location 2) beam waveguide absorber (dashed) and without (solid).

MODAL DAMPING VS. FREQUENCY

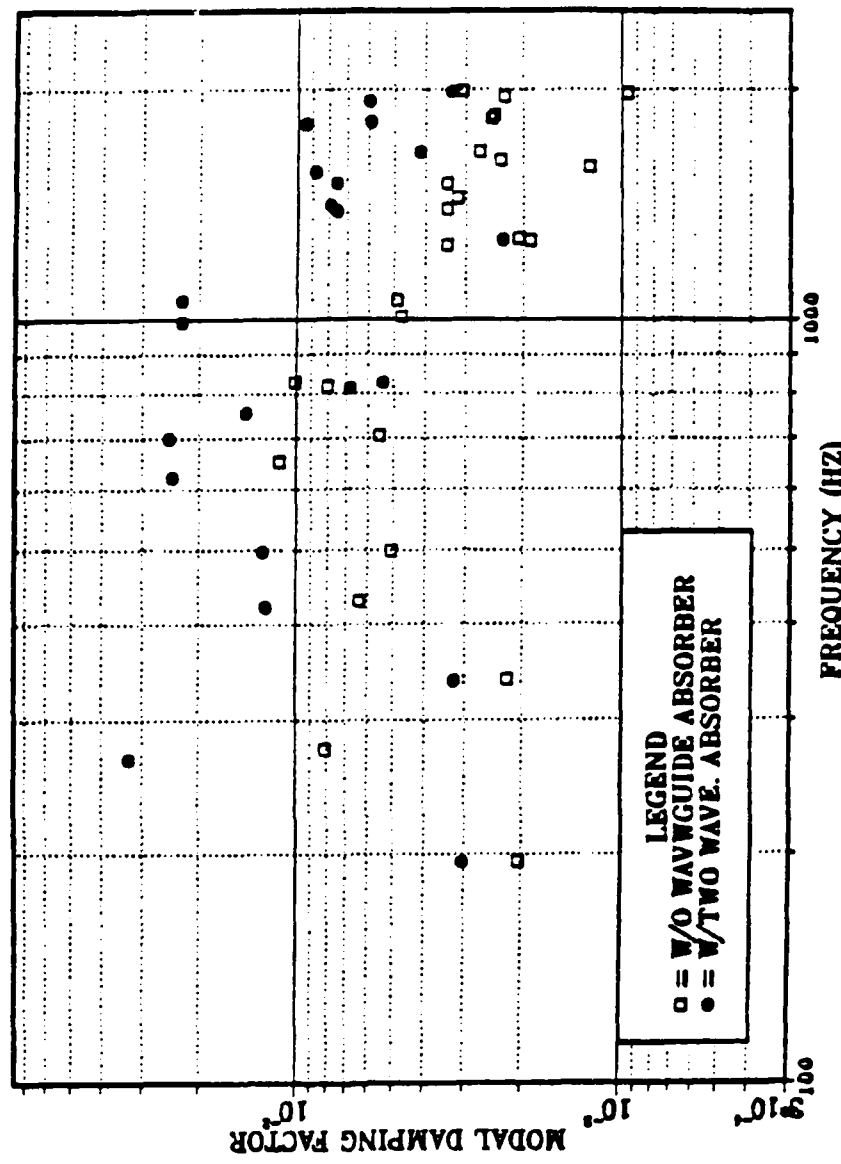


Figure 43. Modal damping factors vs. frequency of the test plate with a 20" viscoelastic (location 1) and a 16" constrained layer (location 2) beam waveguide absorber and without.

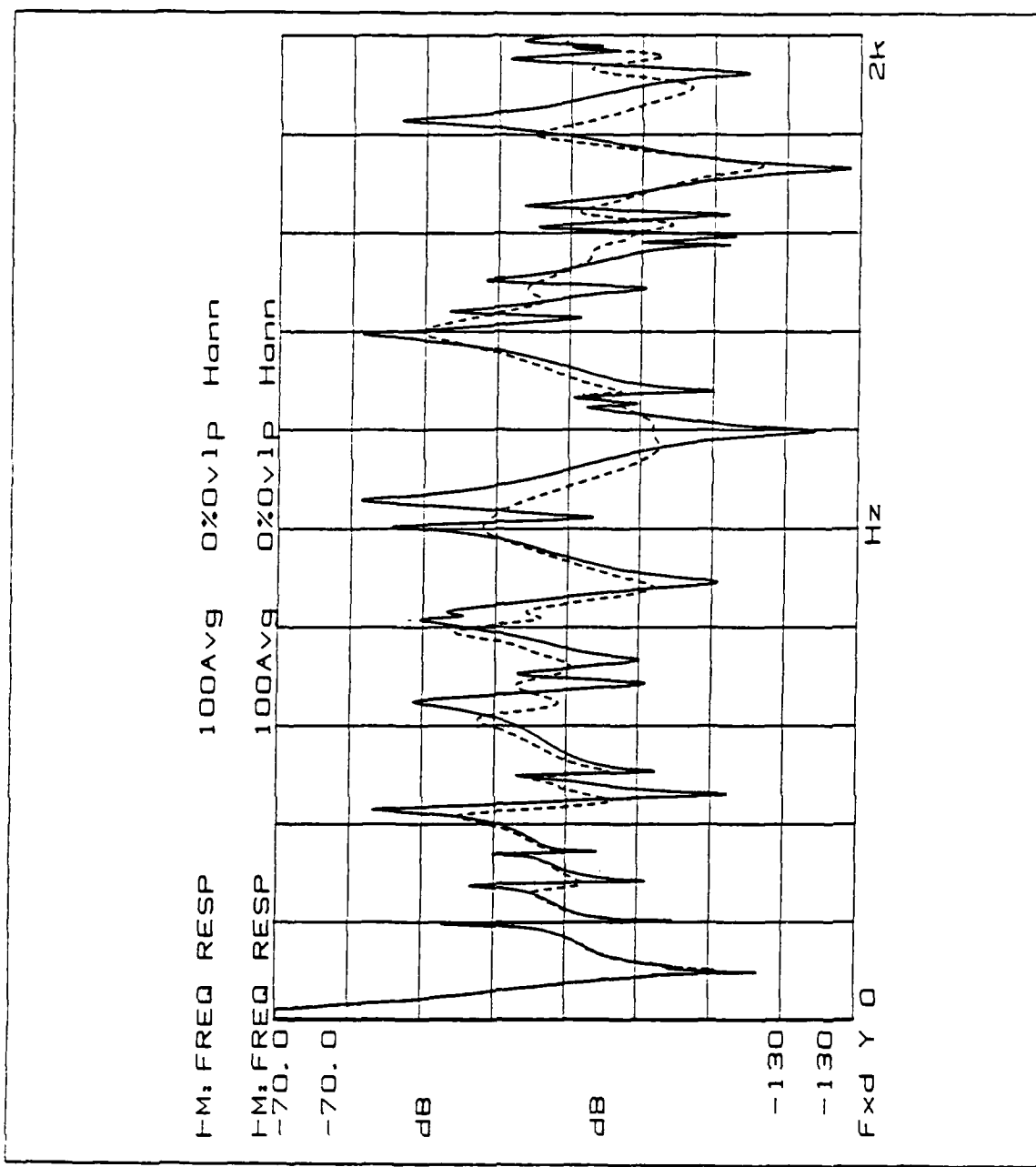


Figure 44. The driving point frequency response of the test plate with a 20" viscoelastic (at location 1), a 16" constrained layer (at location 2) and a 16" viscoelastic (at location 3) beam waveguide absorber (dashed) and without (solid).

MODAL DAMPING VS. FREQUENCY

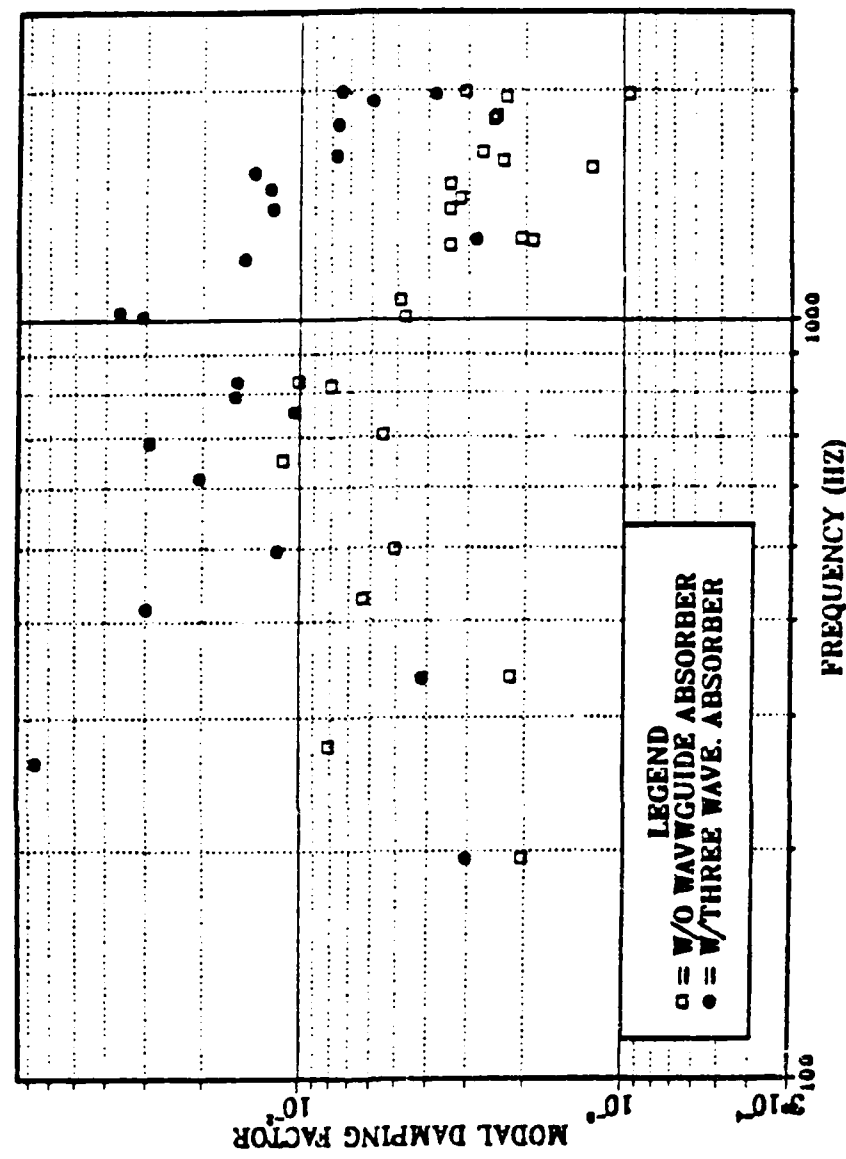


Figure 45. Modal damping factors vs. frequency of the test plate with a 20" viscoelastic (location 1), a 16" constrained layer (location 2) and a 16" viscoelastic beam waveguide absorber and without.

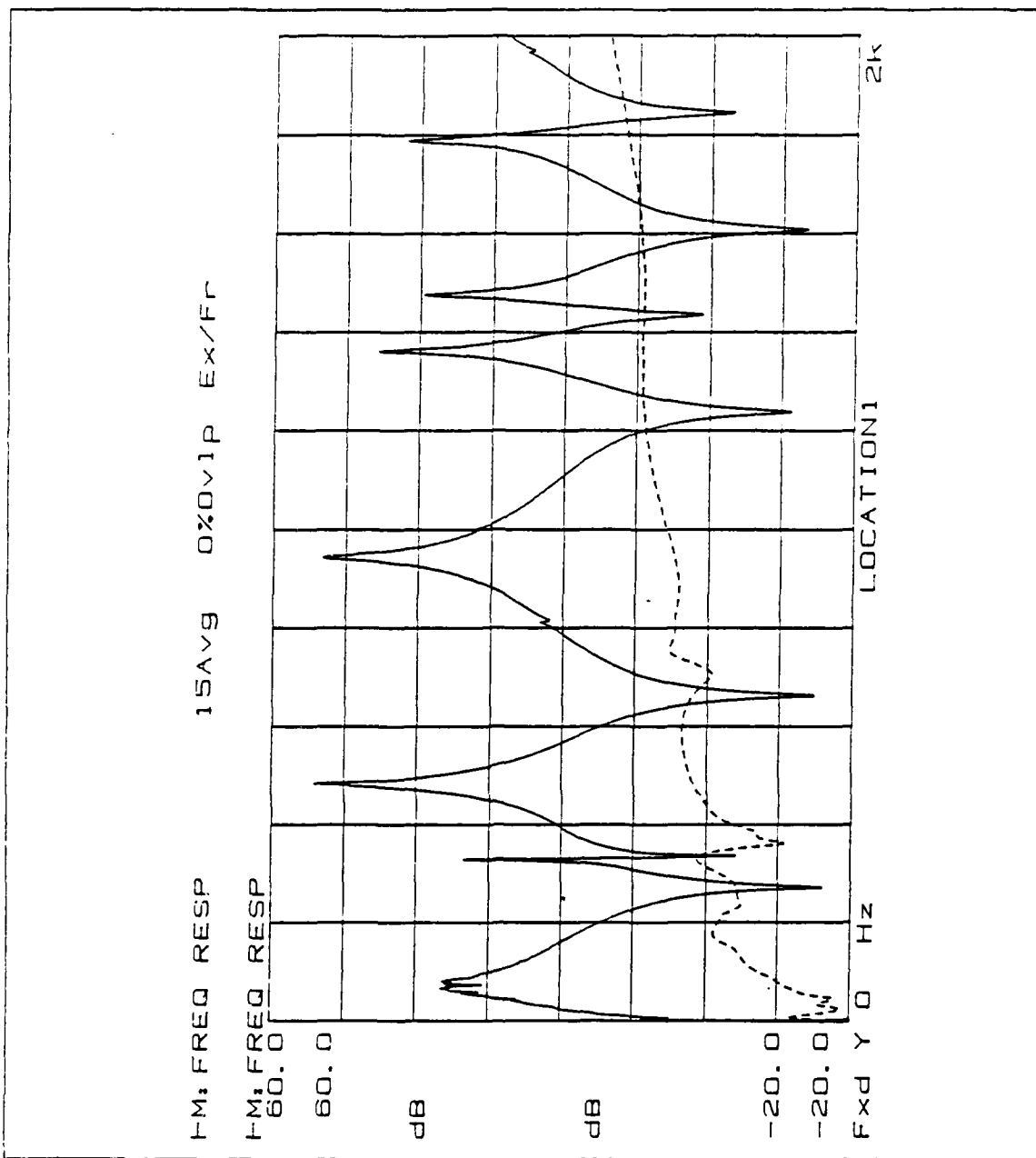


Figure 46. Magnitude impedances of the test plate at location 1 (solid) and of the 20" viscoelastic beam at the driving point (dashed).

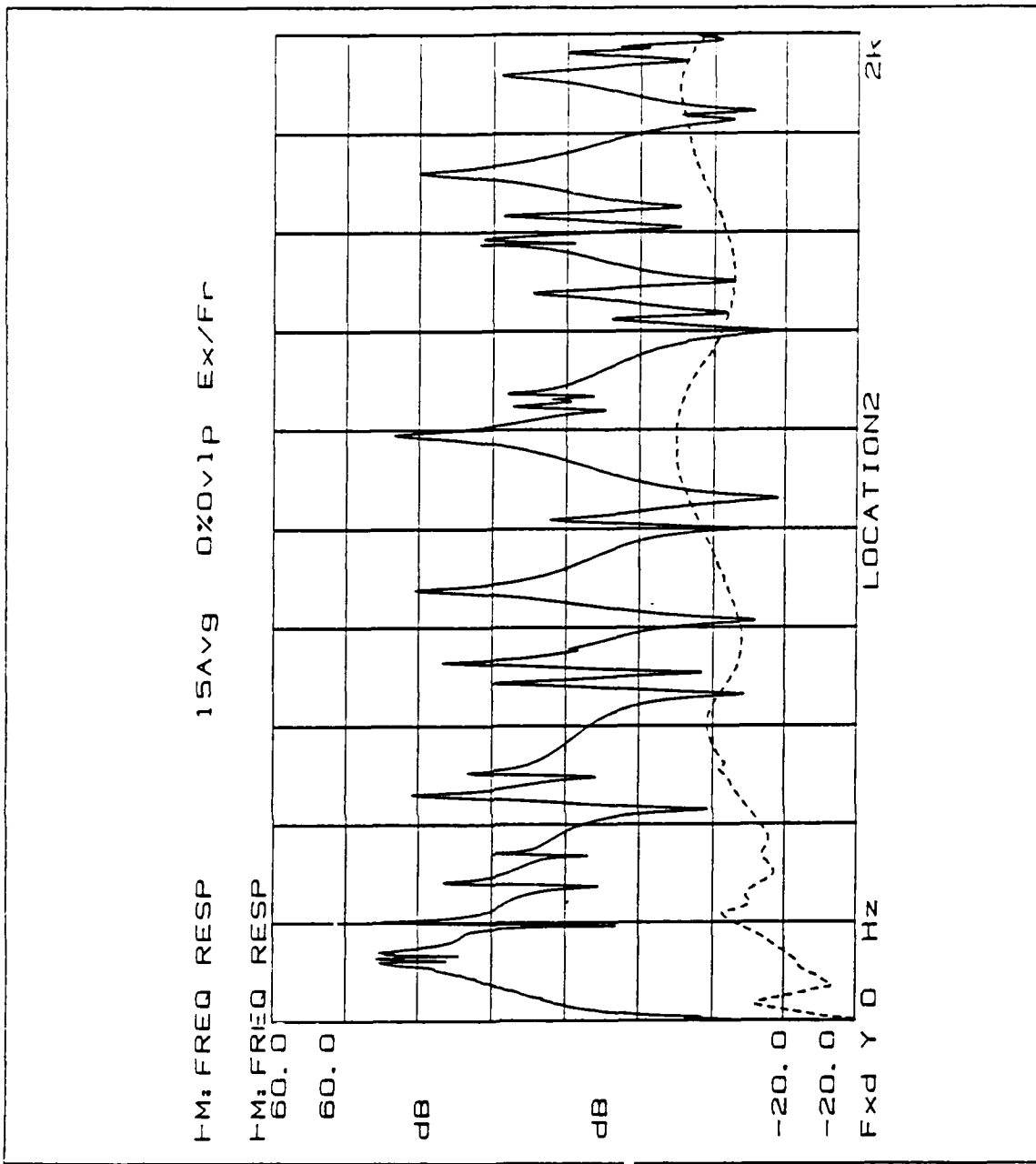


Figure 47. Magnitude impedances of the test plate at location 2 (solid) and of the 16"constrained layer beam at the driving point (dashed).

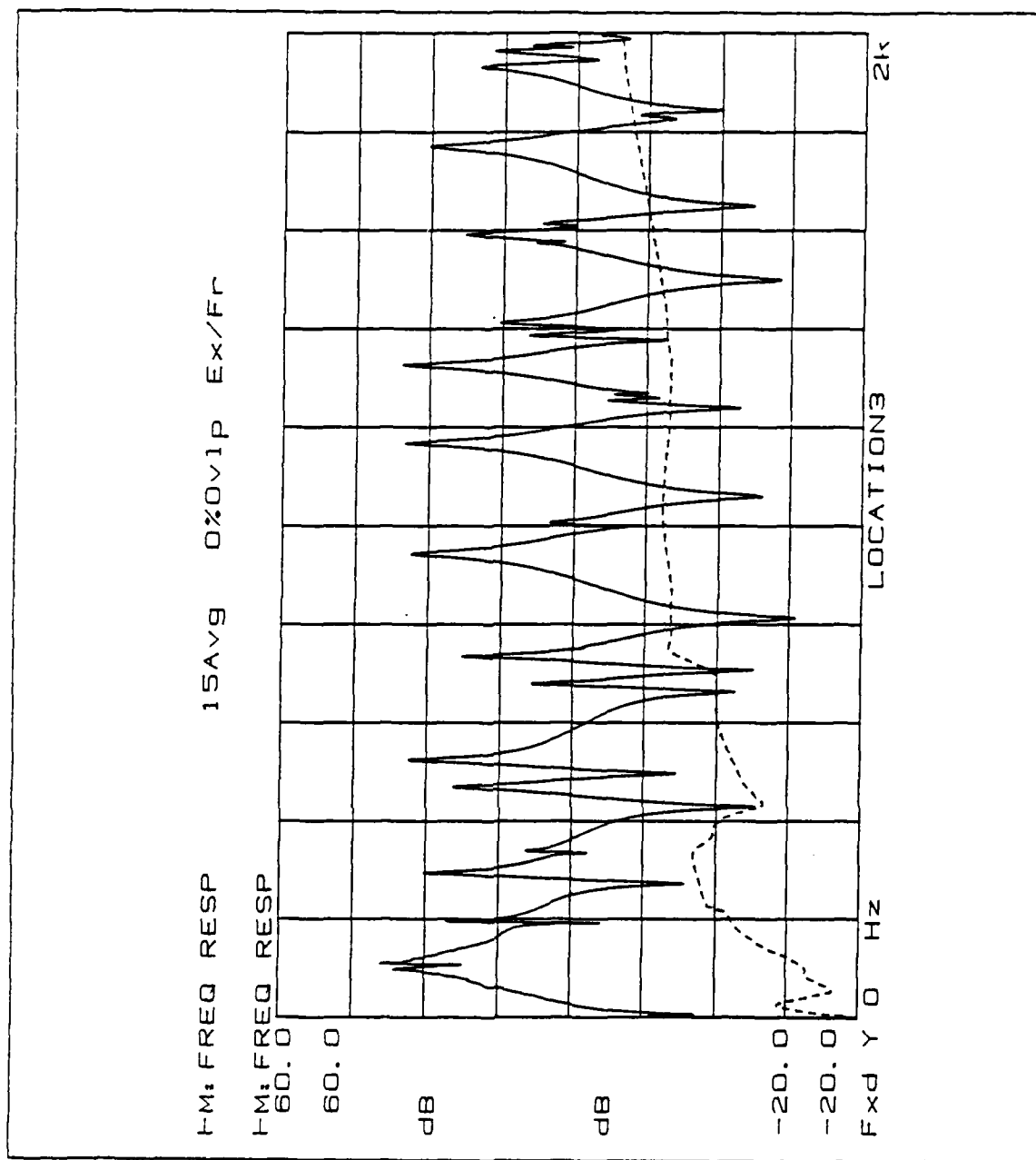


Figure 48. Magnitude impedances of the test plate at location 3 (solid) and of the 16" viscoelastic beam at the driving point (dashed).

V. CONCLUSIONS

The purpose of this study was to develop two kinds of high damping beam waveguide absorbers for application to naval structures over a wide frequency range (100Hz-2000Hz) and to evaluate theoretical prediction schemes using various beam theories. Comparison between theoretical predictions and experimental results show that Timoshenko beam theory and the six order beam theory can be used in the prediction of impedances of viscoelastic beam waveguide absorbers and constrained layer beam waveguide absorbers, respectively.

Application of waveguide absorbers to a test plate structure showed that damping of the test structure can be increased significantly with one waveguide absorber over a frequency range. The magnitude and the frequency range of damping increase depend on the impedance of the waveguide absorber and on the location. The prediction of damping increase due to an attached waveguide absorber, equation (2.7), does not show the effect of waveguide absorber completely since this equation does not include the structure vibration reduction effects due to the waveguide absorber. Since the contribution of each waveguide absorber to the damping of the test plate is additive, the modal damping values of all the vibration modes of the test plate in a wide frequency range can be increased using multiple waveguide absorbers.

VI. RECOMMENDATIONS

From the results of present study following are recommended for future studies on waveguide absorbers:

1. Investigation of the effect of a waveguide absorber on the reduction in vibration of the original structure and derivation of the relation between the impedances and the mode shape of the structure.
2. Theoretical studies on impedance prediction of waveguides of different shape such as circular viscoelastic plates and application to damping increase.
3. Investigation of interaction between waveguide absorber for multiple waveguide absorbers applications, and
4. Optimization of application of waveguide absorbers in design, number, and location.

APPENDIX A.

I. THE IMPEDANCE OF THE INFINITE VISCOELASTIC BEAM USING BERNOULLI-EULER BEAM THEORY

```
*****
* THE THREE REDUCE PROGRAMS WERE USED FOR EVALUATING THE IMPEDANCE *
* OF THE INFINITE VISCOELASTIC BEAM USING BERNOULLI-EULER BEAM *
* THEORY. *
*****
C
C THE FIRST REDUCE PROGRAM DEFINED TRANSVERSE FORCE AND TWO BOUNDARY
C CONDITIONS.
C
YY:=Y1*EXP(I*K1*X)+Y3*EXP(I*K3*X);
PP:=DF(YY,X);
MM:=-EI*DF(PP,X);
FF:=-DF(MM,X);
YO:=SUB(X=0,YY)-Y;
PO:=SUB(X=0,PP)-P;
BYE;
C
C THE SECOND REDUCE PROGRAM SOLVED CONSTANT VARIABLES (Y1 AND Y3).
C
Y0:=Y1+Y3-Y;
PO:=P1*Y1+P3*Y3-P;
SOLVE(LST(Y0,PO),Y1,Y3);
BYE;
C
C THE THIRD REDUCE PROGRAM EVALUATED THE TRANSVERSE FORCE.
C
YY:=Y1*EXP(I*K1*X)+Y3*EXP(I*K3*X);
FFF:=EI*DF(YY,X,3);
FF:=SUB(X=0,FFF);
BYE;

*****
* THIS FORTRAN PROGRAM DEVELOPED THE IMPEDANCE OF THE INFINITE *
* VISCOELASTIC BEAM USING BERNOULLI-EULER BEAM THEORY. *
*
* DEFINED VARIABLES;
* E : COMPLEX YOUNG'S MODULUS OF THE VISCOELASTIC BEAM
* F : FREQUENCY (HZ)
* FF : TRANSVERSE FORCE (LBF)
* G : COMPLEX SHEAR MODULUS OF THE VISCOELASTIC BEAM
* GRAV : GRAVITY (32.6 IN/SEC)
* IMP : IMPEDANCE OF THE VISCOELASTIC BEAM
* POISS : POISSON'S RATIO
* ROH : DENSITY OF THE VISCOELASTIC BEAM
```

```

* XB, XH,XL : DIMENSIONS OF THE BEAM (WIDTH, HEIGHT, LENGTH) *
* XI : AREA MOMENT OF INERTIA *
* XK1, XK2, XK3, XK4 : WAVE NUMBERS *
* XNETA : ENERGY LOSS FACTOR OF THE VISCOELASTIC BEAM *
* V1 : IMAGINARY (0,1) *
* ****
C
COMPLEX V1,G,E,KB1,KB2,XK1,XK2,XK3,XK4,P1,P3,A1,A2,A3,A4,FF,IMP
REAL F,POISS,GRAV,PI,XB,XH,XG,ROH,XI
REAL W,XLOG,XNETA,XA,XCA,XSA,KC,IMPR,IMPI
C
OPEN(UNIT=15,FILE='IFI')
C
CONSTANTS
C
F=10.0
POISS=0.45
GRAV=386.0
PI=3.1415926
V1=CMPLX(0.0,1.0)
C
DIMENSIONS
C
XB=1.0
XH=0.35
C
PROPERTIES
C
ROH=0.05505/GRAV
XI=(XB*XH**3)/12.0
C
FOUR DIFFERENT WAVE NUMBERS
C
DO 100 I=1,100
W=2*PI*F
XLOG=ABS(LOG10(F/62))
XNETA=0.65*EXP(-0.52732*XLOG**1.956)
C
XNETA=0.2
C
XNETA=0.5
XG=0.00002503*F**3-0.1752*F**2+457.5883*F+29280
C
XG=200000
G=XG**CMPLX(1.0,XNETA)
E=2*G*(1+POISS)
XA=ATAN(XNETA)/4.0
XCA=COS(-XA)
XSA=SIN(-XA)
KC=(SQRT(1+XNETA**2))**(-0.25)
KB1=-CSQRT(ROH*XB*XH*W**2/(E*XI))
KB2= CSQRT(ROH*XB*XH*W**2/(E*XI))
XK1= CSQRT(KB1)*KC*CMPLX(XCA,XSA)
XK2=-CSQRT(KB1)*KC*CMPLX(XCA,XSA)
XK3=-CSQRT(KB2)*KC*CMPLX(XCA,XSA)
XK4= CSQRT(KB2)*KC*CMPLX(XCA,XSA)
C

```

```

C      DEFINED CONSTANTS FROM THE THREE REDUCE PROGRAMS
C
C      P1=V1*XK1
C      P2=V1*XK2
C      P3=V1*XK3
C      P4=V1*XK4
C      A1= P3/(P3-P1)
C      A2=0
C      A3=-P1/(P3-P1)
C      A4=0
C      FF=-V1*E*XI*(A1*XK1**3+A3*XK3**3)

C      IMPEDANCES
C
C      IMP=2*FF/(V1*W)
C      IMPR=REAL(IMP)
C      IMPI=AIMAG(IMP)
C      WRITE(15,1000) F,IMPR,IMPI
C      F=F+20.0
100    CONTINUE
1000   FORMAT(1X,D9.3,2X,D12.5,2X,D12.5)
      CLOSE(UNIT=15)
      STOP
      END

```

**2. THE IMPEDANCE OF THE FINITE VISCOELASTIC BEAM USING
BERNOULLI-EULER BEAM THEORY**

```

YY:=Y1*EXP(I*K1*X)+Y2*EXP(I*K2*X)+Y3*EXP(I*K3*X)+Y4*EXP(I*K4*X);
PP:=DF(YY,X);
MM:=-EI*DF(PP,X);
FF:=-DF(MM,X);
Y0:=SUB(X=0,YY)-Y;
PO:=SUB(X=0,PP)-P;
ML:=SUB(X=L,MM);
FL:=SUB(X=L,FF);
BYE;
C
C      THE SECOND REDUCE PROGRAM SOLVED CONSTANT VARIABLES (Y1, Y2, Y3
C      AND Y4).
C
Y0:=Y1+Y2+Y3+Y4-Y;
PO:=P1*Y1+P2*Y2+P3*Y3+P4*Y4-P;
ML:=M1*Y1+M2*Y2+M3*Y3+M4*Y4;
FL:=F1*Y1+F2*Y2+F3*Y3+F4*Y4;
SOLVE(LST(Y0,PO,ML,FL),Y1,Y2,Y3,Y4);
BYE;
C
C      THE THIRD REDUCE PROGRAM EVALUATED THE TRANSVERSE FORCE.
C
YY:=Y1*EXP(I*K1*X)+Y2*EXP(I*K2*X)+Y3*EXP(I*K3*X)+Y4*EXP(I*K4*X);
FFF:=EI*DF(YY,X,3);
FF:=SUB(X=0,FFF);
BYE;

```

```

*****  

*  

* THIS FORTRAN PROGRAM DEVELOPED THE IMPEDANCE OF THE FINITE  

* VISCOELASTIC BEAM USING BERNOULLI-EULER BEAM THEORY.  

*  

* DEFINED VARIABLES;  

* E : COMPLEX YOUNG'S MODULUS OF THE VISCOELASTIC BEAM  

* F : FREQUENCY (HZ)  

* FF : TRANSVERSE FORCE (LBF)  

* G : COMPLEX SHEAR MODULUS OF THE VISCOELASTIC BEAM  

* GRAV : GRAVITY (386 IN/SEC)  

* IMP : IMPEDANCE OF THE VISCOELASTIC BEAM  

* POISS : POISSON'S RATIO  

* ROH : DENSITY OF THE VISCOELASTIC BEAM  

* XB, XH,XL : DIMENSIONS OF THE BEAM (WIDTH, HEIGHT, LENGTH)  

* XI : AREA MOMENT OF INERTIA  

* XK1, XK2, XK3, XK4 : WAVE NUMBERS  

* XNETA : ENERGY LOSS FACTOR OF THE VISCOELASTIC BEAM  

* V1 : IMAGINARY (0,1)  

*  

*****  

C  

      COMPLEX V1,G,E,KB1,KB2,XK1,XK2,XK3,XK4,P1,P2,P3,P4  

      COMPLEX M1,M2,M3,M4,F1,F2,F3,F4,DEN,A1,A2,A3,A4,FF,IMP  

      REAL F,POISS,GRAV,PI,XB,XL,XH,XG,ROH,XI,W,XLOG,XNETA,XA,XCA,XSA  

      REAL KC,KR1,KR2,KR3,KR4,KI1,KI2,KI3,KI4,IMPR,IMPI  

C  

      OPEN(UNIT=15,FILE='FFI')  

C  

C      CONSTANTS  

C  

      F=10.0  

      POISS=0.45  

      GRAV=386.0  

      PI=3.1415926  

      V1=CMPLX(0.0,1.0)  

C  

C      DIMENSIONS  

C  

      XB=1.0  

      XL=8.0  

      XH=0.35  

C  

C      PROPERTIES  

C  

      ROH=0.05505/GRAV  

C  

C      FOUR DIFFERENT WAVE NUMBERS  

C  

      XI=(XB*XH**3)/12.0  

      DO 100 I=1,100  

         W=2*PI**F  

         XLOG=ABS(LOG10(F/62))  

         XNETA=0.65*EXP(-0.52732*XLOG**1.956)  

C  

         XNETA=0.2  

         XNETA=0.5

```

```

C           XG=0. 00002503*F**3-0. 1752*F**2+457. 5883*F+29280
C           XG=200000
C           G=XG*CMPLX( 1. 0 ,XNETA)
C           E=2*G*( 1+POISS)
C           XA=ATAN(XNETA)/4. 0
C           XCA=COS(-XA)
C           XSA=SIN(-XA)
C           KC=( SQRT( 1+XNETA**2 ))**(-0. 25)
C           KB1=-CSQRT( ROH*XB*XH*W**2/( E*XI ))
C           KB2= CSQRT( ROH*XB*XH*W**2/( E*XI ))
C           XK1= CSQRT( KB1)*KC*CMPLX( XCA ,XSA)
C           XK2=-CSQRT( KB1)*KC*CMPLX( XCA ,XSA)
C           XK3=-CSQRT( KB2)*KC*CMPLX( XCA ,XSA)
C           XK4= CSQRT( KB2)*KC*CMPLX( XCA ,XSA)
C           KR1=REAL( XK1)
C           KR2=REAL( XK2)
C           KR3=REAL( XK3)
C           KR4=REAL( XK4)
C           KI1=AIMAG( XK1)
C           KI2=AIMAG( XK2)
C           KI3=AIMAG( XK3)
C           KI4=AIMAG( XK4)

C           DEFINED CONSTANTS FROM THE THREE REDUCE PROGRAMS
C
P1=V1*XK1
P2=V1*XK2
P3=V1*XK3
P4=V1*XK4
M1=EXP( -XL*KI1)*(COS( XL*KR1)+V1*SIN( XL*KR1))*XK1**2
M2=EXP( -XL*KI2)*(COS( XL*KR2)+V1*SIN( XL*KR2))*XK2**2
M3=EXP( -XL*KI3)*(COS( XL*KR3)+V1*SIN( XL*KR3))*XK3**2
M4=EXP( -XL*KI4)*(COS( XL*KR4)+V1*SIN( XL*KR4))*XK4**2
F1=EXP( -XL*KI1)*(COS( XL*KR1)+V1*SIN( XL*KR1))*XK1**3
F2=EXP( -XL*KI2)*(COS( XL*KR2)+V1*SIN( XL*KR2))*XK2**3
F3=EXP( -XL*KI3)*(COS( XL*KR3)+V1*SIN( XL*KR3))*XK3**3
F4=EXP( -XL*KI4)*(COS( XL*KR4)+V1*SIN( XL*KR4))*XK4**3
DEN=( F4*M3*P2-F4*M3*P1-F4*M2*P3+F4*M2*P1+F4*M1*P3-F4*M1*P2
&          -F3*M4*P2+F3*M4*P1+F3*M2*P4-F3*M2*P1-F3*M1*P4+F3*M1*P2
&          +F2*M4*P3-F2*M4*P1-F2*M3*P4+F2*M3*P1+F2*M1*P4-F2*M1*P3
&          -F1*M4*P3+F1*M4*P2+F1*M3*P4-F1*M3*P2-F1*M2*P4+F1*M2*P3)
A1=( F4*M3*P2-F4*M2*P3-F3*M4*P2+F3*M2*P4+F2*M4*P3-F2*M3*P4)
&          /DEN
A2=(-F4*M3*P1+F4*M1*P3+F3*M4*P1-F3*M1*P4-F1*M4*P3+F1*M3*P4)
&          /DEN
A3=( F4*M2*P1-F4*M1*P2-F2*M4*P1+F2*M1*P4+F1*M4*P2-F1*M2*P4)
&          /DEN
A4=(-F3*M2*P1+F3*M1*P2+F2*M3*P1-F2*M1*P3-F1*M3*P2+F1*M2*P3)
&          /DEN
FF=-V1*E*XI*(A1*XK1**3+A2*XK2**3+A3*XK3**3+A4*XK4**3)

C           IMPEDANCES
C
IMP=2*FF/(V1*W)
IMPR=REAL(IMP)
IMPI=AIMAG(IMP)

```

```

        WRITE(15,1000) F,IMPR,IMPI
        F=F+20.0
100   CONTINUE
1000  FORMAT(1K,D9.3,2X,D12.5,2X,D12.5)
      CLOSE(UNIT=15)
      STOP
      END

```

3. THE IMPEDANCE OF THE FINITE VISCOELASTIC BEAM USING TIMOSHENKO BEAM THEORY

```

*****
*
*   THE THREE REDUCE PROGRAMS WERE USED FOR EVALUATING THE IMPEDANCE *
*   OF THE FINITE VISCOELASTIC BEAM USING TIMOSHENKO BEAM THEORY.    *
*
*****
C
C   THE FIRST REDUCE PROGRAM DEFINED SHEAR FORCE AND FOUR BOUNDARY
C   CONDITIONS.
C
YY:=Y1*EXP(I*K1*X)+Y2*EXP(I*K2*X)+Y3*EXP(I*K3*X)+Y4*EXP(I*K4*X);
PP1:=R1*Y1*EXP(I*K1*X)+R2*Y2*EXP(I*K2*X);
PP2:=R3*Y3*EXP(I*K3*X)+R4*Y4*EXP(I*K4*X);
PP:=PP1+PP2;
MM:=DF(PP,X);
SS:=-(DF(YY,X)-PP);
YO:=SUB(X=0,YY)-Y;
PO:=SUB(X=0,PP)-P;
ML:=SUB(X=L,MM);
SL:=SUB(X=L,SS);
BYE;
C
C   THE SECOND REDUCE PROGRAM SOLVED CONSTANT VARIABLES (Y1, Y2,
C   Y3 AND Y4).
C
YO:=Y1+Y2+Y3+Y4-Y;
PO:=R1*Y1+R2*Y2+R3*Y3+R4*Y4-P;
ML:=M1*Y1+M2*Y2+M3*Y3+M4*Y4;
SL:=S1*Y1+S2*Y2+S3*Y3+S4*Y4;
SOLVE(LST(YO,PO,ML,SL),Y1,Y2,Y3,Y4);
BYE;
C
C   THE THIRD REDUCE PROGRAM EVALUATED THE SHEAR FORCE.
C
YY:=Y1*EXP(I*K1*X)+Y2*EXP(I*K2*X)+Y3*EXP(I*K3*X)+Y4*EXP(I*K4*X);
PP1:=R1*Y1*EXP(I*K1*X)+R2*Y2*EXP(I*K2*X);
PP2:=R3*Y3*EXP(I*K3*X)+R4*Y4*EXP(I*K4*X);
PP:=PP1+PP2;
SSS:=-KA*GG*AA*(DF(YY,X)-PP);
SS:=SUB(X=0,SSS);
BYE;

*****
*
*   THIS FORTRAN PROGRAM DEVELOPED THE IMPEDANCE OF THE FINITE

```

```

* VISCOELASTIC BEAM USING TIMOSHENKO BEAM THEORY. *
* DEFINED VARIABLES:
* E : COMPLEX YOUNG'S MODULUS OF THE VISCOELASTIC BEAM *
* F : FREQUENCY (HZ) *
* G : COMPLEX SHEAR MODULUS OF THE VISCOELASTIC BEAM *
* GRAV : GRAVITY (386 IN/SEC) *
* IMP : IMPEDANCE OF THE VISCOELASTIC BEAM *
* KAR : SHAPE OF CROSS SECTION *
* POISS : POISSON'S RATIO *
* ROH : DENSITY OF THE VISCOELASTIC BEAM *
* SS : SHEAR FORCE (LBF) *
* XB, XH, XL : DIMENSIONS OF THE BEAM (WIDTH, HEIGHT, LENGTH) *
* XI : AREA MOMENT OF INERTIA *
* XK1, XK2, XK3, XK4 : WAVE NUMBERS *
* XNETA : ENERGY LOSS FACTOR OF THE VISCOELASTIC BEAM *
* V1 : IMAGINARY (0,1) *
***** C
C      COMPLEX V1,G,E,XKN1,XKN2,XKD,XK1,XK2,XK3,XK4,R1,R2,R3,R4
C      COMPLEX M1,M2,M3,M4,S1,S2,S3,S4,DEN,A1,A2,A3,A4,SS,IMP
C      REAL F,KAR,POISS,GRAV,PI,XB,XL,XH,XG,ROH,XI,W,XLOG,XNETA
C      REAL KR1,KR2,KR3,KR4,KI1,KI2,KI3,KI4,IMPR,IMPI
C      OPEN(UNIT=15,FILE='TIM')
C      CONSTANTS
C      F=10.0
C      KAR=0.83
C      POISS=0.45
C      GRAV=386.0
C      PI=3.1415926
C      V1=CMPLX(0.0,1.0)
C      DIMENSIONS
C      XB=1.0
C      XL=8.0
C      XH=0.35
C      PROPERTIES
C      ROH=0.05505/GRAV
C      XI=(XB*XH**3)/12.0
C      FOUR DIFFERENT WAVE NUMBERS
C      DO 100 I=1,100
C          W=2*PI*F
C          XLOG=ABS(LOG10(F/62))
C          XNETA=0.65*EXP(-0.52732*XLOG**1.956)
C          XNETA=0.2
C          XNETA=0.5

```

```

C XG=0.00002503**F**3-0.1752**F**2+457.5683**F+29280
C XG=200000
C G=XG*CMPLX(1.0,XNETA)
C E=2*G*(1+POISS)
C XKN1=W**2*(KAR*G+E)/ROH
C XKN2= SQRT(W**4*((KAR*G+E)/ROH)**2
C & -4*KAR*G*E*(W**4-KAR*G*XB*XH*W**2/(ROH*XI))
C & /(ROH**2))
C XKD=2*KAR*G*E/(ROH**2)
C XK1= CSQRT((XKN1+XKN2)/XKD)
C XK2=-CSQRT((XKN1+XKN2)/XKD)
C XK3= CSQRT((XKN1-XKN2)/XKD)
C XK4=-CSQRT((XKN1-XKN2)/XKD)
C KR1=REAL(XK1)
C KR2=REAL(XK2)
C KR3=REAL(XK3)
C KR4=REAL(XK4)
C KI1=AIMAG(XK1)
C KI2=AIMAG(XK2)
C KI3=AIMAG(XK3)
C KI4=AIMAG(XK4)

C DEFINED CONSTANTS FROM THE THREE REDUCE PROGRAMS
C
R1=(ROH*W**2-KAR*G*XK1**2)/(V1*KAR*G*XK1)
R2=(ROH*W**2-KAR*G*XK2**2)/(V1*KAR*G*XK2)
R3=(ROH*W**2-KAR*G*XK3**2)/(V1*KAR*G*XK3)
R4=(ROH*W**2-KAR*G*XK4**2)/(V1*KAR*G*XK4)
M1=EXP(-XL*KI1)*(COS(XL*KR1)+V1*SIN(XL*KR1))*V1*XK1*R1
M2=EXP(-XL*KI2)*(COS(XL*KR2)+V1*SIN(XL*KR2))*V1*XK2*R2
M3=EXP(-XL*KI3)*(COS(XL*KR3)+V1*SIN(XL*KR3))*V1*XK3*R3
M4=EXP(-XL*KI4)*(COS(XL*KR4)+V1*SIN(XL*KR4))*V1*XK4*R4
S1=EXP(-XL*KI1)*(COS(XL*KR1)+V1*SIN(XL*KR1))*(R1-V1*XK1)
S2=EXP(-XL*KI2)*(COS(XL*KR2)+V1*SIN(XL*KR2))*(R2-V1*XK2)
S3=EXP(-XL*KI3)*(COS(XL*KR3)+V1*SIN(XL*KR3))*(R3-V1*XK3)
S4=EXP(-XL*KI4)*(COS(XL*KR4)+V1*SIN(XL*KR4))*(R4-V1*XK4)
DEN=( S4*M3*R2-S4*M3*R1-S4*M2*R3+S4*M2*R1+S4*M1*R3-S4*M1*R2
& -S3*M4*R2+S3*M4*R1+S3*M2*R4-S3*M2*R1-S3*M1*R4+S3*M1*R2
& +S2*M4*R3-S2*M4*R1-S2*M3*R4+S2*M3*R1+S2*M1*R4-S2*M1*R3
& -S1*M4*R3+S1*M4*R2+S1*M3*R4-S1*M3*R2-S1*M2*R4+S1*M2*R3 )
A1=( S4*M3*R2-S4*M2*R3-S3*M4*R2+S3*M2*R4+S2*M4*R3-S2*M3*R4 )
& /DEN
A2=(-S4*M3*R1+S4*M1*R3+S3*M4*R1-S3*M1*R4-S1*M4*R3+S1*M3*R4)
& /DEN
A3=( S4*M2*R1-S4*M1*R2-S2*M4*R1+S2*M1*R4+S1*M4*R2-S1*M2*R4)
& /DEN
A4=(-S3*M2*R1+S3*M1*R2+S2*M3*R1-S2*M1*R3-S1*M3*R2+S1*M2*R3)
& /DEN
SS=KAR*G*XB*XH*( A1*(R1-V1*XK1)+A2*(R2-V1*XK2)+A3*(R3-V1*XK3)
& +A4*(R4-V1*XK4) )

C IMPEDANCES
C
IMP=2*SS/(V1*W)
IMPR=REAL(IMP)
IMPI=AIMAG(IMP)

```

```

        WRITE(15,1000) F,IMPR,IMPI
        F=F+20.0
100    CONTINUE
1000   FORMAT(1X,D9.3,2X,D12.5,2X,D12.5)
      CLOSE(UNIT=15)
      STOP
      END

```

4. THE IMPEDANCE OF THE FINITE CONSTRAINED LAYER BEAM USING THE SIXTH ORDER BEAM THEORY

```

*****
*
*   THE THREE REDUCE PROGRAMS WERE USED FOR EVALUATING THE IMPEDANCE *
*   OF THE INFINITE VISCOELASTIC BEAM USING BERNOULLI-EULER BEAM      *
*   THEORY.                                                               *
*
*****
C
C   THE FIRST REDUCE PROGRAM DEFINED TRANSVERSE FORCE AND TWO BOUNDARY
C   CONDITIONS.
C
YY1:=Y1*EXP(I*K1*X)+Y2*EXP(I*K2*X);
YY2:=Y3*EXP(I*K3*X)+Y4*EXP(I*K4*X);
YY3:=Y5*EXP(I*K5*X)+Y6*EXP(I*K6*X);
UU1:=R1*Y1*EXP(I*K1*X)+R2*Y2*EXP(I*K2*X);
UU2:=R3*Y3*EXP(I*K3*X)+R4*Y4*EXP(I*K4*X);
UU3:=R5*Y5*EXP(I*K5*X)+R6*Y6*EXP(I*K6*X);
YYY:=YY1+YY2+YY3;
UUU:=UU1+UU2+UU3;
Y0:=SUB(X=0,YYY)-Y;
P0:=SUB(X=0,DF(YYY,X))-P;
U0:=SUB(X=0,UUU)-U;
SL:=SUB(X=L,(PP*DF(YYY,X,3)+QQ*DF(YYY,X)+RR*UUU));
ML:=SUB(X=L,(PP*DF(YYY,X,2)+SS*DF(UUU,X)));
NL:=SUB(X=L,(TT*DF(UUU,X)));
BYE;
C
C   THE SECOND REDUCE PROGRAM SOLVED CONSTANT VARIABLES (Y4, Y5,
C   AND Y6).
C
Y0:=Y1+Y2+Y3+Y4+Y5+Y6-Y;
P0:=P1*Y1+P2*Y2+P3*Y3+P4*Y4+P5*Y5+P6*Y6-P;
U0:=R1*Y1+R2*Y2+R3*Y3+R4*Y4+R5*Y5+R6*Y6-U;
SL:=S1*Y1+S2*Y2+S3*Y3+S4*Y4+S5*Y5+S6*Y6;
ML:=M1*Y1+M2*Y2+M3*Y3+M4*Y4+M5*Y5+M6*Y6;
NL:=N1*Y1+N2*Y2+N3*Y3+N4*Y4+N5*Y5+N6*Y6;
SOLVE(LST(SL,ML,NL),Y4,Y5,Y6);
BYE;
C
C   THE THIRD REDUCE PROGRAM SOLVED VARIABLES (Y1, Y2 AND Y3) USING
C   Y4, Y5 AND Y6. THE THIRD REDUCE PROGRAM EVALUATED THE SHEAR FORCE.
C
Y4:=B1*Y1+C1*Y2+D1*Y3;
Y5:=B2*Y1+C2*Y2+D2*Y3;
Y6:=B3*Y1+C3*Y2+D3*Y3;
Y0:=Y1+Y2+Y3+Y4+Y5+Y6-Y;

```

```

P0:=P1*Y1+P2*Y2+P3*Y3+P4*Y4+P5*Y5+P6*Y6-P;
U0:=R1*Y1+R2*Y2+R3*Y3+R4*Y4+R5*Y5+R6*Y6-U;
SOLVE(LST(Y0,P0,U0),Y1,Y2,Y3);
YYY1:=Y1*EXP(I*K1*X)+Y2*EXP(I*K2*X);
YYY2:=Y3*EXP(I*K3*X)+Y4*EXP(I*K4*X);
YYY3:=Y5*EXP(I*K5*X)+Y6*EXP(I*K6*X);
YYYY:=YYY1+YYY2+YYY3;
UUU1:=R1*Y1*EXP(I*K1*X)+R2*Y2*EXP(I*K2*X);
UUU2:=R3*Y3*EXP(I*K3*X)+R4*Y4*EXP(I*K4*X);
UUU3:=R5*Y5*EXP(I*K5*X)+R6*Y6*EXP(I*K6*X);
UUUU:=UUU1+UUU2+UUU3;
SSS:=PP*DF(YYYY,X,3)+QQ*DF(YYYY,X)+RR*UUUU;
SS:=SUB(X=0,SSS);
BYE;

```

```

*****
*
* THIS FORTRAN PROGRAM DEVELOPED THE IMPEDANCE OF THE CONSTRAINED
* LAYER BEAM USING THE 6TH ORDER BEAM THEORY.
*
* DEFINED VARIABLES:
* E1, E3 : COMPLEX YOUNG'S MODULUS OF THE CONSTRAINED LAYER
* F : FREQUENCY (HZ)
* G : COMPLEX SHEAR MODULUS OF THE VISCOELASTIC
* GRAV : GRAVITY (386 IN/SEC**2)
* H1, H3 : HEIGHT OF THE CONSTRAINED LAYER
* H2 : HEIGHT OF THE VISCOELASTIC
* I1, I2 : AREA MOMENT OF INERTIA
* IMP : IMPEDANCE OF THE CONSTRAINED LAYER BEAM
* KAR : SHAPE OF CROSS SECTION
* POISS : POISSON'S RATIO
* ROH1 : DENSITY OF THE CONSTRAINED LAYER
* ROH2 : DENSITY OF THE VISCOELASTIC
* SS : SHEAR FORCE (LBF)
* XB, XL : DIMENSIONS OF THE BEAM (WIDTH, LENGTH)
* XK1, XK2, XK3, XK4, XK5, XK6 : WAVE NUMBERS
* XNETA : ENERGY LOSS FACTOR OF THE VISCOELASTIC BEAM
* V1 : IMAGINARY (0,1)
*
*****
```

```

C
COMPLEX*32 V1,G,BB,P1,P2,P3,P4,P5,P6,R1,R2,R3,R4,R5,R6,QQ,RR
COMPLEX*32 S1,S2,S3,S4,S5,S6,M1,M2,M3,M4,M5,M6,N1,N2,N3,N4,N5,N6
COMPLEX*32 B1,C1,D1,B2,C2,D2,B3,C3,D3,DEN1,DEN2,A1,A2,A3
COMPLEX B,D,XK1,XK2,XK3,XK4,XK5,XK6,XXK1,XXK2,XXK3,IMP
REAL*16 F,PI,GRAV,XB,XL,XG,H1,H2,H3,E1,E3,I1,I3,DD,ROH1,ROH2
REAL*16 CC,XM,T1(30),T2(30),T3(30),Q1(30),Q2(30),Q3(30)
REAL*16 XLOG,W,Z,C,BI,CR,DR,DI,FT1,FQ1,DTT1,DTQ1,DQQ1,DQT1
REAL*16 FT2,FQ2,DTT2,DTQ2,DQQ2,DQT2,FT3,FQ3,DTT3,DTQ3,DQQ3,DQT3
REAL*16 XKR1,XKR2,XKR3,XKI1,XKI2,XKI3,KR1,KR2,KR3,KR4,KR5,KR6
REAL*16 KI1,KI2,KI3,KI4,KI5,KI6,PP,SS,TT,IMPR,IMPI
REAL XNETA
```

```

C
OPEN(UNIT=15,FILE='SAN')
C
```

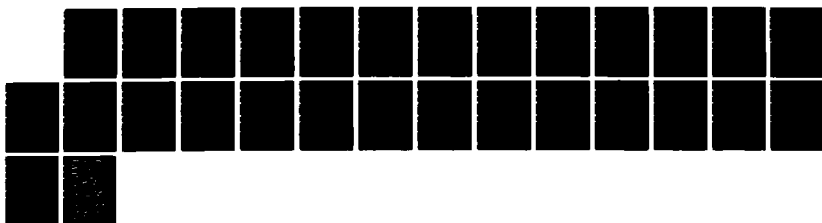
ND-A195 885

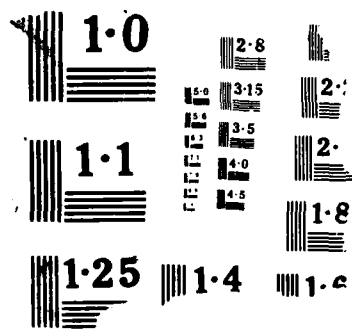
ANALYTICAL AND EXPERIMENTAL STUDIES OF BEAM WAVEGUIDE
ABSORBERS FOR STRUCTURAL DAMPING(U) NAVAL POSTGRADUATE
SCHOOL MONTEREY CA G G LEE MAR 88

2/2

UNCLASSIFIED

F/G 13/10.1 NL





```

C      CONSTANTS
C
C      F=2010
C      PI=3. 1415926
C      GRAV=386. 0
C      V1=CMPLX(0. 0,1. 0)
C
C      DIMENSIONS
C
C      XB=1. 0
C      XL=8. 0
C      H1=0. 0625
C      H2=0. 065
C      H3=0. 0625
C
C      PROPERITIES
C
C      E1=10000000. 0
C      E3=10000000. 0
C      I1=XB**H1**3/12.
C      I3=XB**H3**3/12.
C      DD=E1*I1+E3*I3
C      ROH1=0. 09832/GRAV
C      ROH2=0. 03663/GRAV
C      CC=H1/2.+H2+H3/2.
C      XM=XB*((H1+H3)*ROH1+H2*ROH2)
C
C      INITIAL GUESS WAVE NUMBERS
C
C      T1(1)=-4. 31911862
C      T2(1)=-0. 05139608
C      T3(1)= 3. 77697017
C      Q1(1)=-0. 33835599
C      Q2(1)=-0. 05104052
C      Q3(1)=-0. 27669665
C
C      FIND SIX DIFFERENT WAVE NUMBERS USING NEWTON'S METHOD
C      SIX DIFFERENT WAVE NUMBERS ARE XK1,XK2,XK3,XK4,XK5,XK6
C
C      DO 100 I=1,100
C          W=2*PI*F
C          XLOG=ABS(LOG10(F/800))
C          XNETA=1. 1*EXP(-0. 3906*XLOG**1. 53)
C          XNETA=0. 5
C          XNETA=1. 0
C          KG=-0. 00001258*F**2+0. 2472*F+74. 988
C          XG=1000
C          G=XG*CMPLX(1. 0,XNETA)
C          BB=G*(E1*H1+E3*H3)/(H2*E1*H1*E3*H3)
C          Z=CC**2*E1*H1*E3*H3/(DD*(E1*H1+E3*H3))
C          B=BB*(1. 0+Z)
C          C=-XM*W**2/DD
C          D=-BB*XM*W**2/DD
C          BR=REAL(B)
C          BI=AIMAG(B)
C          CR=C

```

```

DR=REAL(D)
DI=AIMAG(D)
DO 200 J=1,15
  FT1=T1(J)**3+BR*T1(J)**2+(-3*Q1(J)**2-2*BI*Q1(J)+CR)*T1(J)
&           +(-BR*Q1(J)**2+DR)
  FQ1=Q1(J)**3+BI*Q1(J)**2+(-3*T1(J)**2-2*BR*T1(J)-CR)*Q1(J)
&           +(-BI*T1(J)**2-DI)
  DTT1=3*T1(J)**2+2*BR*T1(J)
&           +(-3*Q1(J)**2-2*BI*Q1(J)+CR)
  DTQ1=(-6*T1(J)-2*BR)*Q1(J)-2*BI*T1(J)
  DQQ1=3*Q1(J)**2+2*BI*Q1(J)
&           +(-3*T1(J)**2-2*BR*T1(J)-CR)
  DQT1=(-6*Q1(J)-2*BI)*T1(J)-2*BR*Q1(J)
  T1(J+1)=T1(J)-(DQQ1*FT1-DTQ1*FQ1)/(DTT1*DQQ1-DTQ1*DQT1)
  Q1(J+1)=Q1(J)-(-DQT1*FT1+DTT1*FQ1)/(DTT1*DQQ1-DTQ1*DQT1)
  FT2=T2(J)**3+BR*T2(J)**2+(-3*Q2(J)**2-2*BI*Q2(J)+CR)*T2(J)
&           +(-BR*Q2(J)**2+DR)
  FQ2=Q2(J)**3+BI*Q2(J)**2+(-3*T2(J)**2-2*BR*T2(J)-CR)*Q2(J)
&           +(-BI*T2(J)**2-DI)
  DTT2=3*T2(J)**2+2*BR*T2(J)
&           +(-3*Q2(J)**2-2*BI*Q2(J)+CR)
  DTQ2=(-6*T2(J)-2*BR)*Q2(J)-2*BI*T2(J)
  DQQ2=3*Q2(J)**2+2*BI*Q2(J)
&           +(-3*T2(J)**2-2*BR*T2(J)-CR)
  DQT2=(-6*Q2(J)-2*BI)*T2(J)-2*BR*Q2(J)
  T2(J+1)=T2(J)-(DQQ2*FT2-DTQ2*FQ2)/(DTT2*DQQ2-DTQ2*DQT2)
  Q2(J+1)=Q2(J)-(-DQT2*FT2+DTT2*FQ2)/(DTT2*DQQ2-DTQ2*DQT2)
  FT3=T3(J)**3+BR*T3(J)**2+(-3*Q3(J)**2-2*BI*Q3(J)+CR)*T3(J)
&           +(-BR*Q3(J)**2+DR)
  FQ3=Q3(J)**3+BI*Q3(J)**2+(-3*T3(J)**2-2*BR*T3(J)-CR)*Q3(J)
&           +(-BI*T3(J)**2-DI)
  DTT3=3*T3(J)**2+2*BR*T3(J)
&           +(-3*Q3(J)**2-2*BI*Q3(J)+CR)
  DTQ3=(-6*T3(J)-2*BR)*Q3(J)-2*BI*T3(J)
  DQQ3=3*Q3(J)**2+2*BI*Q3(J)
&           +(-3*T3(J)**2-2*BR*T3(J)-CR)
  DQT3=(-6*Q3(J)-2*BI)*T3(J)-2*BR*Q3(J)
  T3(J+1)=T3(J)-(DQQ3*FT3-DTQ3*FQ3)/(DTT3*DQQ3-DTQ3*DQT3)
  Q3(J+1)=Q3(J)-(-DQT3*FT3+DTT3*FQ3)/(DTT3*DQQ3-DTQ3*DQT3)
200  CONTINUE
XKR1= T1(J)
XKR2= T2(J)
XKR3= T3(J)
XXI1= Q1(J)
XXI2= Q2(J)
XXI3= Q3(J)
XXX1=CMPLX(XKR1,XXI1)
XXX2=CMPLX(XKR2,XXI2)
XXX3=CMPLX(XKR3,XXI3)
XK1= CSQRT(XXX1)
XK2=-CSQRT(XXX1)
XK3= CSQRT(XXX2)
XK4=-CSQRT(XXX2)
XK5= CSQRT(XXX3)
XK6=-CSQRT(XXX3)
KR1= REAL(XK1)

```

```

KR2= REAL(XK2)
KR3= REAL(XK3)
KR4= REAL(XK4)
KR5= REAL(XK5)
KR6= REAL(XK6)
KI1=AIMAG(XK1)
KI2=AIMAG(XK2)
KI3=AIMAG(XK3)
KI4=AIMAG(XK4)
KI5=AIMAG(XK5)
KI6=AIMAG(XK6)

C
C      DEFINED CONSTANTS FROM THE THREE REDUCE PROGRAMS
C

P1=V1*XK1
P2=V1*XK2
P3=V1*XK3
P4=V1*XK4
P5=V1*XK5
P6=V1*XK6
R1=V1*BB*Z*DD*XK1/((XK1**2+BB)*E3*H3*CC)
R2=V1*BB*Z*DD*XK2/((XK2**2+BB)*E3*H3*CC)
R3=V1*BB*Z*DD*XK3/((XK3**2+BB)*E3*H3*CC)
R4=V1*BB*Z*DD*XK4/((XK4**2+BB)*E3*H3*CC)
R5=V1*BB*Z*DD*XK5/((XK5**2+BB)*E3*H3*CC)
R6=V1*BB*Z*DD*XK6/((XK6**2+BB)*E3*H3*CC)
PP=DD
QQ=-DD*BB*Z
RR=DD*BB*Z*(E1*H1+E3*H3)/(CC*E1*H1)
SS=-CC*E3*H3
TT=E3*H3
S1=(-V1*PP*XK1**3+V1*QQ*XK1+RR*R1)*EXP(-XL*KI1)
&   *(COS(XL*KR1)+V1*SIN(XL*KR1))
S2=(-V1*PP*XK2**3+V1*QQ*XK2+RR*R2)*EXP(-XL*KI2)
&   *(COS(XL*KR2)+V1*SIN(XL*KR2))
S3=(-V1*PP*XK3**3+V1*QQ*XK3+RR*R3)*EXP(-XL*KI3)
&   *(COS(XL*KR3)+V1*SIN(XL*KR3))
S4=(-V1*PP*XK4**3+V1*QQ*XK4+RR*R4)*EXP(-XL*KI4)
&   *(COS(XL*KR4)+V1*SIN(XL*KR4))
S5=(-V1*PP*XK5**3+V1*QQ*XK5+RR*R5)*EXP(-XL*KI5)
&   *(COS(XL*KR5)+V1*SIN(XL*KR5))
S6=(-V1*PP*XK6**3+V1*QQ*XK6+RR*R6)*EXP(-XL*KI6)
&   *(COS(XL*KR6)+V1*SIN(XL*KR6))
M1=(V1*SS*R1*XK1-PP*XK1**2)*EXP(-XL*KI1)
&   *(COS(XL*KR1)+V1*SIN(XL*KR1))
M2=(V1*SS*R2*XK2-PP*XK2**2)*EXP(-XL*KI2)
&   *(COS(XL*KR2)+V1*SIN(XL*KR2))
M3=(V1*SS*R3*XK3-PP*XK3**2)*EXP(-XL*KI3)
&   *(COS(XL*KR3)+V1*SIN(XL*KR3))
M4=(V1*SS*R4*XK4-PP*XK4**2)*EXP(-XL*KI4)
&   *(COS(XL*KR4)+V1*SIN(XL*KR4))
M5=(V1*SS*R5*XK5-PP*XK5**2)*EXP(-XL*KI5)
&   *(COS(XL*KR5)+V1*SIN(XL*KR5))
M6=(V1*SS*R6*XK6-PP*XK6**2)*EXP(-XL*KI6)
&   *(COS(XL*KR6)+V1*SIN(XL*KR6))
N1=V1*TT*R1*XK1*EXP(-XL*KI1)

```

```

& *(COS(XL*KR1)+V1*SIN(XL*KR1))
N2=V1*TT*R2*XK2*EXP(-XL*KI2)
& *(COS(XL*KR2)+V1*SIN(XL*KR2))
N3=V1*TT*R3*XK3*EXP(-XL*KI3)
& *(COS(XL*KR3)+V1*SIN(XL*KR3))
N4=V1*TT*R4*XK4*EXP(-XL*KI4)
& *(COS(XL*KR4)+V1*SIN(XL*KR4))
N5=V1*TT*R5*XK5*EXP(-XL*KI5)
& *(COS(XL*KR5)+V1*SIN(XL*KR5))
N6=V1*TT*R6*XK6*EXP(-XL*KI6)
& *(COS(XL*KR6)+V1*SIN(XL*KR6))

B1=(-N6*M5*S1+N6*M1*S5+N5*M6*S1-N5*M1*S6-N1*M6*S5+N1*M5*S6)
& /(N6*M5*S4-N6*M4*S5-N5*M6*S4+N5*M4*S6+N4*M6*S5-N4*M5*S6)
C1=(-N6*M5*S2+N6*M2*S5+N5*M6*S2-N5*M2*S6-N2*M6*S5+N2*M5*S6)
& /(N6*M5*S4-N6*M4*S5-N5*M6*S4+N5*M4*S6+N4*M6*S5-N4*M5*S6)
D1=(-N6*M5*S3+N6*M3*S5+N5*M6*S3-N5*M3*S6-N3*M6*S5+N3*M5*S6)
& /(N6*M5*S4-N6*M4*S5-N5*M6*S4+N5*M4*S6+N4*M6*S5-N4*M5*S6)
B2=(N6*M4*S1-N6*M1*S4-N4*M6*S1+N4*M1*S6+N1*M6*S4-N1*M4*S6)
& /(N6*M5*S4-N6*M4*S5-N5*M6*S4+N5*M4*S6+N4*M6*S5-N4*M5*S6)
C2=(N6*M4*S2-N6*M2*S4-N4*M6*S2+N4*M2*S6+N2*M6*S4-N2*M4*S6)
& /(N6*M5*S4-N6*M4*S5-N5*M6*S4+N5*M4*S6+N4*M6*S5-N4*M5*S6)
D2=(N6*M4*S3-N6*M3*S4-N4*M6*S3+N4*M3*S6+N3*M6*S4-N3*M4*S6)
& /(N6*M5*S4-N6*M4*S5-N5*M6*S4+N5*M4*S6+N4*M6*S5-N4*M5*S6)
B3=(-N5*M4*S1+N5*M1*S4+N4*M5*S1-N4*M1*S5-N1*M5*S4+N1*M4*S5)
& /(N6*M5*S4-N6*M4*S5-N5*M6*S4+N5*M4*S6+N4*M6*S5-N4*M5*S6)
C3=(-N5*M4*S2+N5*M2*S4+N4*M5*S2-N4*M2*S5-N2*M5*S4+N2*M4*S5)
& /(N6*M5*S4-N6*M4*S5-N5*M6*S4+N5*M4*S6+N4*M6*S5-N4*M5*S6)
D3=(-N5*M4*S3+N5*M3*S4+N4*M5*S3-N4*M3*S5-N3*M5*S4+N3*M4*S5)
& /(N6*M5*S4-N6*M4*S5-N5*M6*S4+N5*M4*S6+N4*M6*S5-N4*M5*S6)
DEN1=(R6*P5-R5*P6)*(D3*C2*B1+D3*C2-D3*B2*C1-D3*B2-C3*D2*B1
& -C3*D2+C3*B2*D1+C3*B2+B3*D2*C1+B3*D2
& -B3*C2*D1-B3*C2)
& +(R4*P6-R6*P4)*(D3*C2*B1-D3*B2*C1-D3*C1+D3*B1-C3*D2*B1
& +C3*B2*D1+C3*D1-C3*B1+B3*D2*C1-B3*C2*D1
& -B3*D1+B3*C1)
& +(R5*P4-R4*P5)*(D3*C2*B1-D3*B2*C1-C3*D2*B1+C3*B2*D1
& +B3*D2*C1-B3*C2*D1+D2*C1-D2*B1-C2*D1
& +C2*B1+B2*D1-B2*C1)
DEN2=(R3*P6-R6*P3)*(C3*B2+C3*B1+C3-B3*C2-B3*C1-B3)
& +(R6*P2-R2*P6)*(D3*B2+D3*B1+D3-B3*D2-B3*D1-B3)
& +(R1*P6-R6*P1)*(D3*C2+D3*C1+D3-C3*D2-C3*D1-C3)
& +(R5*P3-R3*P5)*(C3*B2-B3*C2-C2*B1-C2+B2*C1+B2)
& +(R2*P5-R5*P2)*(D3*B2-B3*D2-D2*B1-D2+B2*D1+B2)
& +(R5*P1-R1*P5)*(D3*C2-C3*D2-D2*C1-D2+C2*D1+C2)
& +(R4*P3-R3*P4)*(C3*B1-B3*C1+C2*B1-B2*C1-C1+B1)
& +(R2*P4-R4*P2)*(D3*B1-B3*D1+D2*B1-B2*D1-D1+B1)
& +(R4*P1-R1*P4)*(D3*C1-C3*D1+D2*C1-C2*D1-D1+C1)
& +(R3*P2-R2*P3)*(B3+B2+B1+1)
& +(R1*P3-R3*P1)*(C3+C2+C1+1)
& +(R2*P1-R1*P2)*(D3+D2+D1+1)

A1=( R6*( P5*D3*C2-P5*C3*D2+P4*D3*C1-P4*C3*D1-P3*C3+P2*D3)
& + R5*(-P6*D3*C2+P6*C3*D2+P4*D2*C1-P4*C2*D1-P3*C2+P2*D2)
& + R4*(-P6*D3*C1+P6*C3*D1-P5*D2*C1+P5*C2*D1-P3*C1+P2*D1)
& + R3*( P6*C3+P5*C2+P4*C1+P2)
& + R2*(-P6*D3-P5*D2-P4*D1-P3) )/(DEN1+DEN2)
A2=( R6*(-P5*D3*B2+P5*B3*D2-P4*D3*B1+P4*B3*D1+P3*B3-P1*D3)

```

```

& + R5*( P6*D3*B2-P6*B3*D2-P4*D2*B1+P4*B2*D1+P3*B2-P1*D2)
& + R4*( P6*D3*B1-P6*B3*D1+P5*D2*B1-P5*B2*D1+P3*B1-P1*D1)
& + R3*(-P6*B3-P5*B2-P4*B1-P1)
& + R1*( P6*D3+P5*D2+P4*D1+P3) )/(DEN1+DEN2)
A3=( R6*( P5*C3*B2-P5*B3*C2+P4*C3*B1-P4*B3*C1-P2*B3+P1*C3)
& + R5*(-P6*C3*B2+P6*B3*C2+P4*C2*B1-P4*B2*C1-P2*B2+P1*C2)
& + R4*(-P6*C3*B1+P6*B3*C1-P5*C2*B1+P5*B2*C1-P2*B1+P1*C1)
& + R2*( P6*B3+P5*B2+P4*B1+P1)
& + R1*(-P6*C3-P5*C2-P4*C1-P2) )/(DEN1+DFN2)

C
C IMPEDANCES
C

IMP=2*( (R4*RR+V1*QQ*XK4-V1*PP*XK4**3)*(D1*A3+C1*A2+B1*A1)
& + (R5*RR+V1*QQ*XK5-V1*PP*XK5**3)*(D2*A3+C2*A2+B2*A1)
& + (R6*RR+V1*QQ*XK6-V1*PP*XK6**3)*(D3*A3+C3*A2+B3*A1)
& + RR*(R3*A3+R2*A2+R1*A1)
& + V1*QO*(XK3*A3+XK2*A2+XK1*A1)
& -V1*PP*(K3**3*A3+K2**3*A2+K1**3*A1) )/(V1*W)
IMPR=REAL(IMP)
IMPI=AIMAG(IMP)
WRITE(15,1000)F,IMPR,IMPI
F=F-20
T1(1)=T1(J)
T2(1)=T2(J)
T3(1)=T3(J)
Q1(1)=Q1(J)
Q2(1)=Q2(J)
Q3(1)=Q3(J)
100 CONTINUE
1000 FORMAT(1X,D9.3,2X,D12.5,2X,D12.5)
CLOSE(UNIT=15)
STOP
END

```

APPENDIX B.

IMPEDANCES VS. FREQUENCY

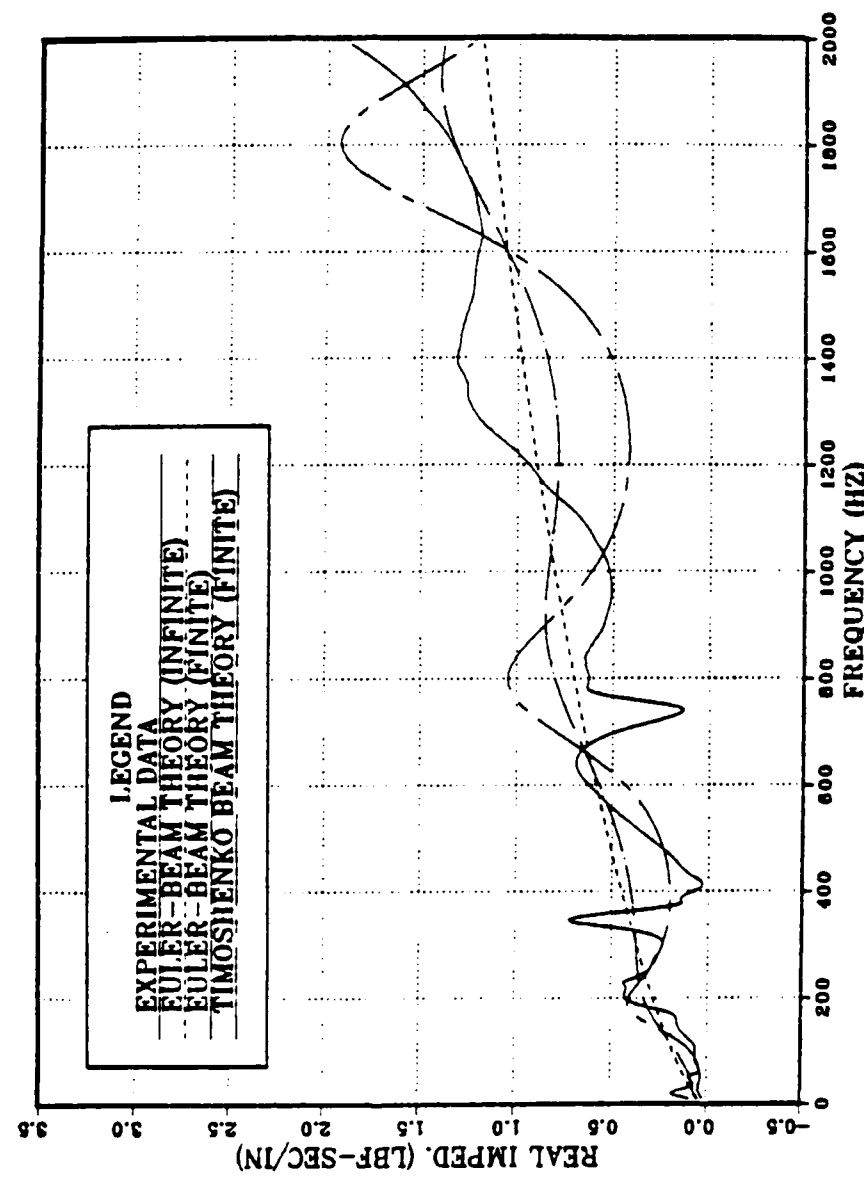


Figure 49. Real part of the 20" viscoelastic beam waveguide absorber impedances at the center of the beam.

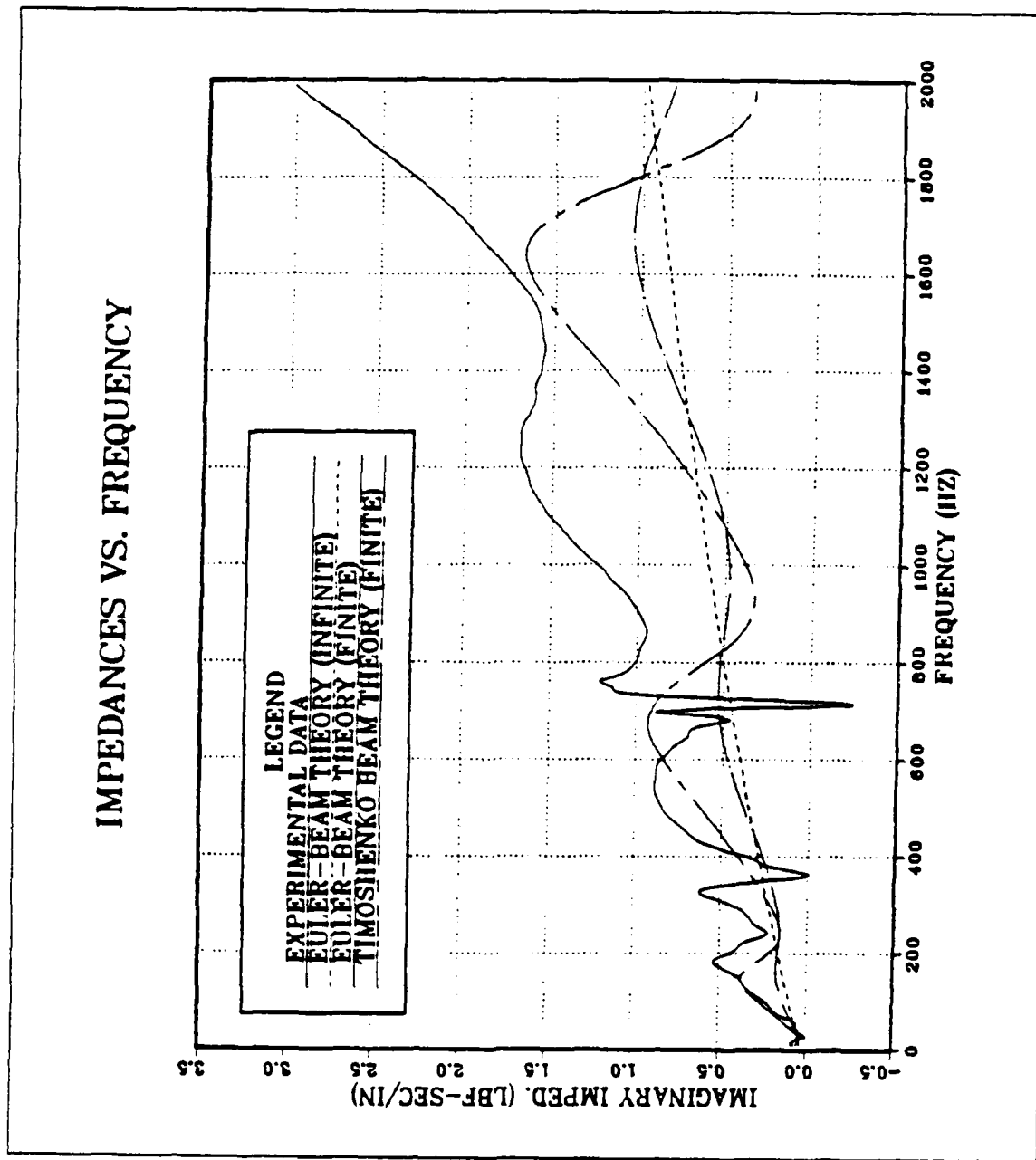


Figure 50. Imaginary part of the 20" viscoelastic beam waveguide absorber impedances at the center of the beam.

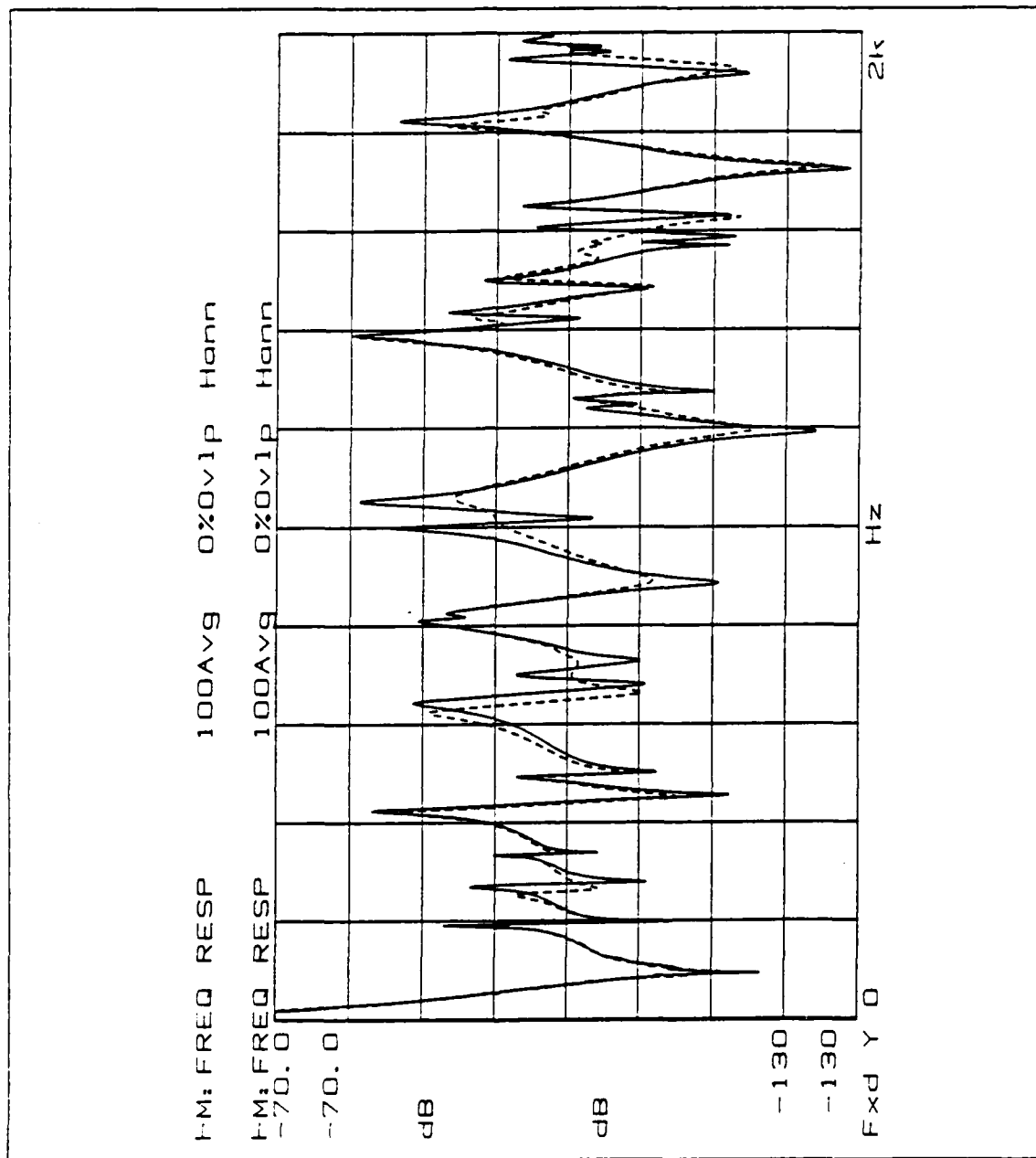


Figure 51. The driving point frequency response of the test plate with a 16" viscoelastic beam waveguide absorber (dashed) at location 1 and without (solid).

MODAL DAMPING VS. FREQUENCY

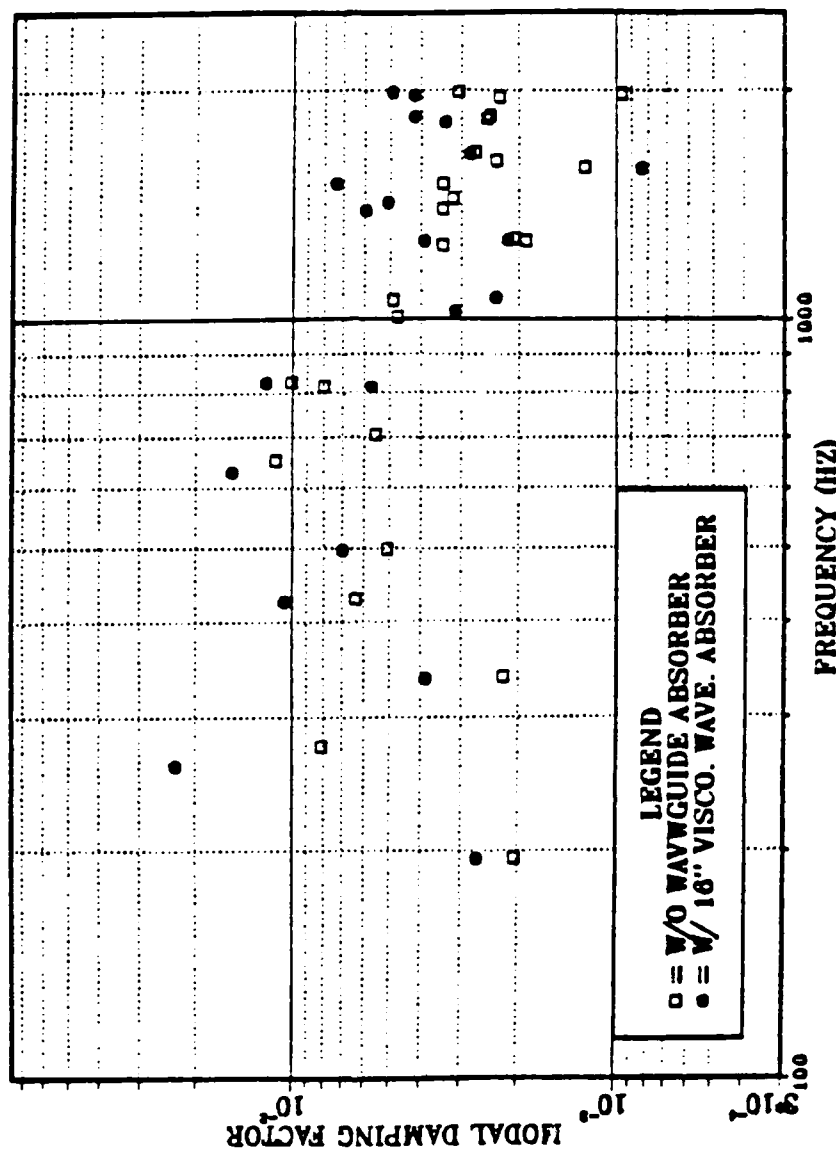


Figure 52. Modal damping factors vs. frequency of the test plate with a 16" viscoelastic beam waveguide absorber at location 1 and without.

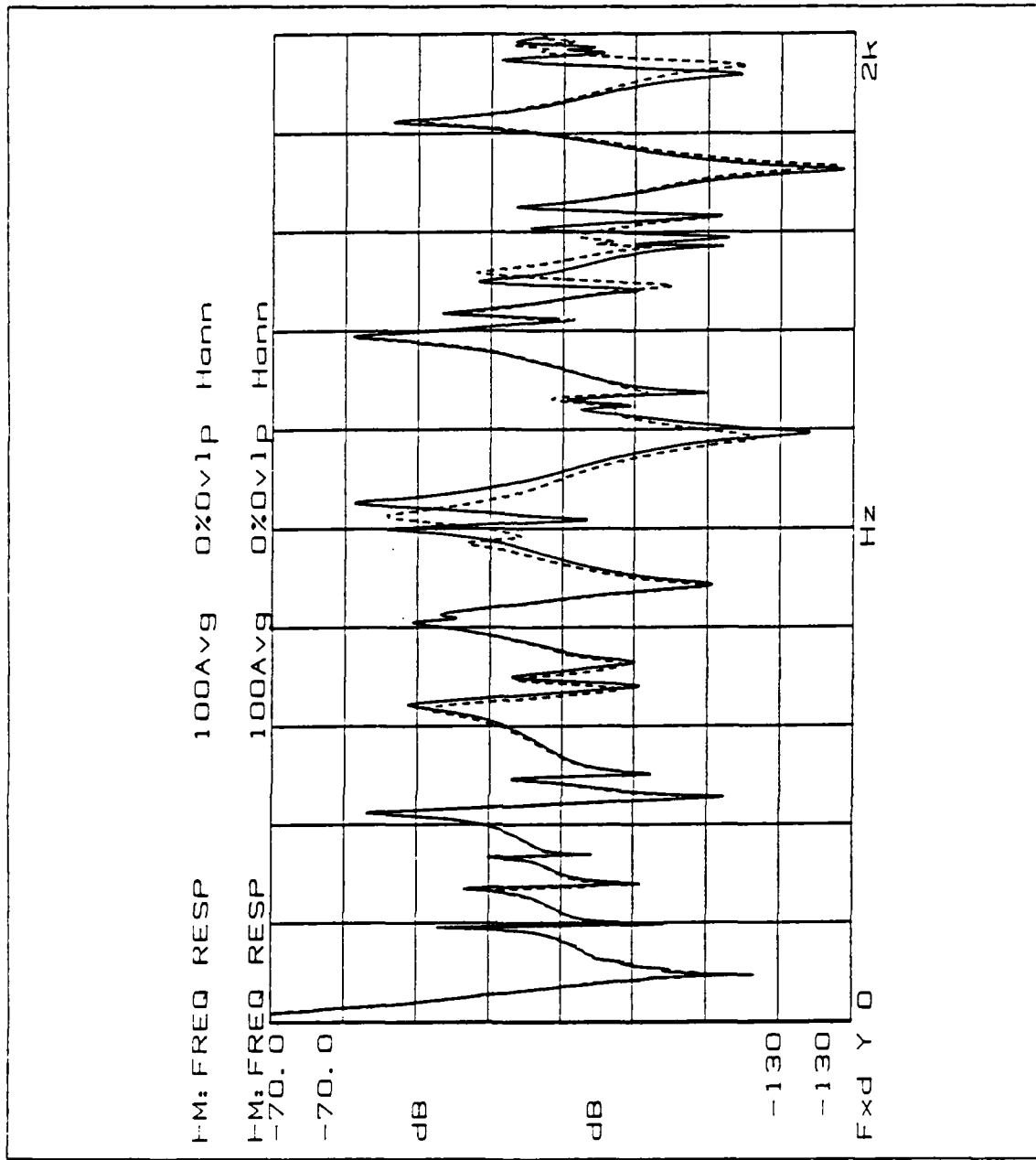


Figure 53. The driving point frequency response of the test plate with a 20" constrained layer beam waveguide absorber (dashed) at location 1 and without (solid).

MODAL DAMPING VS. FREQUENCY

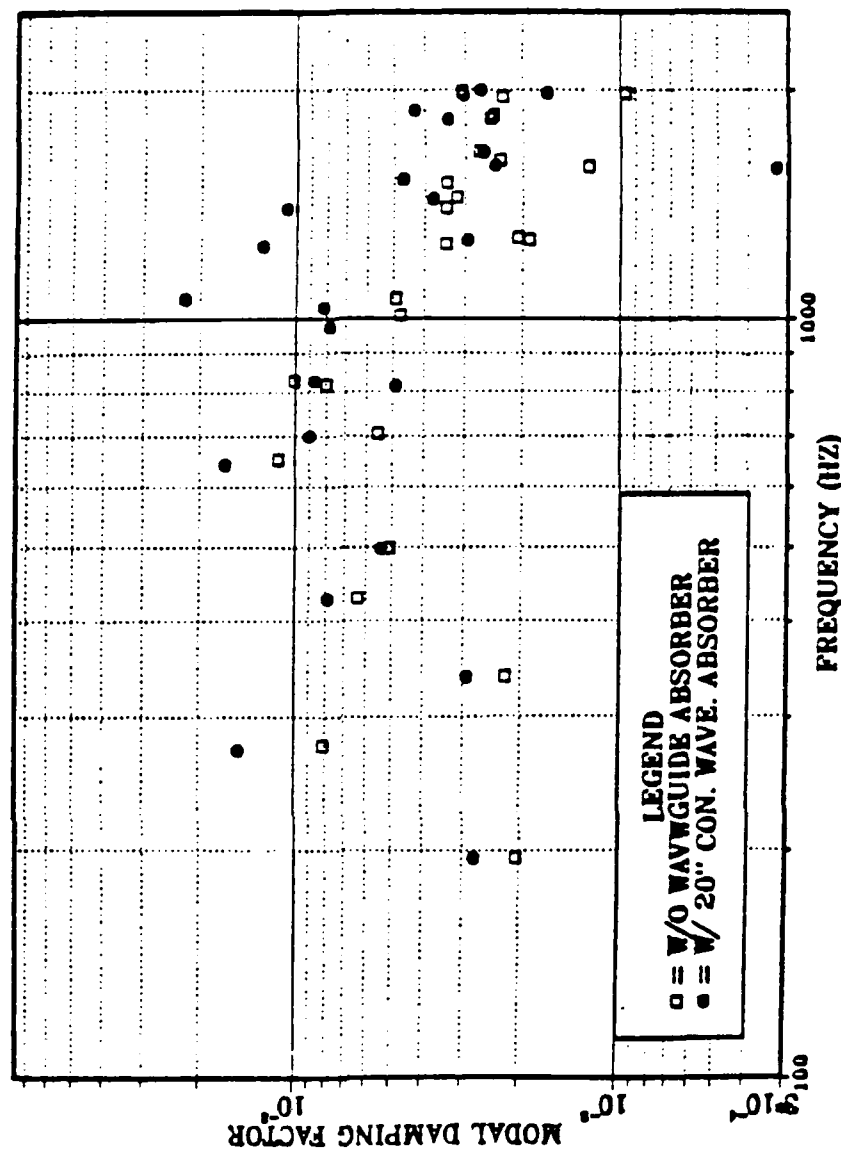


Figure 54. Modal damping factors vs. frequency of the test plate with a 20" constrained layer beam waveguide absorber at location 1 and without.

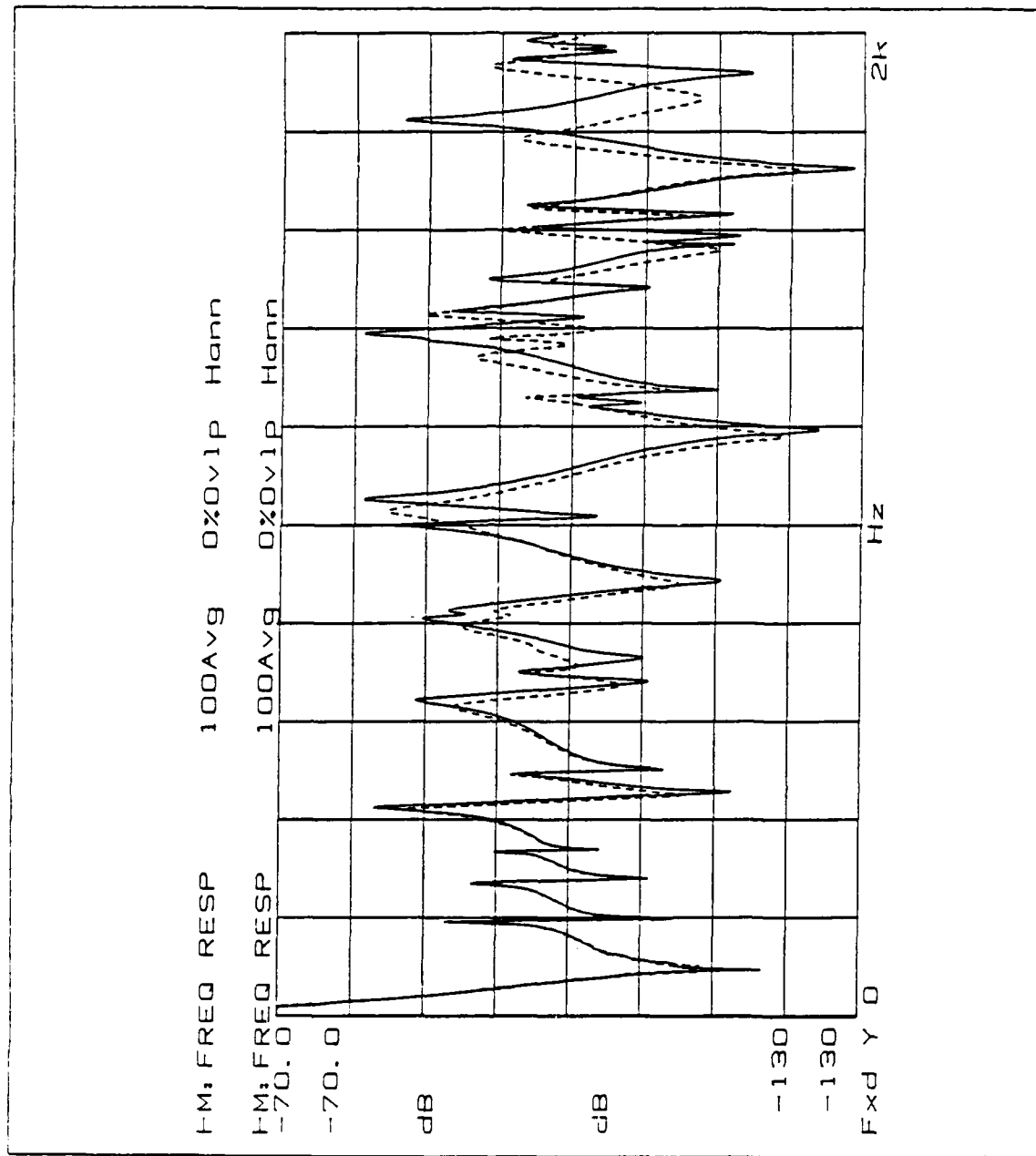


Figure 55. The driving point frequency response of the test plate with a 16" viscoelastic beam waveguide absorber (dashed) at location 2 and without (solid).

MODAL DAMPING VS. FREQUENCY

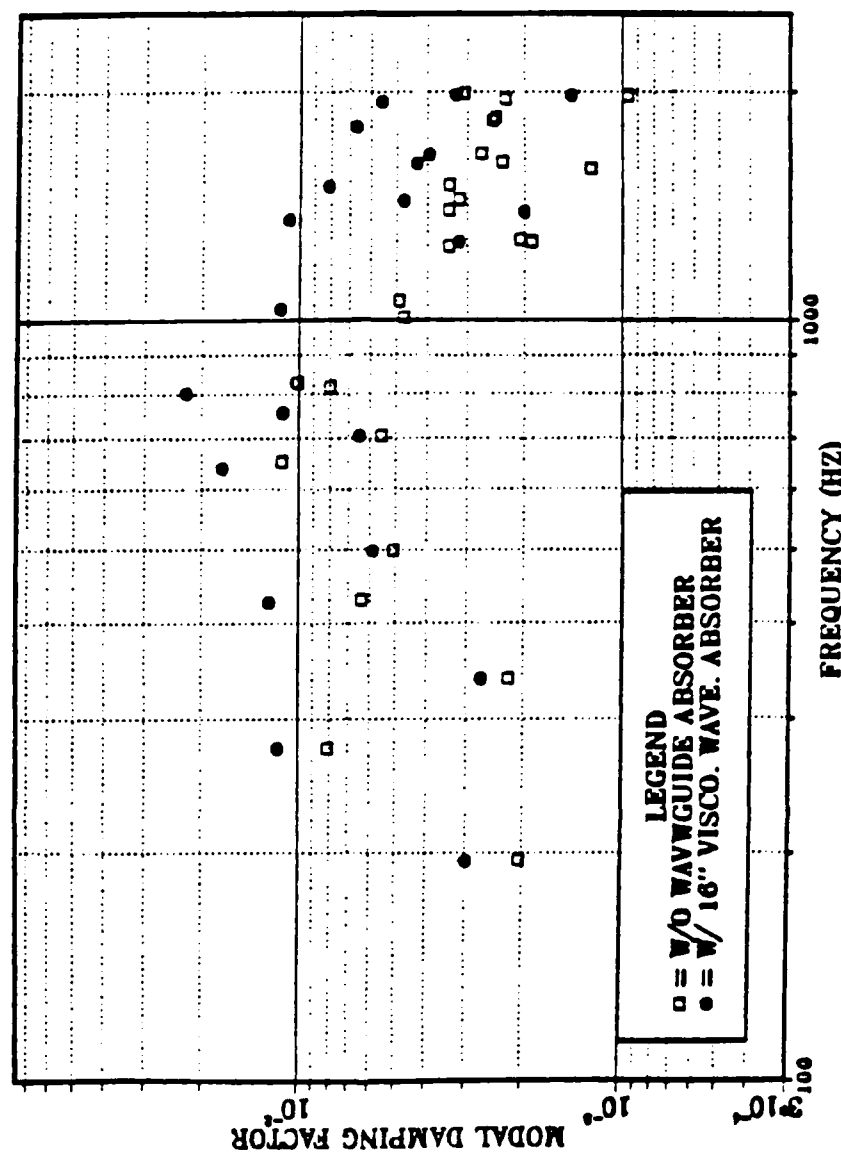


Figure 56. Modal damping factors vs. frequency of the test plate with a 16" viscoelastic beam waveguide absorber at location 2 and without.

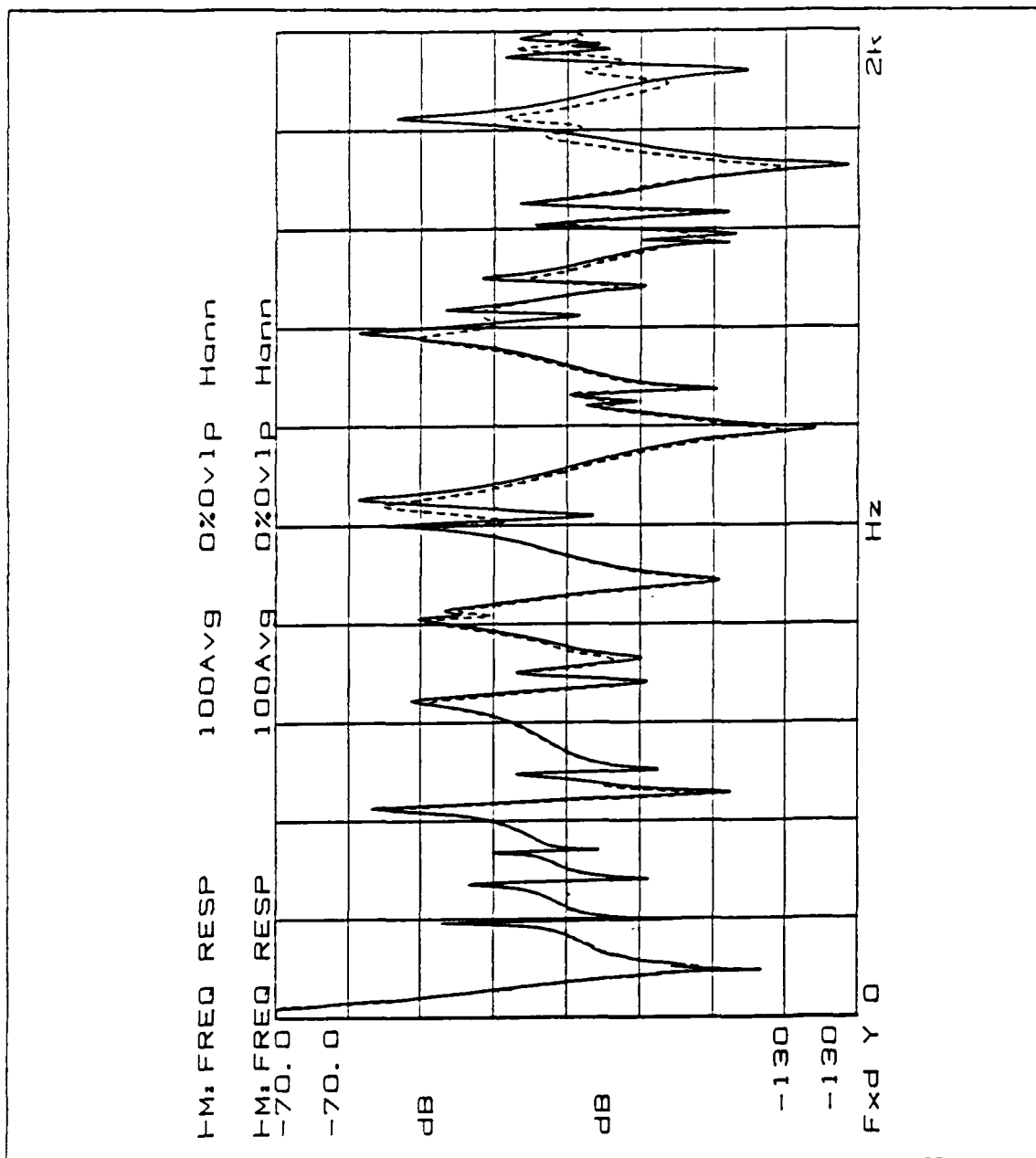


Figure 57. The driving point frequency response of the test plate with a 16" constrained layer beam waveguide absorber (dashed) at location 2 and without (solid).

MODAL DAMPING VS. FREQUENCY

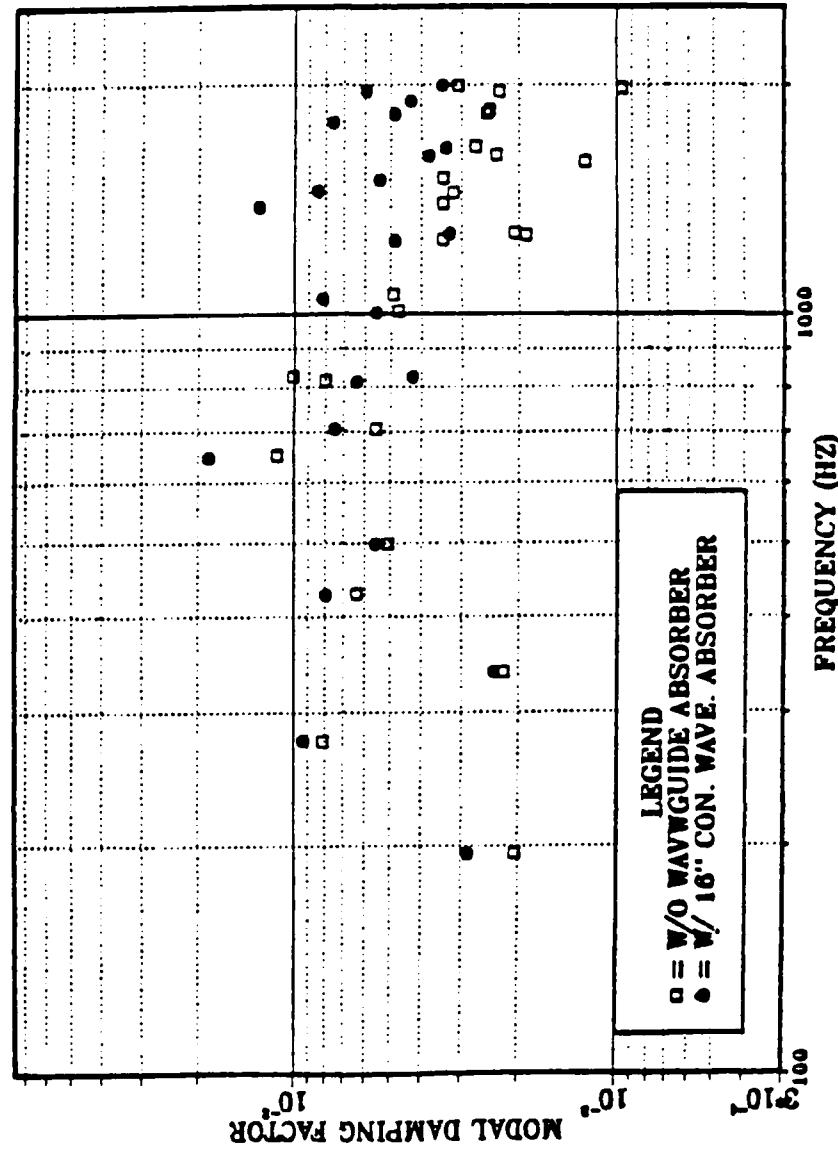


Figure 58. Modal damping factors vs. frequency of the test plate with a 16" constrained layer beam waveguide absorber at location 2 and without.

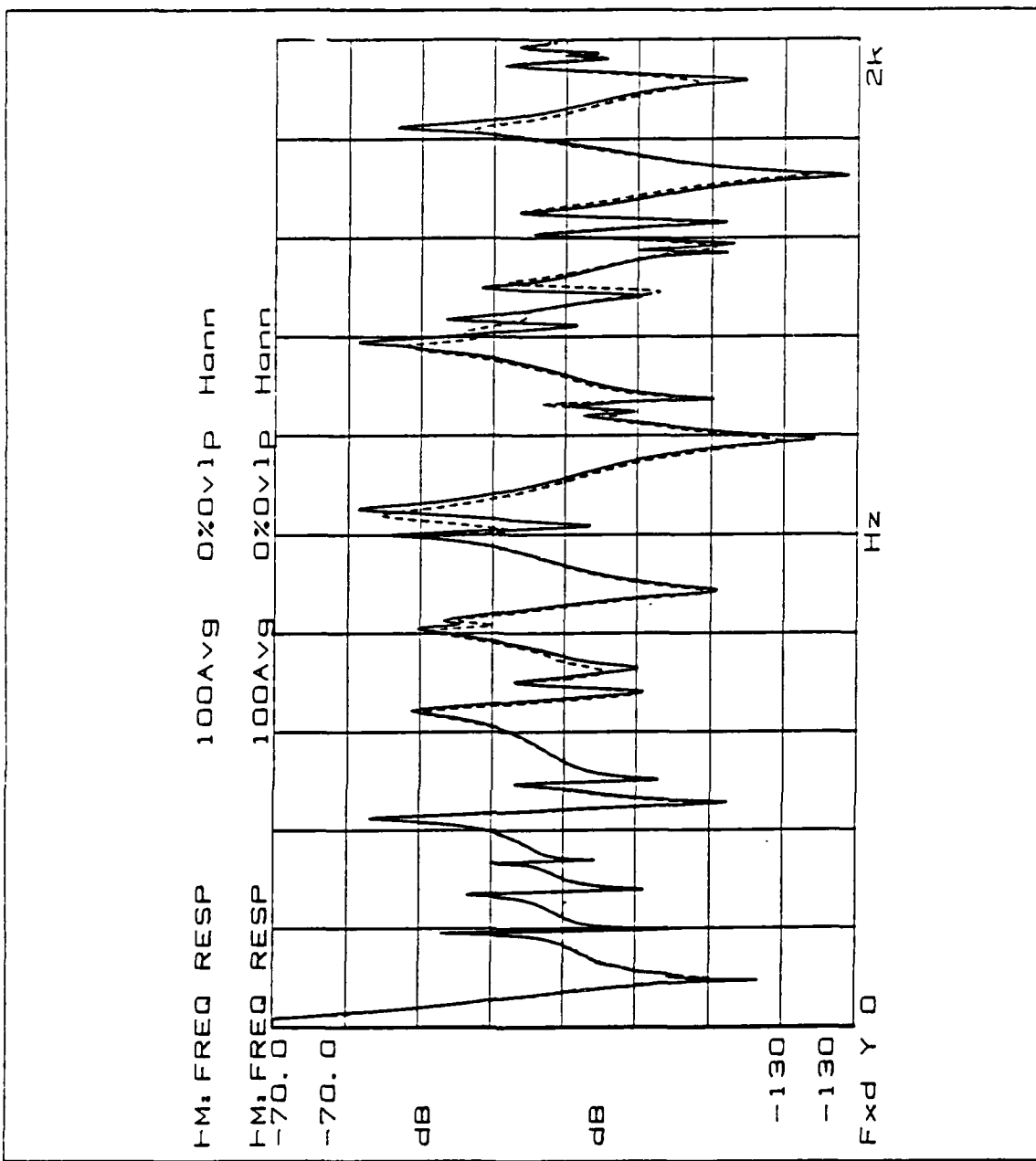


Figure 59. The driving point frequency response of the test plate with a 20" constrained layer beam waveguide absorber (dashed) at location 2 and without (solid).

MODAL DAMPING VS. FREQUENCY

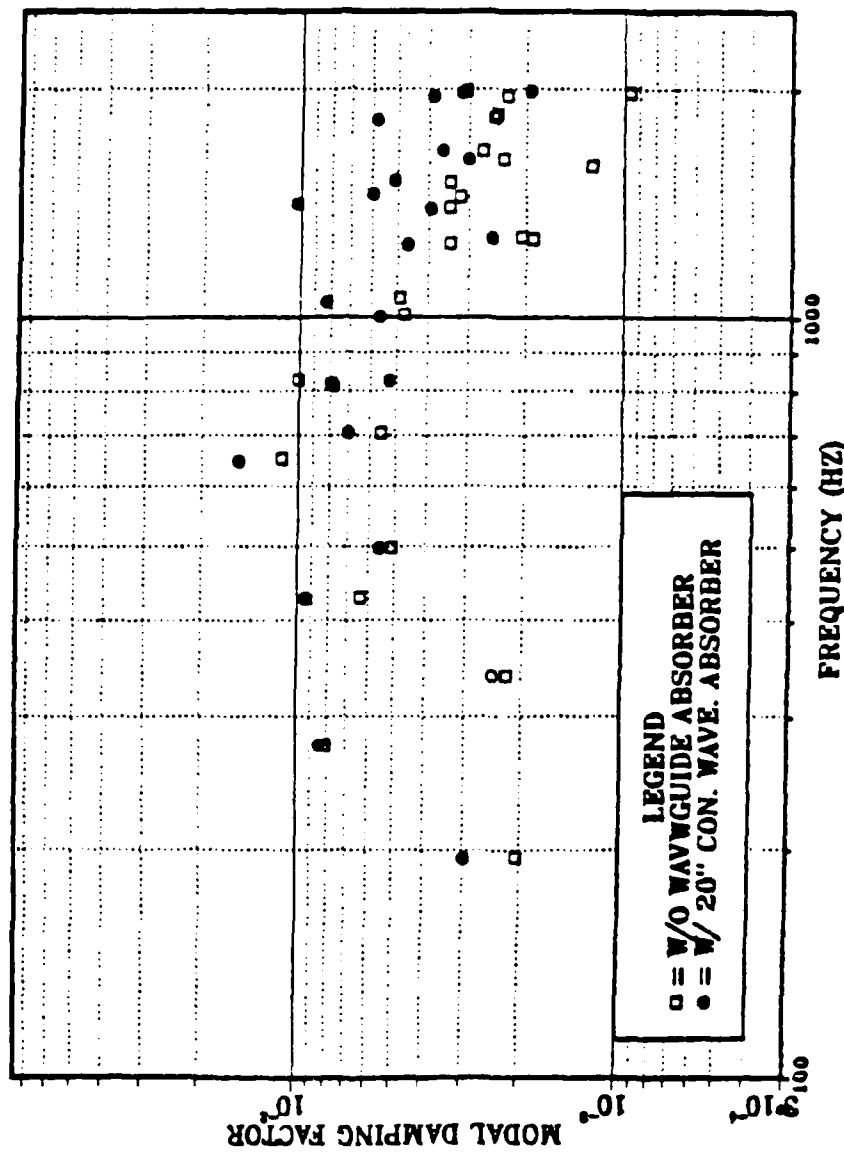


Figure 60. Modal damping factors vs. frequency of the test plate with a 20" constrained layer beam waveguide absorber at location 2 and without.

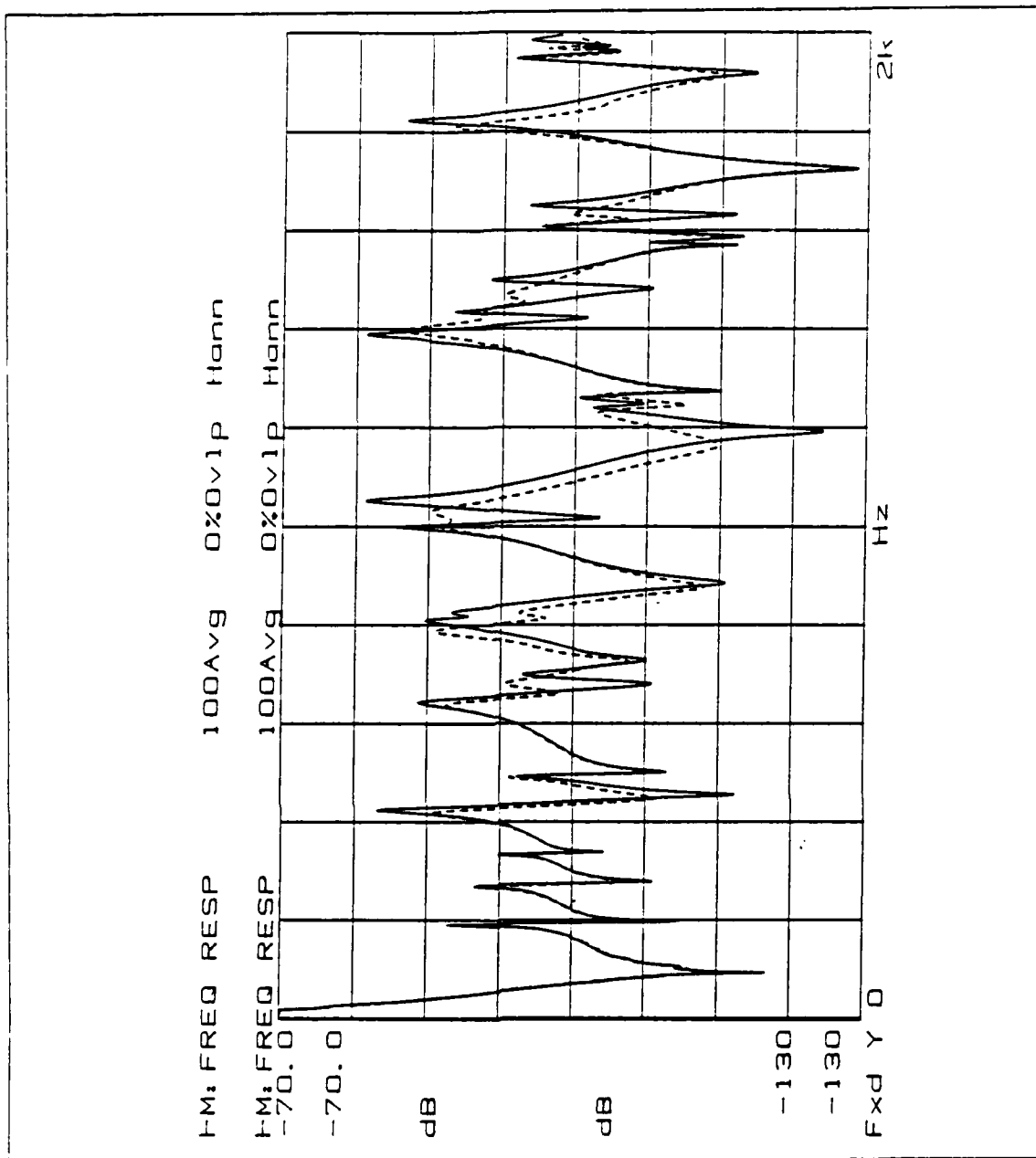


Figure 61. The driving point frequency response of the test plate with a 16" viscoelastic beam waveguide absorber (dashed) at location 3 and without (solid).

MODAL DAMPING VS. FREQUENCY

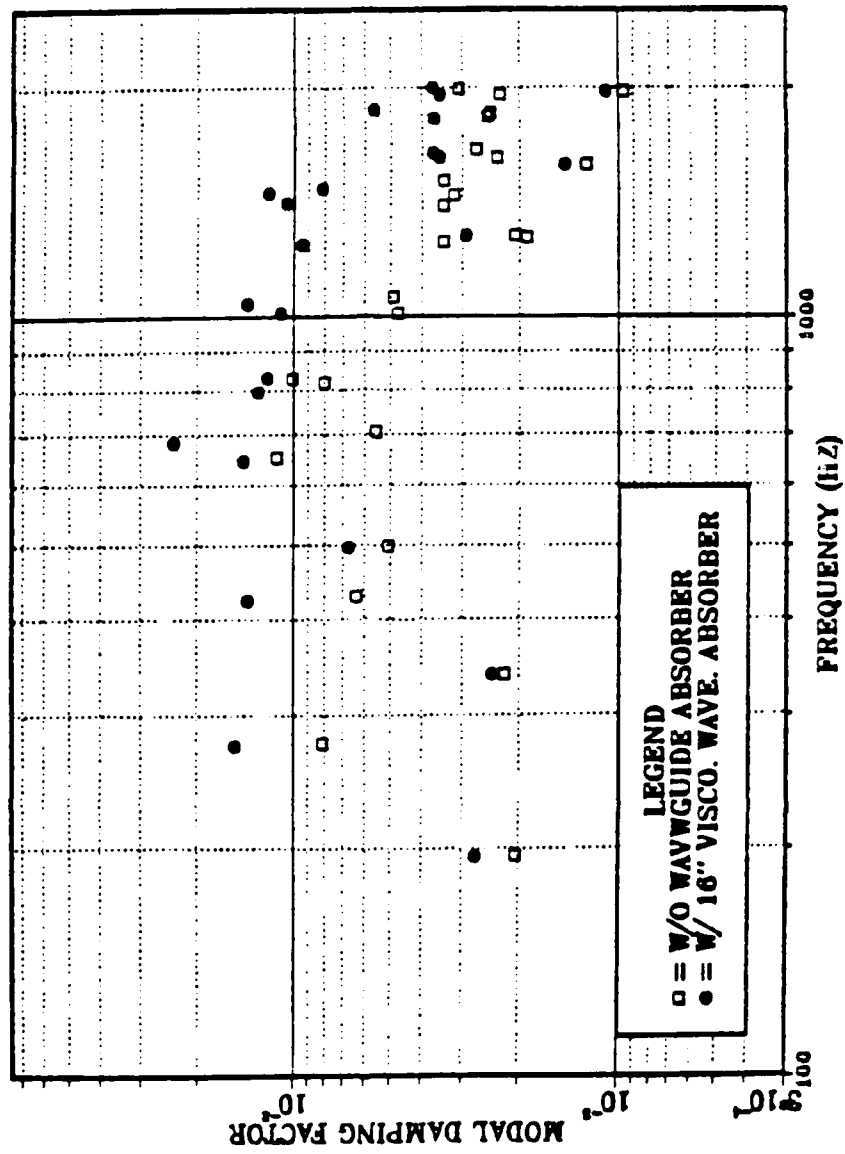


Figure 62. Modal damping factors vs. frequency of the test plate with a 16" viscoelastic beam waveguide absorber at location 3 and without.

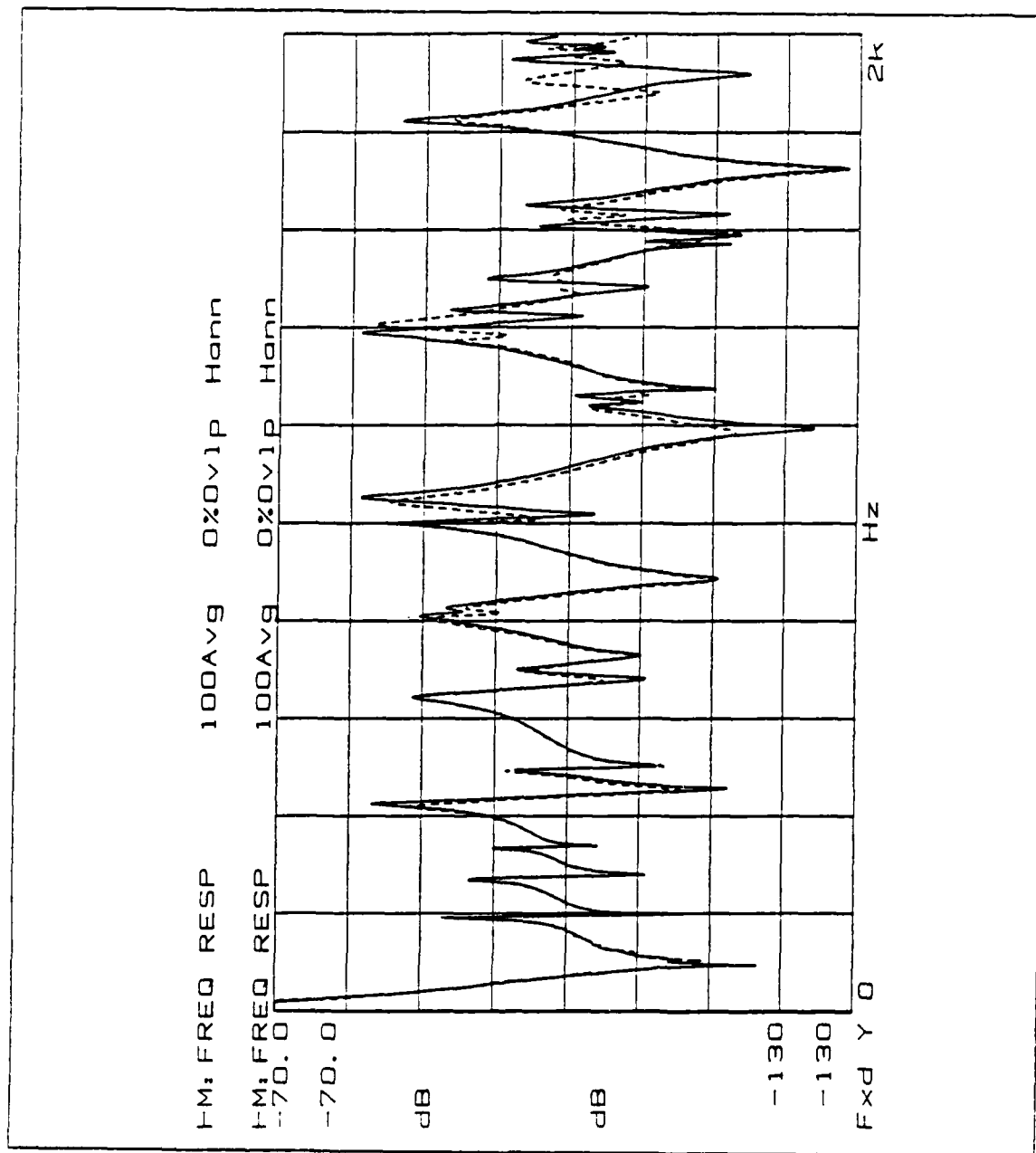


Figure 63. The driving point frequency response of the test plate with a 16" constrained layer beam waveguide absorber (dashed) at location 3 and without (solid).

MODAL DAMPING VS. FREQUENCY

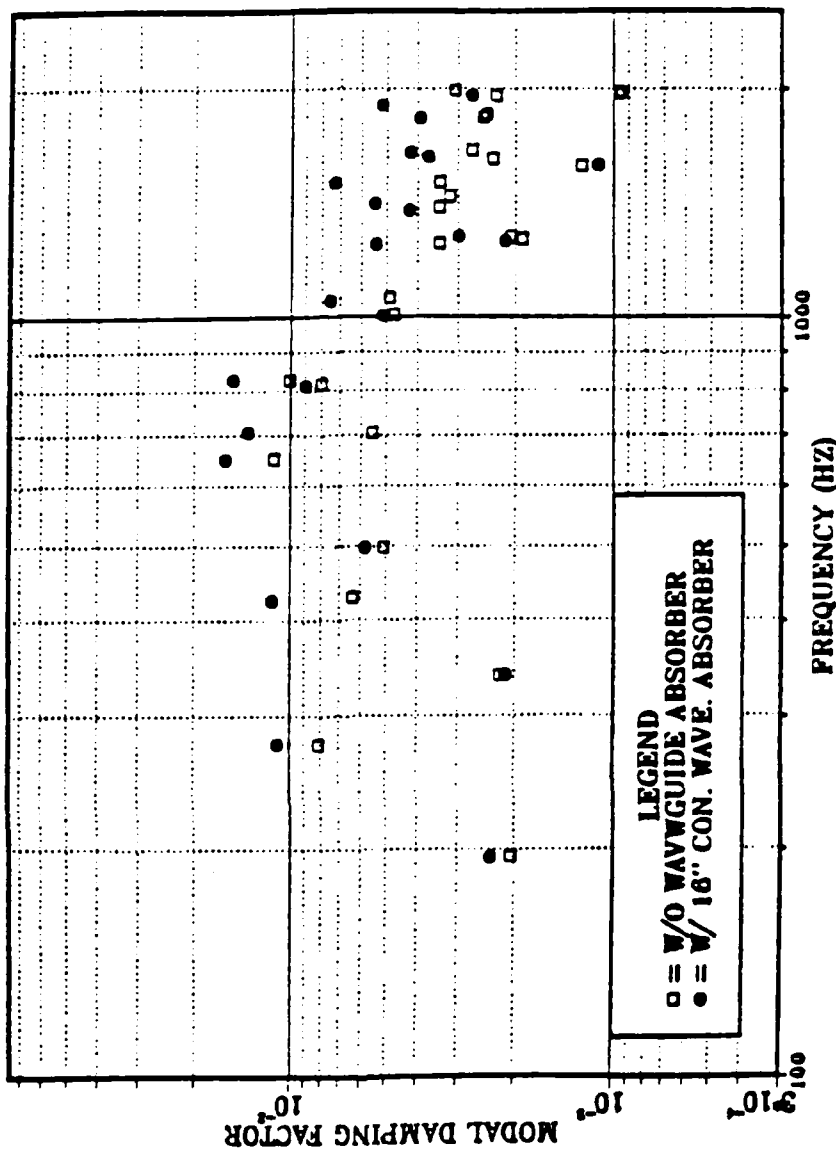


Figure 64. Modal damping factors vs. frequency of the test plate with a 16" constrained layer beam waveguide absorber at location 3 and without.

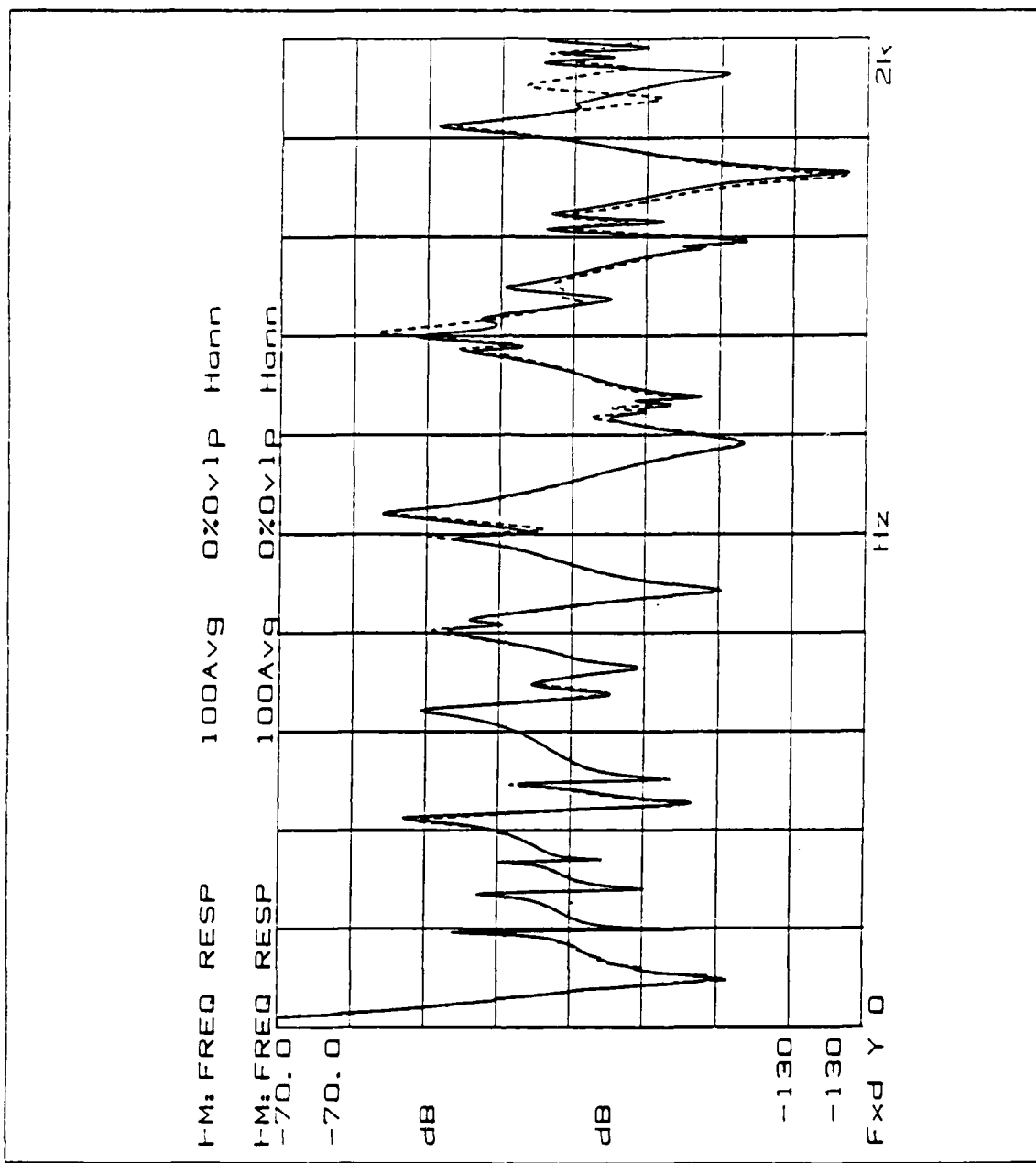


Figure 65. The driving point frequency response of the test plate with a 20" constrained layer beam waveguide absorber (dashed) at location 3 and without (solid).

MODAL DAMPING VS. FREQUENCY

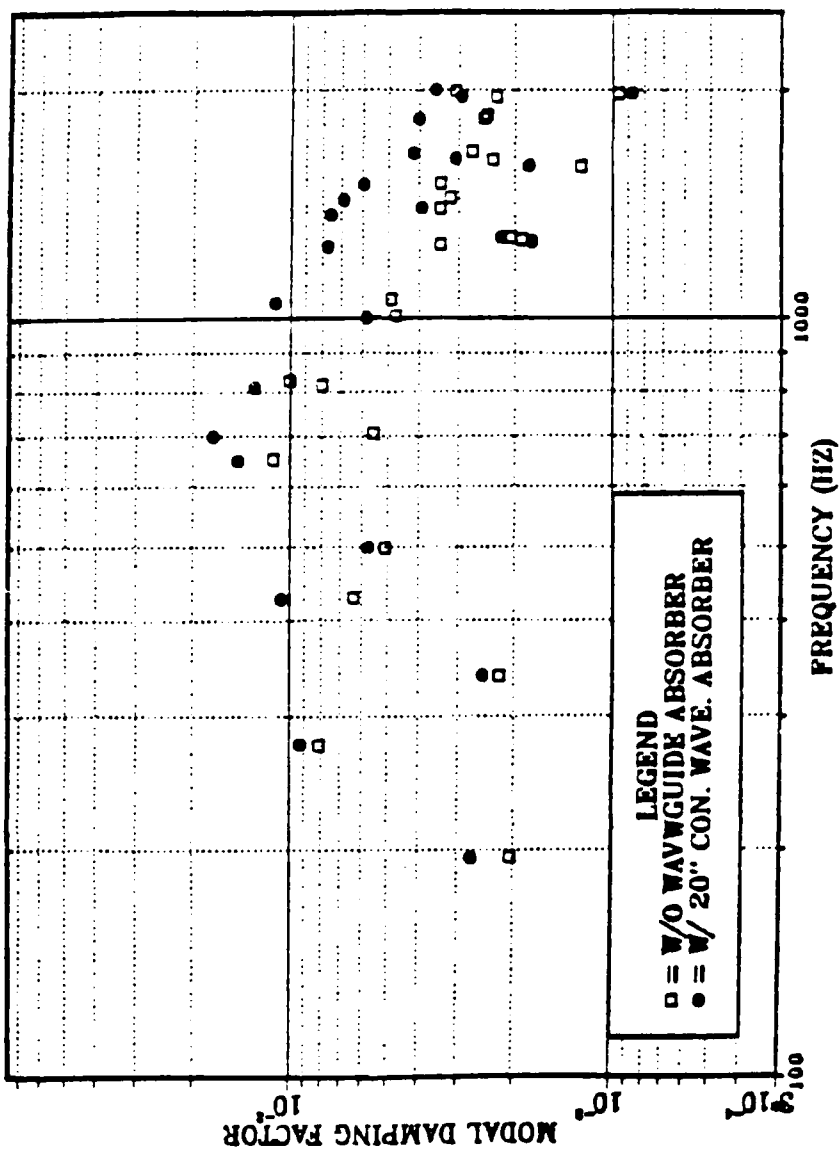


Figure 66. Modal damping factors vs. frequency of the test plate with a 20" constrained layer beam waveguide absorber at location 3 and without.

LIST OF REFERENCES

1. Ungar, E. E. and Kurzweil, L. G., Structural Damping Potential of Waveguide Absorbers, in Vibration Damping 1984 Workshop Proceedings, edited by Lynn Rogers, Air Force Wright Aeronautical Laboratories, AFWAL-TR-84-3064, pp. CC.1-CC.15, Nov. 1984.
2. Ungar, E. E. and Kurzweil, L. G., Preliminary Evaluation of Waveguide Vibration Absorbers, Flight Dynamics Laboratory, Air Force Wright Aeronautical Laboratories Report AFWAL-TR-83-3125 Jan. 1984.
3. Ungar, E. E. and Williams, B. F., A study to guide the development and use of waveguide absorbers for structural damping, David Taylor Naval Ship Research and Development Center, Report No.6463 Mar. 1987.
4. Crandall, S. H., DYNAMICS of mechanical and electromechanical system, Department of Mechanical Engineering, Massachusetts Institute of Technology, pp. 332-363, 1968.
5. Ditaranto, R. A., "Theory of Vibratory Bending for Elastic and Viscoelastic Layered Finite-Length Beams", Journal of Applied Mechanics (Transactions of the ASME), pp. 881-886, Dec. 1965.
6. Kerwin, E. M. Jr., "Damping of flexural Waves by a Constrained Visco-Elastic layer," Journal of the Acoustical Society of America, vol.31, pp. 952-962, 1959.
7. Mead, Mead and Markus, S., "The Forced Vibration of a Three-layer, Damped Sandwich Beam Arbitrary Boundary Conditions", Journal of the Sound Vibrations, pp. 163-175, Oct. 1969.
8. Hearn, A. C., Reduce user's manual, Rand Publication CP78, Apr. 1983.

9. Nashif, A. D., Jones, D. I. G., and Henderson, J. P., Vibration damping, A Wiley-interscience publication, 1985.
10. Thomson, W. T., Theory of vibration with applications, Prentice-Hall Engilewood Cliffs, 1981.
11. HP-3562A Dynamic signal analyzer operating manual, Oct. 1985.

INITIAL DISTRIBUTION LIST

| | No. Copies |
|---|------------|
| 1. Defense Technical Information Center Cameron Station Alexandria, VA 22304-6145 | 2 |
| 2. Library, Code 0142 Naval Postgraduate School Monterey, CA 93943-5002 | 2 |
| 3. Dean of Science and Engineering, Code 06 Naval Postgraduate School Monterey, CA 93943-5000 | 2 |
| 4. Research Administrations Office, Code 012 Naval Postgraduate School Monterey, CA 93943-5000 | 1 |
| 5. Department Chairman, Code 69 Department of Mechanical Engineering Naval Postgraduate School Monterey, CA 93943-5000 | 1 |
| 6. Professor Young S. Shin, Code 69Sg Department of Mechanical Engineering Naval Postgraduate School Monterey, CA 93943-5000 | 4 |
| 7. Professor Kilsoo S. Kim, Code 69Ki Department of Mechanical Engineering Naval Postgraduate School Monterey, CA 93943-5000 | 1 |
| 8. Dr. Arthur Kilcullen, Code 1962 David W. Taylor Naval Ship R&D Center Bethesda, MD 20084 | 2 |
| 9. Mr. Robert Hardy, Code 2803 David W. Taylor Naval Ship R&D Center Annapolis, MD 21402 | 1 |
| 10. Library of the Naval Academy Kyoung Nam Jin-Hae Si Anggok Dong South Korea | 1 |
| 11. Mr. V.J. Castelli, Code 2844 David W. Taylor Naval Ship R&D Center Annapolis, MD 21402 | 1 |

- | | | |
|-----|--|---|
| 12. | Dr. Lawrence Maga, Code 196 David W. Taylor Naval Ship R&D Center Ship Acoustics Department (196) Bethesda, MD 20084 | 1 |
| 13. | Dr. B. Whang, Code 1750.2 David W. Taylor Naval Ship R&D Center Hull Group Head, Submarine Protection Div. Bethesda, MD 20084 | 1 |
| 14. | Dr. N. T. Tsai Defence Nuclear Agency SPSS Washington, D.C. 20305-1000 | 1 |
| 15. | Dr. E. E. Ungar BBN Laboratory Inc. 10 Moulton st. Cambridge, MA 02238 | 1 |
| 16. | Department of Mechanical Engineering Naval Academy Kyoung Nam Jin-Hae Si Anggok Dong South Korea | 1 |
| 17. | Gi G. Lee 530-00 Jeon Buk Namwon Si Kwang-chi Dong 273 South Korea | 1 |
| 18. | Chil K. Baek SMC #1646 Naval Postgraduate School Monterey, CA 93943 | 1 |
| 19. | Dong R. Shin SMC #1732 Naval Postgraduate School Monterey, CA 93943 | 1 |
| 20. | Joo N. Sur SMC #1655 Naval Postgraduate School Monterey, CA 93943 | 1 |
| 21. | Gerald F. Nies 20026 Viking Crest N.E. APT. 1-202 Poulsbo, WA 98370 | 1 |
| 22. | Joseph Chan 208-A S. Gold Canyon Ridgecrest, CA 93555 | 1 |

END

DATED

FILM

8-88

DTIC